

Normal State Transport Properties of Novel Superconductors

THÈSE N° 4230 (2009)

PRÉSENTÉE LE 23 JANVIER 2009

À LA FACULTE SCIENCES DE BASE

Laboratoire de nanostructures et nouveaux matériaux électroniques

SECTION DE PHYSIQUE

ÉCOLE POLYTECHNIQUE FÉDÉRALE DE LAUSANNE

POUR L'OBTENTION DU GRADE DE DOCTEUR ÈS SCIENCES

PAR

Balázs SIPOS

acceptée sur proposition du jury:

Prof. R. Schaller, président du jury

Prof. L. Forró, directeur de thèse

Prof. A. Gauzzi, rapporteur

Prof. M. Grioni, rapporteur

Dr E. Tütis, rapporteur



ÉCOLE POLYTECHNIQUE
FÉDÉRALE DE LAUSANNE

Lausanne, EPFL

2009

NORMAL STATE PROPERTIES OF NOVEL
SUPERCONDUCTORS

Version abrégée

La découverte de la supraconductivité à haute température dans les cuprates en 1986 a stimulé la recherche de matériaux fortement corrélés. La compréhension des phénomènes dans les matériaux à haut T_c et l'espoir de découvrir ou de fabriquer des matériaux avec des très hauts T_c reste la principale motivation dans ce domaine. Parallèlement à l'étude détaillée des cuprates, la communauté de l'état solide s'oriente vers la recherche de nouveaux matériaux dont la découverte trouve un intérêt d'un point de vue technologique mais aussi car ils pourraient permettre une meilleure compréhension des phénomènes « haut T_c ».

Mes travaux de thèse s'articule autour de trois points : i) étudier le rôle de l'inhomogénéité dans les matériaux sous dopés. Ceci reste une des énigmes des cuprates supraconducteurs ; ii) Etudier l'effet du désordre dans MgB_2 , supraconducteur ayant des potentiels pour les applications ; iii) la découverte de nouveaux matériaux supraconducteurs dans les dichalcogénures de métaux de transition. Tous ces matériaux sont, d'un certain point de vue, des supraconducteurs non conventionnels : les cuprates par leur haute T_c et par la symétrie du paramètre d'ordre ; MgB_2 par la supraconductivité à deux bandes et un T_c de 39 K ; et enfin les dichalcogénures dont la supraconductivité apparaît dans le bruit de fond de la compétition entre les interactions.

Nous avons utilisé des mesures de propriétés de transport, tels que la résistivité et le pouvoir thermoélectrique, pour comprendre le comportement de ces matériaux. En plus de la température, nous avons appliqué des hautes pressions, des champs magnétiques extrêmes et nous avons contrôlé le désordre créé par irradiation électronique rapide.

Dans la première partie, je présente la dépendance en température de matériaux de la famille dichalcogénures qui possèdent une structure 1T : 1T-TiSe₂ et 1T-TaS₂, pour lesquels un état supraconducteur n'a jamais été observé dans l'état non transformé. 1T-TiSe₂ présente une phase CDW (onde de densité de charge) à température inférieure à 220 K dont l'origine reste une question ouverte. L'exis-

tence de cette phase peut être le résultat d'un mécanisme excitonique ou d'une distorsion de type Jahn-Teller. Nous avons montré que 1T-TiSe₂ est supraconducteur dans une gamme de pression comprise entre 3 et 4 GPa. Cette gamme de pression coïncide avec le petit domaine CDW fluctuante avant sa disparition à plus haute pression. Si l'état CDW est dû à des interactions excitoniques, alors nos observations suggèrent qu'elles peuvent être aussi à l'origine de la supraconductivité.

Le second dichalcogénure étudié est 1T-TaS₂, pour lequel une phase isolante de Mott apparaît superposée à un état CDW commensurable. Avec l'application d'une pression supérieure à 2.5 GPa, le matériau devient supraconducteur avec une T_c de 5.9 K. De manière inattendue, la supraconductivité apparue à partir d'une phase non métallique reste stable jusqu'au plus hautes pressions appliquées de 24 GPa.

Dans la deuxième partie, j'ai essayé d'apporter ma contribution à la thématique « supraconducteurs haute T_c ». Quelques cristaux de très bonne qualité de Bi₂Sr₂Pr_xCa_{1-x}Cu₂O_{8-δ} sous dopés ont été sélectionnés. Nous avons étudié la nature de l'état fondamental à basse température en appliquant de hauts champs magnétiques. Même si des mesures ont déjà été effectuées par d'autres groupes et ont montré qu'à fort sous dopage, l'état fondamental était isolant ; nous avons montré qu'un échantillon avec un T_c de 15 K présente un comportement métallique jusqu'à une pression de 60 T. De plus, nous avons montré qu'une distribution inhomogène des dopants peut masquer entièrement l'état intrinsèque d'un supraconducteur haut T_c .

Dans la dernière partie, nous avons étudié MgB₂ supraconducteur à deux bandes par diffusion entre les bandes grâce à la règle de Matthiessen. Nous avons fait une étude systématique de l'influence des défauts créés par une irradiation rapide d'électrons. Nous avons trouvé que la loi de Matthiessen peut être appliquée pour une concentration de défauts de la gamme obtenue. Nous avons par la suite comparé l'influence de défauts sur la température critique et sur la résistivité résiduelle dans MgB₂ avec des supraconducteurs avec divers paramètres d'ordre.

Nous avons trouvé que la vitesse de décroissance de T_c dans notre système est dans la gamme de réponse d'un supraconducteur avec un paramètre d'ordre d'onde s.

Mots-clés : Supraconductivité, Propriétés de transport, Supraconducteurs haute T_c , Dichalcogénures

Abstract

The discovery of high temperature superconductivity in the cuprates in 1986 has boosted the research in strongly correlated materials. One strong motivation was and stays the understanding the high- T_c phenomenon with the hope that one can ultimately engineer new materials with even higher T_c . Besides the in-depth investigation of cuprates, there is a strong tendency in the solid state community to find new superconductors, which by themselves are interesting for applications, or by their properties they can contribute to the understanding of the high- T_c phenomenon.

The program of my doctoral thesis was three-fold: i) to address one important issue in the cuprate superconductors, that of the role of homogeneity in the underdoped part of the phase diagram; ii) what is the effect of disorder in MgB_2 superconductor, which has high potentials for applications; iii) to discover new superconductors in the family of transition metal dichalcogenides. All these materials are in some sense unconventional superconductors. The cuprates by their high T_c and the symmetry of the order parameter, MgB_2 by its two-band superconductivity and T_c of 39 K, and the dichalcogenides by the appearance of superconductivity on the background of competing interactions.

Measurements of transport properties, such as resistivity and thermoelectric power, were used to get insight in the behavior of these materials. Besides temperature as variable, I applied high pressure, extreme magnetic fields and controlled disorder introduced by fast electron irradiation.

In the first part I present the pressure dependent study of two members of the transition metal dichalcogenides having 1T structure, 1T-TiSe₂ and 1T-TaS₂, where superconductivity was never observed in a pristine sample. 1T-TiSe₂ has a CDW phase below 220 K which origin, weather it is driven by an excitonic mechanism or by a Jahn-Teller distortion, is an ongoing question. By applying pressure I showed that the pristine sample is superconducting in the pressure range of 2.0–4.0 GPa. This range remarkably coincides with the short range

fluctuating CDW before its disappearance at the upper pressure value. If CDW is due to excitonic interactions than our observation suggest that it can be at the origin of superconductivity, as well.

The second dichalcogenide is the 1T-TaS₂, where a Mott-insulator phase appears on the top of a commensurate CDW. By applying pressure I was able to melt that Mott-phase, and reveal that the material is superconducting above 2.5 GPa with T_c of 5.9 K. Unexpectedly, superconductivity is born from a non-metallic phase, and stays remarkably stable up to the highest applied pressure of 24 GPa.

In the second part I tried to give my contribution to the field of high- T_c superconductors. I carefully selected few high quality underdoped Bi₂Sr₂Pr_xCa_{1-x}Cu₂O_{8- δ} sample, to address the nature of the low temperature ground state by applying high magnetic field. Although former measurements by other groups showed that at high underdoping, the ground state is an insulator, I found that a sample with as low T_c as 15 K exhibits metallic behavior up to 60 T. Furthermore, I showed that a inhomogeneous distribution of the doping atoms can completely mask the intrinsic normal state of a high- T_c superconductor.

In the last part of my thesis I focused on the two-band superconductor MgB₂ by studying the scattering between the

bands by the means of the Matthiessen's rule. I made a systematic study of the influence of defects created by fast electron irradiation, and found that the the Matthiessen's rule is satisfied for the defect concentration range I induced. I further compare the influence of defects on the critical temperature and the residual resistivity in MgB₂ with superconductors with various order parameters, and found that the decrease-rate of T_c in our system is within the range of a response of a superconductor with an s-wave order parameter.

Keywords: Superconductivity, Transport properties, High- T_c superconductors, Dichalcogenides

Contents

1	Introduction	1
2	Electronic properties of two-dimensional conductors	11
2.1	Electron-electron correlations	11
2.2	The Hubbard model	12
2.2.1	Different ground states	13
2.3	Electron-phonon interaction	18
2.3.1	Peierls instability, charge density waves	19
2.3.2	Jahn-Teller distortion	25
2.4	Superconductivity	26
3	Transition metal dichalcogenides	31
3.1	Introduction to the transition metal dichalcogenides	31
3.1.1	Crystal structure and polytypes	31
3.1.2	Electronic structure	34
3.1.3	Intercalation complexes	36
3.2	1T-TiSe ₂	37
3.2.1	Presentation of 1T-TiSe ₂	37
3.2.2	Results	45
3.3	1T-TaS ₂	52
3.3.1	Presentation of 1T-TaS ₂	52
3.3.2	Goal of the experiment	58
3.3.3	Results	60

3.3.4	Discussion	64
4	Underdoped $\text{Bi}_2\text{Sr}_2\text{CaCu}_2\text{O}_{8-\delta}$ high T_c superconductor	79
4.1	Introduction	80
4.2	Sample and measurements	88
4.2.1	Results	90
4.2.2	Magnetoresistance in the normal state	92
4.2.3	Superconducting fluctuations near T_c	95
4.2.4	A minimal model for the resistivity of inhomogeneous superconductor.	98
4.3	Conclusion	102
5	MgB_2	111
5.1	Introduction	111
5.1.1	Crystal structure	112
5.1.2	Isotope effect	114
5.1.3	Specific heat measurement	114
5.1.4	Point contact spectroscopy	115
5.1.5	Electronic structure calculation and the proof of the two gap model	116
5.2	The goal of our experiment	117
5.3	Experimental setup	120
5.4	Results	122
5.5	Conclusion	126
6	Conclusion	133
A	Calculation the Coulomb energy for different domain sizes in the case of 1T-TaS_2	137

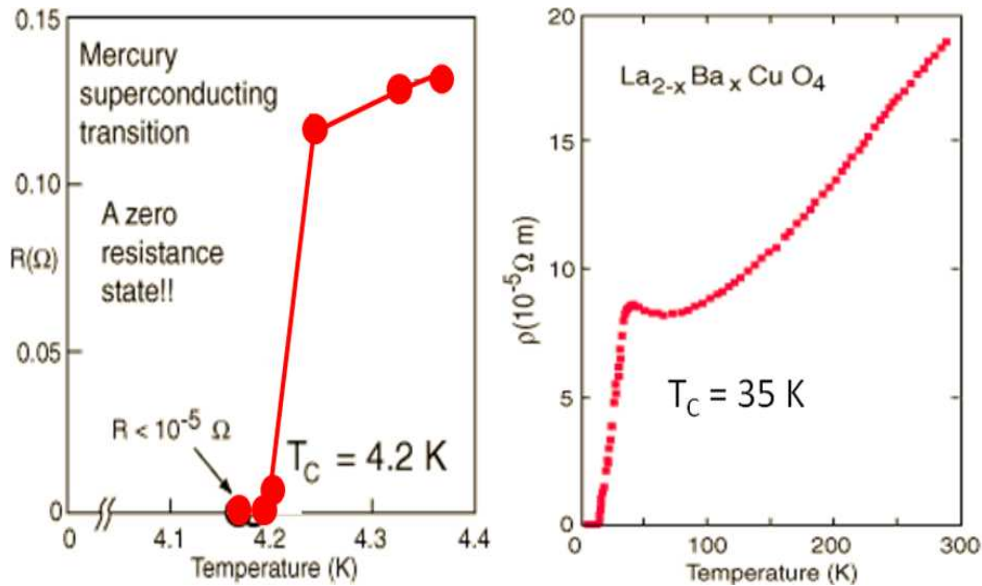
Chapter 1

Introduction

Superconductivity looks like a miracle. The fact that one can transport electrical charge without resistance, without “paying” anything for this transport, without heating up the wires, is far from being an ordinary thing. Furthermore, this zero resistance state arrives without a herald: the resistance drops from a finite value to zero suddenly at a critical temperature T_c . When Kamerlingh Onnes’ student reported him the zero resistance state below 4.1 K of Mercury in 1911 [1](Fig. 1.1(a)), the supervisor was suspicious. They had to repeat the experiment several times before it became evident that they were facing a genuine discovery. This sudden and fundamental disappearance of resistance was rewarded by the Nobel Prize in 1913.

During the decades new superconductors were discovered, a wealth of experimental results were accumulated which finally led to the understanding of the microscopic mechanism of superconductivity by Bardeen, Cooper and Schrieffer in 1957 [2]. The description of this macroscopic coherent quantum state by the BCS theory merited also a Nobel Prize in 1972.

Because of the lossless electrical transport, magnetic levitation, quantum interference etc., it was clear that this phenomenon is very important for applications and that the increase of T_c would be very beneficial. If T_c went above liquid nitrogen temperature (77 K) one could dispense with the costly helium



(a) The first observation of superconductivity by measuring the resistivity of Mercury. (after H. K. Onnes, [1]).

(b) This ceramic material was the first of a new class of high temperature superconductors (after Bednorz and Müller, [6]).

Figure 1.1: The two most important milestones in superconductivity. Both of them have been awarded with a Nobel Prize.

liquefaction. Until the mid-seventies physicists and material scientists managed to increase T_c up to 23 K (Nb_3Ge) [3, 4, 5] but it seemed that it leveled off at this value. Theorists suspected that there was an intrinsic upper limit for T_c , in the 30 K ballpark.

The report of Bednorz and Müller in 1986 [6] which stated that in an oxide material T_c might be higher than 30 K (Fig. 1.1(b)) arrived as a *deus ex machina*! A few months later Wu and colleagues reported T_c of 93 K in $\text{YBa}_2\text{Cu}_3\text{O}_6$ [7]. After that it seemed that the sky was the limit for T_c and a “gold-rush” started for higher and higher critical temperatures. Besides many non-confirmed room temperature or even higher T_c superconductors the overall accepted highest ambient pressure T_c is at 135 K in HgBaCuO superconductor [8]. The very same compound under 15 GPa of pressure shows the onset of superconductivity at 164 K, the highest T_c known today (see. Fig. 1.2) [9]. The heroes of this new era, Bednorz and Müller received the Nobel Prize in 1989.

The conventional superconductors (those discovered before 1974) and the

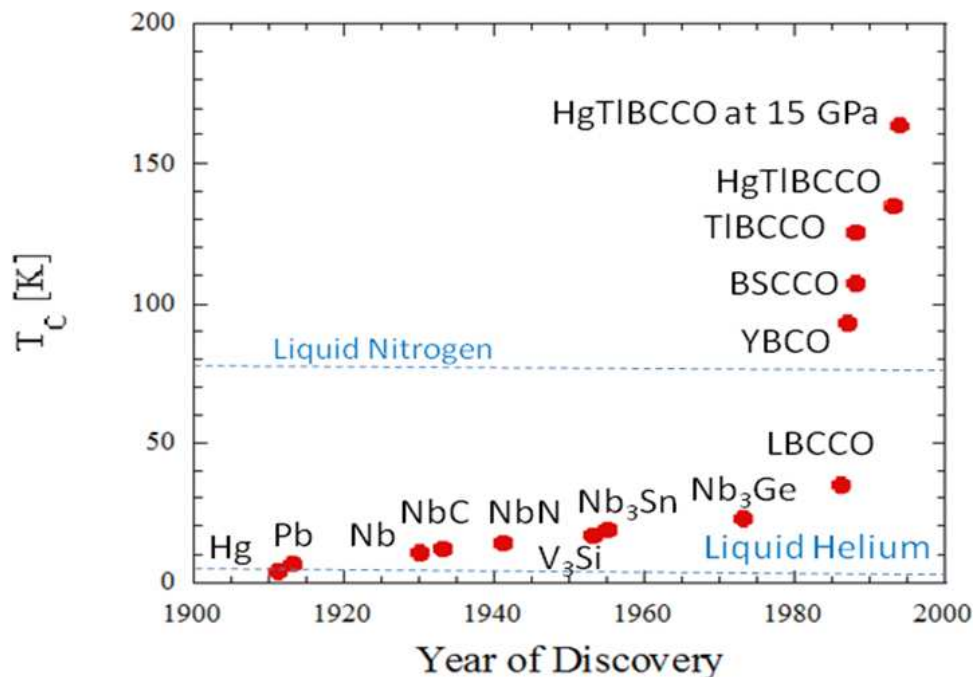


Figure 1.2: The evolution of the superconducting transition temperature (T_c) during the years. The drastic change in slope has happened in 1986 with the discovery of high temperature superconductors.

high- T_c oxide superconductors are only two chapters in superconductivity. There are many others which show that superconductivity is a robust phenomenon in condensed matter.

Figure 1.3 summarizes, with a somewhat personal choice, the most interesting superconducting families discovered in the last 30 years. Organic materials which were considered as the archetypes of the electrical insulator still, the quasi-one-dimensional $(\text{TMTSF})_2\text{PF}_6$ showed superconductivity in 1980 [10]. Since then, by increasing the dimensionality of the organic conductors T_c has gone up to 30 K in Rb_3C_{60} [11, 12]. The latest member of the carbon-based superconductors is the calcium intercalated graphite [13], which was surprising not because of its “high” T_c , but by the fact that it had been missed in the heydays of graphite intercalation in the 60’s and 70’s. It has been a subject of discussion whether the mechanism of superconductivity in the low-dimensional organics is the same as in e.g. lead, described by the BCS theory, where the coupling between

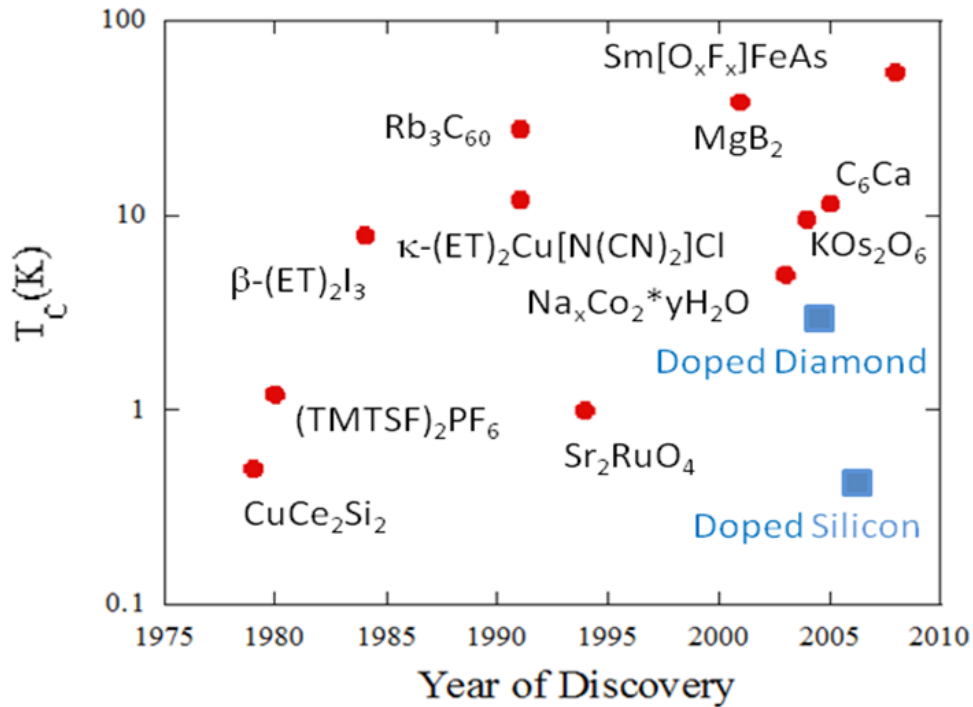


Figure 1.3: Another subset of superconductors discovered in the last 3 decades, excepting the cuprate superconductors. The large number of newly discovered superconductors shows the vivacity of this topic in the condensed matter community.

electrons into pairs (the current carrying units in superconductors) is mediated by lattice vibrations. There is less debate about the unconventional nature of superconductivity in heavy fermion systems (discovered in CuCe_2Si_2 in 1979 by Steglich [14]) and in Sr_2RuO_4 reported by Maeno in 1994 [15]. Probably these materials are in the same class of superconductors as superconducting cobaltates [16] and the high temperature cuprate superconductors where the role of strong Coulomb repulsion and magnetism in the coupling is also suspected. They are the subject of vivid interest among the theorists, trying to describe the microscopic mechanism of superconductivity in these families.

In the case of MgB_2 [17] the excitement had a different origin. Although MgB_2 does have a lower transition temperature (T_c of 39 K, which is still rather high) than some of the oxide-based, high- T_c superconductors, but since MgB_2 appears to be a simple, old-fashioned superconductor, it is much easier to work with and

appears easier to manipulate. There is a very real likelihood that wires of this material will be used to make superconducting electromagnets that will produce the magnetic fields for machines such as magnetic resonance imaging devices found in many hospitals. In addition there is also the hope that MgB_2 will prove to be useful for electronic applications as well. There are several advantages that MgB_2 has over traditional superconductors. First of all, a transition temperature of 40 K means that it will be useful when cooled to temperatures near 20 K. Whereas this is still a very low temperature (about -250 C) it is easily reached by closed cycle refrigeration. This means that superconducting devices made from MgB_2 could be cooled without the need for liquid cryogenes. In addition MgB_2 is lightweight and it has a very low electrical resistivity in the non-superconducting state.

At the moment of writing this dissertation the hype is turned towards the Fe-oxipnictide superconductors, which show T_c as high as 54 K. The major question is related to the role of the magnetic Fe ion in superconductivity. Knowing the speed of scientific progress, it would not be surprising that by the end of this PhD work, all the questions would be answered!

In no lesser extent was the scientific community surprised by the superconductivity of the pillar of the information technologies, silicon, which also shows zero resistance state with suitable doping. This is also true for the boron doped diamond.

The mystery of superconductivity also stems from the fact that many of these superconductors were discovered just by chance. One can have a feeling that finding them is just a question of luck, like finding a jewel in the desert. For example the cobaltate superconductor was discovered by a salesman who wanted to sell a magnetometer and for demonstration he took off the shelf a longly forgotten sample; MgB_2 was known fifty years before it was cooled down below liquid nitrogen temperature, etc. It also gives the false impression that by random mixing of elements one can discover new, high temperature superconductors. However, most of the superconductors are the fruits of tedious, well-thought

research. Just to mention the case of the cuprates, Alex Müller has been working on related compounds for many-many years among the oxides, even when nobody gave a credit for his ideas.

It is widely believed that superconductivity will gain importance in the future when energy will become more and more precious. Not only because using superconductors the transport and energy storage will be more cost effective, but relying on electrical energy will preserve in a greater extent our environment. Using high magnetic fields and quantum interference devices in health care will gain in importance, as well. Research and development in superconductivity are picking up worldwide.

My research program during these four years was to refine a few parameters in the already known superconductors $\text{Ba}_2\text{Sr}_2\text{CaCu}_2\text{O}_{8+\delta}$ and MgB_2 . In the former case the question I wanted to answer is the ground state of an underdoped cuprate superconductor. I have challenged the well accepted concept, that its ground state is an insulator. In the case of MgB_2 I have addressed the issue of defects on T_c and the fulfillment or not of the Matthiessen's rule. By introducing point defects by fast electron irradiation I have performed a systematic study of the resistivity of this compound.

Last but not least, my task was also to discover new superconductors by applying high pressure as a tuning parameter. Two layered conductors were chosen, 1T-TaS₂ and 1T-TiSe₂, which are different from cuprates in the sense that the major interaction is not magnetism but the formation of charge density waves by strong electron-phonon or excitonic interactions. I have managed to find a superconducting phase in both compounds, and to map out the pressure-temperature phase diagram.

Bibliography

- [1] H. K. Onnes. *Commun. Phys. Lab.*, 12:120, 1911.
- [2] J. Bardeen, L. N. Cooper, and J. R. Schrieffer. Microscopic theory of superconductivity. *Physical Review*, 106(1):162–164, 1957.
- [3] J. R. Gavaler. Superconductivity in Nb-Ge films above 22 K. *Applied Physics Letters*, 23(8):480–482, 1973.
- [4] L. R. Newkirk, F. A. Valencia, A. L. Giorgi, E. G. Szklarz, and T. C. Wallace. Bulk superconductivity above 20 k in Nb₃Ge. *Ieee Transactions On Magnetism*, MA11(2):221–224, 1975.
- [5] L. R. Testardi, J. H. Wernick, and W. A. Royer. Superconductivity with onset above 23 K in Nb-Ge sputtered films. *Solid State Communications*, 15(1):1–4, 1974.
- [6] J. G. Bednorz and K. A. Muller. Possible high- T_c superconductivity in the Ba-La-Cu-O system. *Zeitschrift Fur Physik B-Condensed Matter*, 64(2):189–193, 1986.
- [7] M. K. Wu, J. R. Ashburn, C. J. Torng, P. H. Hor, R. L. Meng, L. Gao, Z. J. Huang, Y. Q. Wang, and C. W. Chu. Superconductivity at 93 K in a new mixed-phase Y-Ba-Cu-O compound system at ambient pressure. *Physical Review Letters*, 58(9):908–910, March 1987.

- [8] C. W. Chu, L. Gao, F. Chen, Z. J. Huang, R. L. Meng, and Y. Y. XUE. Superconductivity above 150 K in $\text{HgBa}_2\text{Ca}_2\text{Cu}_3\text{O}_{8+\delta}$ at high-pressures. *Nature*, 365(6444):323–325, September 1993.
- [9] L. Gao, Y. Y. Xue, F. Chen, Q. Xiong, R. L. Meng, D. Ramirez, C. W. Chu, J. H. Eggert, and H. K. Mao. Superconductivity up to 164 K in $\text{HgBa}_2\text{Ca}_{m-1}\text{Cu}_m\text{O}_{2m+2+\delta}$ ($m=1, 2,$ and 3) under quasihydrostatic pressures. *Phys. Rev. B*, 50(6):4260–4263, Aug 1994.
- [10] D. Jerome, A. Mazaud, M. Ribault, and K. Bechgaard. Superconductivity in a synthetic organic conductor $(\text{TMTSF})_2\text{PF}_6$. *Journal De Physique Lettres*, 41(4):L95–L98, 1980.
- [11] Karoly Holczer, Olivier Klein, Shiou Mei Huang, Richard B. Kaner, Ke Jian Fu, Robert L. Whetten, and Francois Diederich. Alkali-fulleride superconductors: synthesis, composition, and diamagnetic shielding. *Science*, 252:1154–1157, 1991.
- [12] M. J. Rosseinsky, A. P. Ramirez, S. H. Glarum, D. W. Murphy, R. C. Haddon, A. F. Hebard, T. T. M. Palstra, A. R. Kortan, S. M. Zahurak, and A. V. Makhija. Superconductivity at 28 K in Rb_xC_{60} . *Phys. Rev. Lett.*, 66(21):2830–2832, May 1991.
- [13] T. E. Weller, M. Ellerby, S. S. Saxena, R. P. Smith, and N. T. Skipper. Superconductivity in the intercalated graphite compounds C_6Yb and C_6Ca . *Nature Physics*, 1(1):39–41, October 2005.
- [14] F. Steglich, J. Aarts, C. D. Breidl, W. Lieke, D. Meschede, W. Franz, and H. Schäfer. Superconductivity in the presence of strong pauli paramagnetism: CeCu_2Si_2 . *Phys. Rev. Lett.*, 43(25):1892–1896, Dec 1979.
- [15] Y. Maeno, H. Hashimoto, K. Yoshida, S. Nishizaki, T. Fujita, J. G. Bednorz, and F. Lichtenberg. Superconductivity in a layered perovskite without copper. *Nature*, 372(6506):532–534, December 1994.

-
- [16] K. Takada, H. Sakurai, E. Takayama-Muromachi, F. Izumi, R. A. Dilanian, and T. Sasaki. Superconductivity in two-dimensional CoO_2 layers. *Nature*, 422(6927):53–55, March 2003.
- [17] Jun Nagamatsu, Norimasa Nakagawa, Takahiro Muranaka, Yuji Zenitani, and Jun Akimitsu. Superconductivity at 39 K in magnesium diboride. *Nature*, 410(6824):63–64, March 2001.

Chapter 2

Electronic properties of two-dimensional conductors

One would naively expect that more dimensions results in deeper physics. However, research in the last 40 years has shown that Nature has chosen differently – as we delve deeper into the physics of low dimensional materials, we find more and more interesting phenomena to explain. Although some of the theories are old, discussion is still running hot on many topics, mainly due to the subtle balance existing between electronic phases, resulting in rich but rather complicated phase diagrams containing a multitude of exotic states. In the following section I will attempt to give a brief introduction to the constantly growing and exciting field of low dimensional physics, focusing on phenomena that are important in understanding experimental results shown in the following chapters.

2.1 Electron-electron correlations

The simplest definition of a correlated electron system is a negative statement: An electronic system is correlated when the electrons within it are not free. In the free electron model description of metals, the valence electrons of the constituent atoms become conduction electrons and move freely through the volume of the

metal. They form a free electron Fermi gas, which is subject to the Pauli principle. [1]

2.2 The Hubbard model

Usually electrons in a solid can be described using two basis set, the Wannier, and the Bloch-basis. Let us choose in this section the Wannier [2] basis $\phi_n(\mathbf{r} - \mathbf{R}_i)$. For these states we can introduce the standard creation $c_{ni\sigma}^\dagger$ and annihilation $c_{ni\sigma}$ operators. They create and destroy the n -th localized Wannier state with spin σ on the atom at the position \mathbf{R}_i . First we only consider the two simplest processes; the Coulomb repulsion between electrons on the same site, and the kinetic (hopping) term, which describes the quantum mechanical amplitude that an electron may hop from site R_i to R_j (or from R_j to R_i).

By using only these two terms in our model, we have already made one approximation. In the standard Hubbard model [3, 4, 5] we assume that each atom has only one electron orbit and the corresponding orbital state is non-degenerate. Of course, actual atoms can have more than one orbital and more than two electrons in the corresponding states. The philosophy behind the Hubbard model is that those electrons in other states do not play significant roles in the low-energy physics of the system, and can be “forgotten” for the moment. Using the two simple terms described above the Hamilton operator of the system can be written as

$$H = \sum_{ij\sigma} t_{i,j} c_{i\sigma}^\dagger c_{j\sigma} + U_H \sum_i n_{i\uparrow} n_{i\downarrow} \quad (2.1)$$

where $n_{i\sigma}$ stands for $c_{i\sigma}^\dagger c_{i\sigma}$ and is the electron number operator. In this form there is no explicit long range interaction present, and the only two-electron term acts between two electrons on the same site. However, there is a hidden long range force in this description, which makes the situation much more complicated; the *Pauli exclusion principle* (PEP). Electrons are fermions, and so the many body

wave function must be antisymmetric under interchange of any two electrons. It is possible to further simplify the formula by expressing it in terms of the dimensionless quantity U/t , which indicates whether the hopping or the Coulomb repulsion force dominates. However, it is still not possible to determine the relative importance of the two in relation to the Pauli exclusion principle, which depends on the probability of finding two electrons on the same site. This quantity is somewhat accounted for by the second crucial parameter involved in the model, the electron density per spin $n = \frac{1}{2N} \sum_{i\sigma} c_{i\sigma}^\dagger c_{j\sigma}$ which controls the total number of electrons in the system. Each atom has space for at most two electrons, so n can be in the range of 0 to 1.

2.2.1 Different ground states

The interpretation of the behavior of the Hubbard model is centered around the competition of the three forces described above, on-site repulsion, hopping, and PEP, controlled by the parameters t and U , and the correlations between electrons that they induce.

Hubbard model in the case of a half filled band

Let's first assume that on each atom we have one electron. In this case we have a perfect half filled band. In the Hubbard model to put an extra electron on that system we have to pay the energy cost of the Coulomb repulsion. If that energy U is big the band will split into two subbands, with a gap in the middle. If n is not perfectly equal to 0.5 the Fermi energy will cross either the upper, or the lower Hubbard band, and in case of the perfect crystal, the material will behave like a metal, however in the case of the half filled band $n = 0.5$ we have an insulator.

So we have one electron on each site. Let's come back to the half-filled band. Half of the electrons has up spin, and half of them down. Due to the overlap between the neighboring sites, the process when one electron jumps to one of

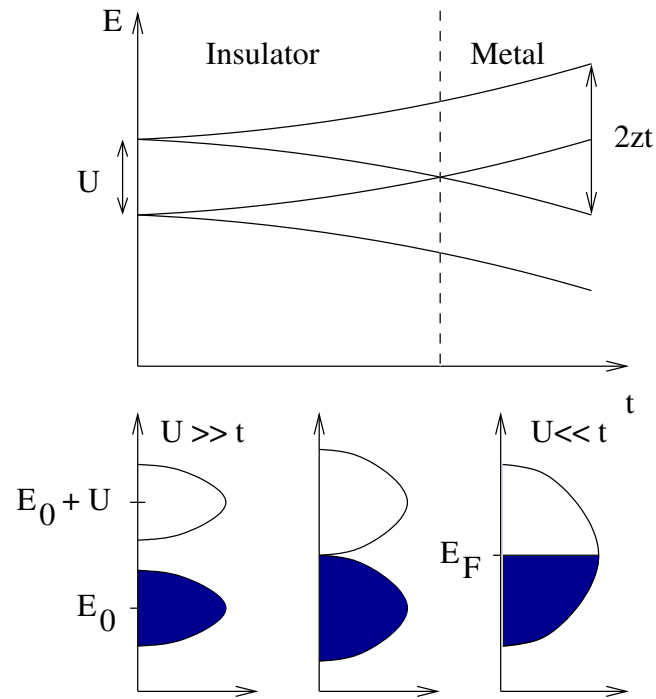


Figure 2.1: The broadening of the bands (upper), and the density of the states in the Hubbard model

its neighbors, and then back has finite probability. That process will cause the broadening of the electron state to a band, and a lowering of the overall energy. This hopping, again owing to the PEP can only take place if the spins of the two electrons are antiparallel. Thus the $U \gg t > 0$ introduces antiferromagnetic correlation between neighbouring sites, and can be accounted for an effective antiferromagnetic coupling between the neighboring spins. In the half filled band we have an antiferromagnetic insulator, the Mott-insulator.

For that reasoning we used the condition that we have two separate Hubbard bands. We have seen, that the hopping broadens the Hubbard band, and the bandwidth is $2zt$, where z is the number of the nearest-neighbor sites. In a square lattice $2zt = 8t$. As we increase t , for example by decreasing the distance between the sites, there will be a point when the two Hubbard subbands will overlap, and the material becomes a metal (Fig. 2.1). This is called the Mott-transition.

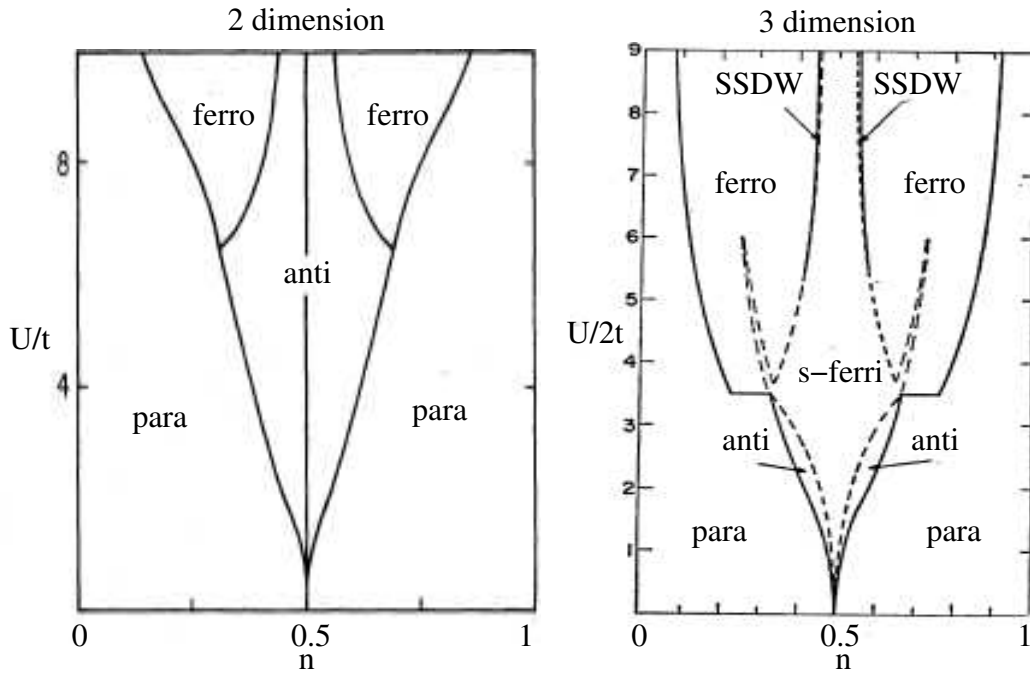


Figure 2.2: Phase diagram of the two and tree dimensional Hubbard-model in a mean field approximation, as a function U/t and n . It shows antiferromagnetic (anti), ferromagnetic (ferro), paramagnetic (para), spiral-ferrimagnetic (s-ferri), and spiral spin density wave (SSDW) states.(Figures from [6] (2D) and [7] (3D))

Ground states of the non half-filled band

In the last section we saw how the systems behaves in the case of half filled band. It is even more interesting, what happens with the Hubbard-model if we can control the number of carriers, either by adding extra electrons in the upper Hubbard band, or by creating holes in the lower. In the mean field theory calculation in two and three dimension shows the appearance of several new phases. (Fig. 2.2) The mean field approximation seems to give back many of the features of the tree dimensional metal. But in lower dimension, there are many fine details and complications, like Van Hove singularities, nesting Fermi surfaces, what might give rise to new phases. One of the most spectacular of them is the non-conventional superconductivity with $d_{x^2-y^2}$ symmetry, as in the case of High- T_c superconductors. Several calculation shows that despite the fact that in

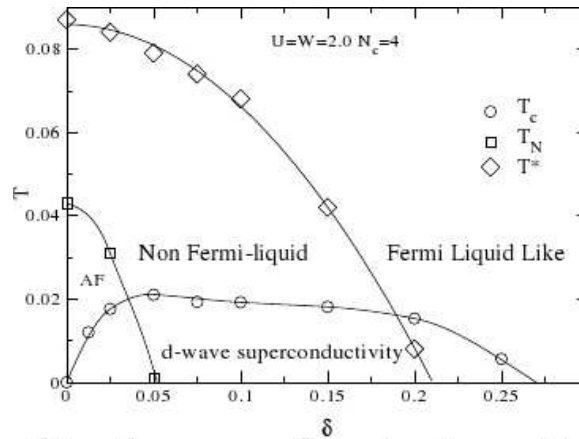


Figure 2.3: The phase diagram as a function of hole concentration δ , on finite temperature, coming from numerical calculation of the two dimensional Hubbard model. (Figure from [8])

the Hubbard model, there is no explicit attractive interaction, the energetically favorable ground state might be the condensate of Cooper-pairs [8], which can be even further stabilized by adding new terms to the Hamiltonian. One of the most common extensions is to add the possibility of hopping to further sites. In the simplest case that means the second-nearest-neighbor interaction t' . The importance of t' can be better seen if we look on the theory proposed first by P.W. Anderson [9]. As we start to remove electrons from the Mott insulator (Fig. 2.4(a)), we create holes, and they can freely jump, and behave as free carriers (Fig. 2.4(b)). But we still have the rest of the electrons, in an antiferromagnetic state. It is somewhat natural to form singlets from the neighboring atoms, and make a condensate of it (Fig. 2.4(c)). As we allow the next-nearest-neighbor hopping, the possibilities to create resonating singlets is even more (Fig. 2.4(d)). The ground state will be the superposition of all those singlet configurations, without those where we have doubly occupied states.

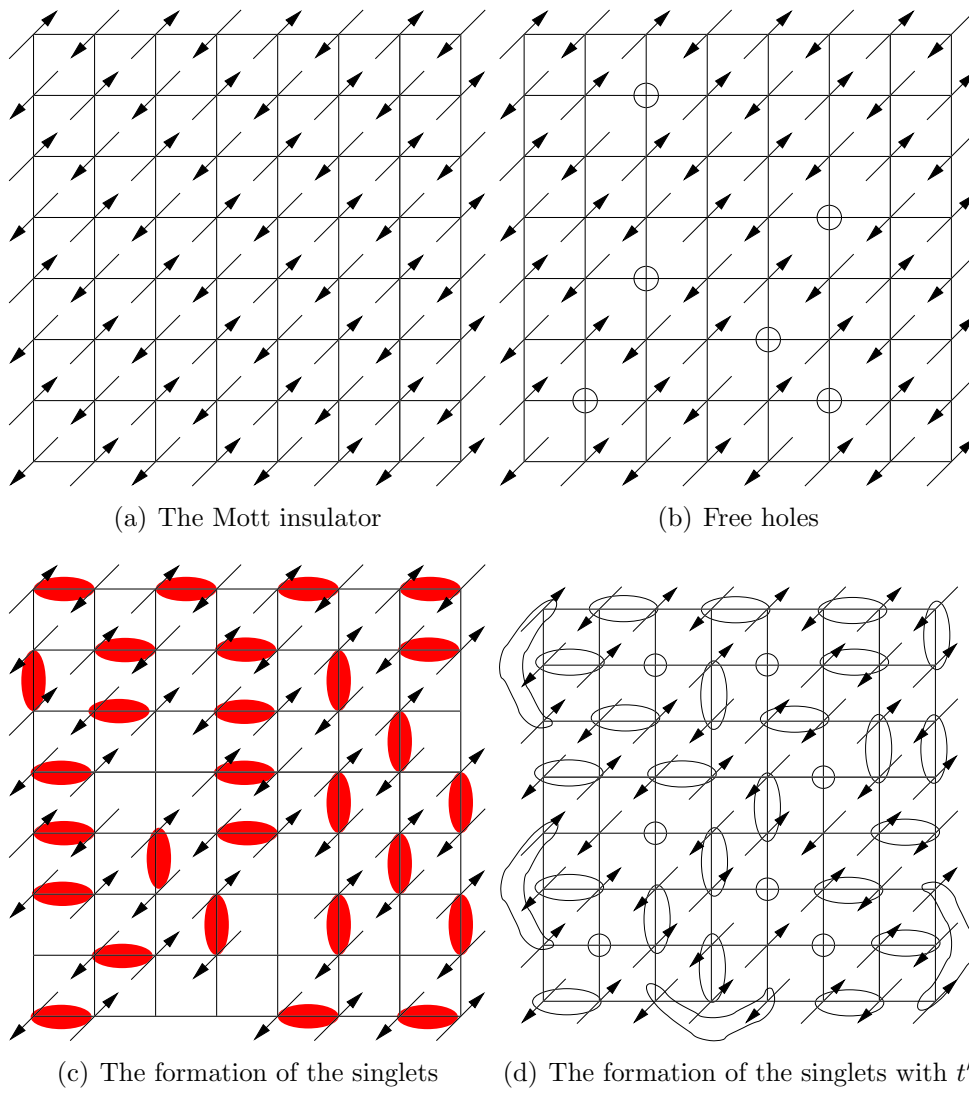


Figure 2.4: The cartoon of the Anderson model.

2.3 Electron–phonon interaction

In the last section we were only focusing on the electrons, neglecting any interaction between them except the bare Coulomb-repulsion. In this part I will introduce some part of the physics involving the elemental excitation of the vibration of the ions forming the lattice.

The Hamiltonian of an electron-phonon system can usually be written in the form

$$H = H_{el} + H_{ph} + H_{el-ph} \quad (2.2)$$

where the terms can be expressed in the second quantised formalism,

$$\begin{aligned} H_{el} &= \sum_{\mathbf{k}} \epsilon_{\mathbf{k}} c_{\mathbf{k}}^{\dagger} c_{\mathbf{k}} \\ H_{ph} &= \sum_{\mathbf{q}} \omega_{\mathbf{q}} a_{\mathbf{q}}^{\dagger} a_{\mathbf{q}} \\ H_{el-ph} &= \frac{1}{\sqrt{N}} \sum_{\mathbf{q}, \mathbf{k}} g(\mathbf{q}, \mathbf{k}) \left(a_{-\mathbf{q}}^{\dagger} + a_{\mathbf{q}} \right) c_{\mathbf{k}+\mathbf{q}}^{\dagger} c_{\mathbf{k}} \end{aligned} \quad (2.3)$$

for simplicity the spin and polarization indexes have been neglected. $c_{\mathbf{k}}^{\dagger}(c_{\mathbf{k}})$ and $a_{\mathbf{q}}^{\dagger}(a_{\mathbf{q}})$ are electron and phonon creation (annihilation) operators respectively, $\epsilon_{\mathbf{k}}$ is the bare electron energy, $\omega_{\mathbf{q}}$ is the phonon energy and $g(\mathbf{q}, \mathbf{k})$ is the e^{-} -ph interaction describing the scattering of electrons by phonons.

The above Hamiltonian can be understood as follows: In a lattice where the atoms are oscillating around their equilibrium position, the free electron Bloch-states are no longer eigenstates of the system. Due to charge-conservation, the number of electrons is constant, but the number of phonons can change. Thus, the electrons can interact with an oscillation of the lattice by creating, or annihilating a phonon. It is important to notice that the total momentum of the crystal is no longer conserved in this description. To fix this problem we describe the vibration

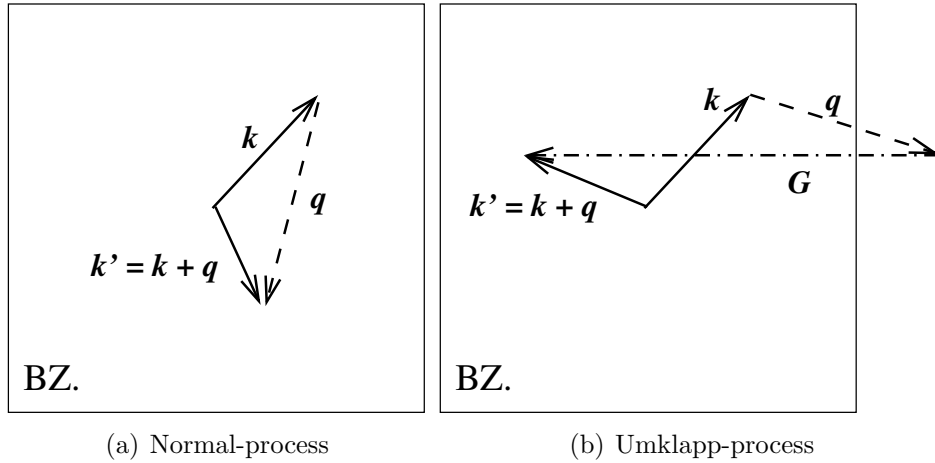


Figure 2.5: The two types of the electron phonon interactions

of the crystal using phonons, and we use the reciprocal vectors of the lattice as a parameter for the phonons and the electrons as well.

Now we can consider the joint set of the phonons and the electrons, and observe that the total momentum is now conserved. Since the crystal momentum is only defined modulo any vector \mathbf{G} in reciprocal space, we can define two types of processes. A normal process is when the electron momentum after the creation or annihilation of a phonon remains in the Brillouin zone. In a so-called Umklapp process, however, the final electron state has to be shifted by a reciprocal vector \mathbf{G} from an equivalent state in the first BZ.

2.3.1 Peierls instability, charge density waves

Due to the interaction described in the last section the energy of the electrons and phonons are renormalized. The lowering in energy of a phonon mode, or phonon softening, at a given \mathbf{q} can be strong enough such that the expectation value of the phonon number operator $\langle a_{\mathbf{q}}^\dagger a_{\mathbf{q}} \rangle$ is nonzero. From that point, the numbers of phonons with momentum \mathbf{q} is finite, resulting in a condensation, which means a deformation of the lattice. The order parameter of the resulting phase can be

defined as

$$\Delta = \frac{1}{\sqrt{L}}g \left[\langle a_{\mathbf{q}} \rangle + \langle a_{-\mathbf{q}}^\dagger \rangle \right] \quad (2.4)$$

where g is the electron-phonon coupling constant, and L is the characteristic length of the system.

The real space representation of this condensation is a modulation of the crystal structure. The changes of atomic position can then be written in the form

$$\langle \delta \mathbf{R}_n \rangle \sim \frac{2|\Delta|}{g} \cos(\mathbf{q}\mathbf{R}_n + \phi) \quad (2.5)$$

But why would such a distortion be energetically favorable? There are two competing energies involved in the CDW phase transition: on one hand the loss of lattice energy associated with the distortion and on the other the gain of electronic energy from the lowering of E near $\frac{\pi}{2a}$

As a result of the distortion, a gap will open at the boundary of the BZ. If the new periodicity is chosen such that the gap opens at the Fermi energy, the system achieves the maximal energy reduction. In order to observe the appearance of the gap and calculate the energy reduction we will use the Fröhlich-Hamiltonian (2.3). Since we are in the condensed state, the phonon operators can be replaced by their average. We have seen as well that the periodicity of the new order will be the Fermi wavelength, and therefore we will use $\mathbf{q} = \mathbf{k}_F$.

$$\mathcal{H} = \sum_{\mathbf{k}} \epsilon_{\mathbf{k}} c_{\mathbf{k}}^\dagger c_{\mathbf{k}} + \sum_{\mathbf{k}} \left[\Delta^* c_{\mathbf{k}-2\mathbf{k}_F}^\dagger c_{\mathbf{k}} + \Delta c_{\mathbf{k}}^\dagger c_{\mathbf{k}+2\mathbf{k}_F} \right] \quad (2.6)$$

It is useful to measure the energy from the Fermi-level. Using this convention we can distinguish the c^\dagger and d^\dagger operators, which measure the energy at the \mathbf{k}_F and $-\mathbf{k}_F$ points respectively. Using these operators the previous Hamiltonian 2.2

becomes,

$$\mathcal{H} = \sum_{\mathbf{k}} \left[\epsilon_{\mathbf{k}_F+\mathbf{k}} c_{\mathbf{k}_F+\mathbf{k}}^\dagger c_{\mathbf{k}_F+\mathbf{k}} + \epsilon_{-\mathbf{k}_F+\mathbf{k}} d_{-\mathbf{k}_F+\mathbf{k}}^\dagger d_{-\mathbf{k}_F+\mathbf{k}} \right] \quad (2.7)$$

$$+ \sum_{\mathbf{k}} \left[\Delta^* d_{-\mathbf{k}_F+\mathbf{k}}^\dagger c_{\mathbf{k}_F+\mathbf{k}} + \Delta c_{\mathbf{k}_F+\mathbf{k}}^\dagger d_{-\mathbf{k}_F+\mathbf{k}} \right] \quad (2.8)$$

in matrix form;

$$\mathcal{H} = \sum_{\mathbf{k}} = \begin{pmatrix} c_{\mathbf{k}_F+\mathbf{k}}^\dagger & d_{-\mathbf{k}_F+\mathbf{k}}^\dagger \end{pmatrix} \begin{pmatrix} \epsilon_{\mathbf{k}_F+\mathbf{k}} & \Delta \\ \Delta^* & \epsilon_{-\mathbf{k}_F+\mathbf{k}} \end{pmatrix} \begin{pmatrix} c_{\mathbf{k}_F+\mathbf{k}} \\ d_{-\mathbf{k}_F+\mathbf{k}} \end{pmatrix} \quad (2.9)$$

The beauty of this definition is that it is already in a bi-linear form, and therefore can be diagonalized with a well chosen unitary transformation. To achieve this we choose two new fermionic operator pairs in place of c and d .

$$\begin{pmatrix} \alpha_{\mathbf{k}} \\ \beta_{\mathbf{k}} \end{pmatrix} = \begin{pmatrix} u_{\mathbf{k}} & v_{\mathbf{k}} \\ -v_{\mathbf{k}}^* & u_{\mathbf{k}}^* \end{pmatrix} \begin{pmatrix} c_{\mathbf{k}_F+\mathbf{k}} \\ d_{-\mathbf{k}_F+\mathbf{k}} \end{pmatrix} \quad (2.10)$$

and

$$\begin{pmatrix} \alpha_{\mathbf{k}}^\dagger & \beta_{\mathbf{k}}^\dagger \end{pmatrix} = \begin{pmatrix} c_{\mathbf{k}_F+\mathbf{k}}^\dagger & d_{-\mathbf{k}_F+\mathbf{k}}^\dagger \end{pmatrix} \begin{pmatrix} u_{\mathbf{k}}^* & -v_{\mathbf{k}} \\ v_{\mathbf{k}}^* & u_{\mathbf{k}}^* \end{pmatrix}. \quad (2.11)$$

To satisfy the unitarity,

$$|u_{\mathbf{k}}|^2 + |v_{\mathbf{k}}|^2 = 1 \quad (2.12)$$

the correct u and v must be found to diagonalize the Hamiltonian.

$$\mathcal{H} = \sum_{\mathbf{k}} = E_{\mathbf{k}}^{(\alpha)} \alpha_{\mathbf{k}}^\dagger \alpha_{\mathbf{k}} + E_{\mathbf{k}}^{(\beta)} \beta_{\mathbf{k}}^\dagger \beta_{\mathbf{k}} \quad (2.13)$$

After a short calculation we can arrive at following forms for u and v :

$$u_{\mathbf{k}}^2 = \frac{1}{2} \left[1 + \frac{\xi_{\mathbf{k}}}{\sqrt{\xi_{\mathbf{k}}^2 + |\Delta|^2}} \right], \quad v_{\mathbf{k}}^2 = \frac{1}{2} \left[1 - \frac{\xi_{\mathbf{k}}}{\sqrt{\xi_{\mathbf{k}}^2 + |\Delta|^2}} \right] \quad (2.14)$$

where

$$\xi_{\mathbf{k}} = \frac{\epsilon_{\mathbf{k}_F+k} - \epsilon_{-\mathbf{k}_F+k}}{2}. \quad (2.15)$$

According to the equations above,

$$E_{\mathbf{k}}^{(\alpha)} = \epsilon_{\mathbf{k}_F+k} |u_{\mathbf{k}}^2|^2 + \epsilon_{-\mathbf{k}_F+k} |v_{\mathbf{k}}^2|^2 + (\Delta + \Delta^*) u_{\mathbf{k}} v_{\mathbf{k}}, \quad (2.16)$$

$$E_{\mathbf{k}}^{(\beta)} = \epsilon_{\mathbf{k}_F+k} |u_{\mathbf{k}}^2|^2 + \epsilon_{-\mathbf{k}_F+k} |v_{\mathbf{k}}^2|^2 - (\Delta + \Delta^*) u_{\mathbf{k}} v_{\mathbf{k}} \quad (2.17)$$

These are the dispersion relations of the new quasi particles. By the (2.14) definitions of u and v , and the approximation that bare electron energy near the Fermi surface can be assumed linear,

$$\epsilon_{\mathbf{k}_F+\mathbf{k}} = \mu + \xi_{\mathbf{k}} = \mu + \hbar v_F |\mathbf{k}| \quad (2.18)$$

$$\epsilon_{-\mathbf{k}_F+\mathbf{k}} = \mu + \xi_{\mathbf{k}} = \mu - \hbar v_F |\mathbf{k}| \quad (2.19)$$

, we find for the dispersion relation of the new quasiparticles,

$$E_{\mathbf{k}}^{(\alpha)} = \mu + \sqrt{(\hbar v_F |\mathbf{k}|) + |\Delta|^2} \quad (2.20)$$

$$E_{\mathbf{k}}^{(\beta)} = \mu - \sqrt{(\hbar v_F |\mathbf{k}|) + |\Delta|^2} \quad (2.21)$$

$$(2.22)$$

In Fig. 2.6, these two dispersions can be seen in addition to the opening of a gap with a magnitude of 2Δ . Since the gap opens at the top of the Fermi-level, the one dimensional system becomes an insulator. This is referred to as the Peierls instability [10].

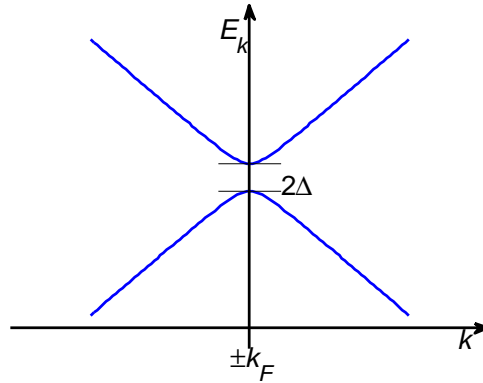


Figure 2.6: The one particle excitation spectrum of the spin density wave state.

Now we have seen that reducing the size of the Brillouin-zone lowers the overall energy of the electronic system by reducing the energy of electrons at the Fermi-surface, a process which involves modulation of the positions of the atoms in the crystal.

We have to emphasize that the formalism we derived is only strictly valid in one dimension. In two dimensions the energy balance between the introduced crystal stress and the lowering in of the electron energy is more subtle. To see that we have to use the electron susceptibility $\chi(\mathbf{q})$. It tells us how an electron system, described by the electronic density $\rho(\mathbf{q})$ behaves under the influence of an external potential $V(\mathbf{q})$.

$$\rho(\mathbf{q}) = -\chi(\mathbf{q})V(\mathbf{q}) \quad (2.23)$$

The susceptibility can be written in the form first derived by Lindhard in 1954 [11]. In the static limit

$$\chi(\mathbf{q}) = \sum_{\mathbf{k}} \frac{f_{\mathbf{k}+\mathbf{q}} - f_{\mathbf{k}}}{E_{\mathbf{k}+\mathbf{q}} - E_{\mathbf{k}}}, \quad (2.24)$$

where $f_{\mathbf{k}}$ and $E_{\mathbf{k}}$ stands for the Fermi-Dirac function and the energy eigenvalues at the given \mathbf{k} vector, respectively.

That can be explicitly calculated in the one dimensional case if we take a

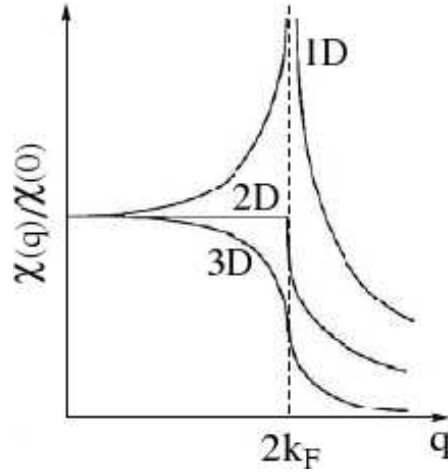


Figure 2.7: The Lindhard function in one two and three dimension

linear dispersion relation near E_F .

$$\chi(\mathbf{q})_{1D} = -e^2 n(\epsilon_F) \ln \left| \frac{\mathbf{q} + 2\mathbf{k}_F}{\mathbf{q} - 2\mathbf{k}_F} \right| \quad (2.25)$$

$n(\epsilon_F)$ is the density of states at the Fermi energy, and e is the elemental charge. This function has a logarithmic singularity at $2\mathbf{k}_F$, what means that the electron system is unstable against any perturbation with a characteristic wavelength $\lambda = \pi/\mathbf{k}_F$.

The singularity of the susceptibility can be understood if we take a closer look on the original Lindhard form 2.24. In the denominator we have the difference of the electron energy in two points of the Brillouin zone, separated by the \mathbf{q} vector. If we take the simplest isotropic case in three dimension, the Fermi surface is a sphere. After shifting it with the \mathbf{q} vector, the intersection of is a ring. The total volume of that ring compared to the surface of the sphere is small. In two dimension where the intersections are two point the result is still finite. But in one dimension the Fermi surface consist of two points, which can be overlapped by a single translation. That produces singularity, and we get the 2.25 form of the susceptibility. Those three cases are plotted in Figure 2.7.

In 3D materials the susceptibility can be enhanced if two parts of the Fermi

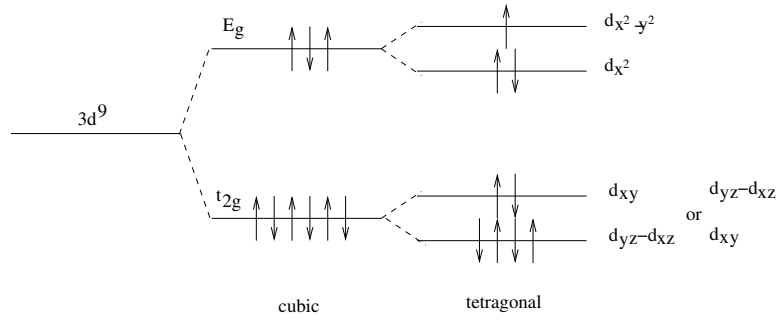


Figure 2.8: The band splitting of the Cu^{2+} $S = 1/2$, $L = 2$ band in a cubic environment (without Jahn–Teller distortion), and in a tetragonal environment (with Jahn–Teller distortion)

surface are parallel. Those are called the nesting Fermi surfaces. That is still favors the one dimension, because in case of the Fermi “line”, very big portion of it can be mapped to each other. In two dimension it is more difficult to imagine a geometry where important parts of the Fermi surface are parallel. Therefore is it questioned if the nesting can be driving force of the charge density wave formation in two dimensional materials [12].

2.3.2 Jahn–Teller distortion

In the previous subsection it was shown that in low dimensional systems where the electrons are confined by strong electron-lattice coupling, distortion of the crystal can be energetically favourable.

It is however also possible to imagine a situation where the lowering of the energy of the “core” electrons yields the displacement of the atoms. This is called the Jahn–Teller effect [13].

Picture a crystal where Cu^{2+} (d^9) ions are coordinated in an octahedral environment (i.e. a cubic crystal field). The local crystal field splits the 5-fold degenerate $L = 2$ levels split into two groups: The threefold degenerate t_{2g} level consists of the d_{xy} , d_{yz} and d_{zx} orbitals, and are filled with 6 electrons. The upper e_g states consist of the d_{x^2} and $d_{x^2-y^2}$ orbitals and are occupied by the three remaining electrons.

If we now for example distort all the octahedra along the z-axis, the symmetry of the crystal is reduced to tetragonal and a further splitting is induced in the scheme discussed above. This splitting may be easily calculated if the distortion is sufficiently small so that it can be treated as a perturbation. The t_{2g} level is now split into a low lying doubly degenerate level containing four electrons (d_{xz} , d_{yz}), and a higher energy state (d_{yz}) with two electrons. The total energy of the three states, however, remains unaffected. On the other hand, the upper e_g level is split into a lower d_{x^2} level containing two electrons and a higher $d_{x^2-y^2}$ with the final electron occupying it, resulting in a lowering of energy. While this energy gain is proportional to the size of the distortion, it is balanced against the stress induced in the structure, which generally scales as the square of the distortion parameter. Thus, the Jahn–Teller occurs mainly for small displacements.

2.4 Superconductivity

The third phenomena that might be the last in that chapter, but the most important, is superconductivity. Superconductivity has been long considered the most extraordinary and mysterious property of metals. The basic and still most comprehensive theory was developed by Bardeen, Cooper, and Schrieffer in 1957 [14]. They showed that in case of an existing attractive interaction between the electrons, the bound two electron states are energetically favorable. They can be looked as an effective boson, what can condensate without breaking the Pauli exclusion principle.

They have discovered as well, that the mediating attractive potential is created by the exchange of phonons. The fact that so far no other mediating force has been confirmed (although there were several proposed), shows the geniality of that discovery.

The Hamilton operator of the BCS theory, is the most intuitive in a second quantized formalism. Here for the simplicity we will only consider the case where the two electrons have opposite momentum. It can be shown, that Cooper-pairs

having zero total momentum, have the lowest energy, therefore that simplification is valid.

$$\mathcal{H}_{BCS} = \sum_{\mathbf{k},\sigma} \epsilon_{\mathbf{k}} c_{\mathbf{k},\sigma}^{\dagger} c_{\mathbf{k},\sigma} + \frac{1}{2} \sum_{\mathbf{k},\mathbf{k}',\sigma,\sigma'} V_{\mathbf{k},\mathbf{k}'} c_{\mathbf{k}',\sigma}^{\dagger} c_{-\mathbf{k}',\sigma'}^{\dagger} c_{-\mathbf{k},\sigma'} c_{\mathbf{k},\sigma}. \quad (2.26)$$

The first part is the usual kinetic energy term. And the second term describes the scattering of a bound electron pair with opposite momentum. If we restrict the pairs to the spin singlet state, as it is in the nature, we can further simplify the form:

$$\mathcal{H}_{BCS} = \sum_{\mathbf{k}} \epsilon_{\mathbf{k}} \left(c_{\mathbf{k},\uparrow}^{\dagger} c_{\mathbf{k},\uparrow} + c_{\mathbf{k},\downarrow}^{\dagger} c_{\mathbf{k},\downarrow} \right) + \sum_{\mathbf{k},\mathbf{k}'} V_{\mathbf{k},\mathbf{k}'} c_{\mathbf{k}',\uparrow}^{\dagger} c_{-\mathbf{k}',\downarrow}^{\dagger} c_{-\mathbf{k},\downarrow} c_{\mathbf{k},\uparrow}. \quad (2.27)$$

. From that point we can follow almost step by step the development, what we used for the charge density waves. First we define an order parameter, with the operator what have a non-vanishing average. In the case of the superconductivity, those are the Cooper-pairs. Therefore the order parameter has the form of:

$$\Delta_{\mathbf{k}} = - \sum_{\mathbf{k}'} V_{\mathbf{k},\mathbf{k}'} \langle c_{-\mathbf{k}',\downarrow} c_{\mathbf{k}',\uparrow} \rangle, \quad \Delta_{\mathbf{k}}^* = - \sum_{\mathbf{k}'} V_{\mathbf{k},\mathbf{k}'} \langle c_{\mathbf{k}',\uparrow}^{\dagger} c_{-\mathbf{k}',\downarrow}^{\dagger} \rangle \quad (2.28)$$

Since in the case of superconductivity we are not restricted in one dimension, the momentum dependence of the potential and therefore the order parameter has to be explicitly written. Now if we use the general mean field approach, we can write the 2.26 in the following form:

$$\mathcal{H}_{BCS} = \sum_{\mathbf{k}} \epsilon_{\mathbf{k}} \left(c_{\mathbf{k},\uparrow}^{\dagger} c_{\mathbf{k},\uparrow} + c_{\mathbf{k},\downarrow}^{\dagger} c_{\mathbf{k},\downarrow} \right) + \sum_{\mathbf{k},\mathbf{k}'} V_{\mathbf{k},\mathbf{k}'} c_{\mathbf{k}',\uparrow}^{\dagger} c_{-\mathbf{k}',\downarrow}^{\dagger} \langle c_{-\mathbf{k},\downarrow} c_{\mathbf{k},\uparrow} \rangle \quad (2.29)$$

$$+ \sum_{\mathbf{k},\mathbf{k}'} V_{\mathbf{k},\mathbf{k}'} \langle c_{\mathbf{k}',\uparrow}^{\dagger} c_{-\mathbf{k}',\downarrow}^{\dagger} \rangle c_{-\mathbf{k},\downarrow} c_{\mathbf{k},\uparrow} + \sum_{\mathbf{k},\mathbf{k}'} V_{\mathbf{k},\mathbf{k}'} \langle c_{\mathbf{k}',\uparrow}^{\dagger} c_{-\mathbf{k}',\downarrow}^{\dagger} \rangle \langle c_{-\mathbf{k},\downarrow} c_{\mathbf{k},\uparrow} \rangle. \quad (2.30)$$

It is often convenient not to fix the total number of electrons, by introducing the

chemical potential μ . Therefore from now we use $\xi_k = \epsilon_k - \mu$. By writing $\Delta_{\mathbf{k}}$ into 2.29 we get the following equation:

$$\mathcal{H}_{BCS} = \sum_{\mathbf{k}} \xi_{\mathbf{k}} \left(c_{\mathbf{k},\uparrow}^\dagger c_{\mathbf{k},\uparrow} + c_{\mathbf{k},\downarrow}^\dagger c_{\mathbf{k},\downarrow} \right) \quad (2.31)$$

$$- \sum_{\mathbf{k}} \left(\Delta_{\mathbf{k}} c_{\mathbf{k},\uparrow}^\dagger c_{-\mathbf{k},\downarrow}^\dagger + \Delta_{\mathbf{k}}^* c_{-\mathbf{k},\downarrow} c_{\mathbf{k},\uparrow} \right) + \sum_{\mathbf{k},\mathbf{k}'} V_{\mathbf{k},\mathbf{k}'} \left\langle c_{\mathbf{k}',\uparrow}^\dagger c_{-\mathbf{k}',\downarrow}^\dagger \right\rangle \left\langle c_{-\mathbf{k},\downarrow} c_{\mathbf{k},\uparrow} \right\rangle. \quad (2.32)$$

That equation has the same form as 2.6, except an extra constant term. Therefore we can use the same method to diagonalize the Hamiltonian. The only thing we have to be aware of is the \mathbf{k} dependence of Δ .

It isn't surprising that we can use the same formalism for both phenomena. The two can be brought even further, if in case of the charge density waves, we forget about the explicit form of the phonon operators, and use them only as an effective potential. The operator that will have a non vanishing average in that case will be the $c_{\mathbf{k}+\mathbf{q}}^\dagger c_{\mathbf{k}}$. The average of that operator will represent the modulation of the charge density with a period of \mathbf{q} . The first mentioning of superconductivity together with the charge density waves was done by Frölich, who suggested that the sliding movement of a long range ordered CDW would happen without resistivity. Although his derivation was correct, any small perturbation of the potential (impurity, finite phonon lifetime, or the commensurability of the wave with the underlying lattice) would pin the density wave, and prevent the zero resistivity conductance.

Recently Gabovic *et. al* showed, using a Green-function approach, that the two symmetry breaking phases are closely related [15, 16].

Therefore it is natural to expect that superconductivity and charge density wave can compete or even coexist in some materials, depending on the fine details of the electronic structure.

Bibliography

- [1] W. Pauli. Über den Zusammenhang des Abschlusses der Elektronengruppen im Atom mit der Komplexstruktur der Spektren. *Zeitschrift für Physik*, 31:765–783, 1925.
- [2] Gregory H. Wannier. The structure of electronic excitation levels in insulating crystals. *Phys. Rev.*, 52(3):191–197, Aug 1937.
- [3] Martin C. Gutzwiller. Correlation of electrons in a narrow s band. *Phys. Rev.*, 137(6A):A1726–A1735, Mar 1965.
- [4] J. Hubbard. Electron correlations in narrow energy bands. *Proceedings Of The Royal Society Of London Series A-Mathematical And Physical Sciences*, 276(DEC):238–&, 1963.
- [5] J. Kanamori. Electron correlation and ferromagnetism of transition metals. *Progress Of Theoretical Physics*, 30(3):275–289, 1963.
- [6] J. E. Hirsch. Two-dimensional hubbard model: Numerical simulation study. *Phys. Rev. B*, 31(7):4403–4419, Apr 1985.
- [7] David R. Penn. Stability theory of the magnetic phases for a simple model of the transition metals. *Phys. Rev.*, 142(2):350–365, Feb 1966.
- [8] M. Jarrell, Th Maier, M. H. Hettler, and A. N. Tahvildarzadeh. Phase diagram of the hubbard model: Beyond the dynamical mean field, 2000.

- [9] P. W. Anderson. The resonating valence bond state in La_2CuO_4 and superconductivity. *Science*, 235(4793):1196–1198, March 1987.
- [10] R. Peierls. Zur Theorie der elektrischen und thermischen Leitfähigkeit von Metallen. *Annalen der Physik*, 396(2):121–148, 1930.
- [11] J. Lindhard. On the properties of a gas of charged particles. *Matematisk-Fysiske Meddelelser Kongelige Danske Videnskabernes Selskab*, 28(8):1–57, 1954.
- [12] M. D. Johannes and I. I. Mazin. Fermi surface nesting and the origin of charge density waves in metals. *Phys. Rev. B*, 77(16):165135–8, April 2008.
- [13] HA Jahn and E. Teller. Stability of polyatomic molecules in degenerate electronic states. I. orbital degeneracy. *Proceedings of the Royal Society of London. Series A, Mathematical and Physical Sciences*, 161(905):220–235, 1937.
- [14] J. Bardeen, L. N. Cooper, and J. R. Schrieffer. Microscopic theory of superconductivity. *Physical Review*, 106(1):162–164, 1957.
- [15] A. M. Gabovich, A. I. Voitenko, J. F. Annett, and M Ausloos. Charge- and spin-density wave superconductors. *Sup. Sci. and Tech.*, 14(4):R1, 2001.
- [16] A. M. Gabovich, A. I. Voitenko, and M. Ausloos. Charge- and spin-density waves in existing superconductors: competition between Cooper pairing and peierls or excitonic instabilities. *Phys. Rep.*, 367(6):583, September 2002.

Chapter 3

Transition metal dichalcogenides

3.1 Introduction to the transition metal dichalcogenides

3.1.1 Crystal structure and polytypes

Layered transition metal dichalcogenides have attracted a widespread interest because of their unique electronic properties. Originally they were discovered as the prototypical 2D CDW compounds, however later on the discovery of superconductivity at low temperature made them subject to an intense study. Their general formula is TX_2 , where T stands for the transition metal (usually Nb, Ti or Ta) and X for the chalcogenide (S, Se or Te). They are layered materials where the transition metal layer is sandwiched between two chalcogenide layers. The bond between the T and X atoms in a sandwich is a strong (largely covalent) one, and these atoms form a two-dimensional hexagonal lattice. The TX_2 layers are coupled in the crystal by weak van der Waals forces. The structure of the crystals is schematically shown in Fig. 3.1. The weak van der Waals interaction between the layers admits various ways for the relative position of for the TX_2 sandwiches in a crystal along the axis perpendicular to the layers (the c axis). Therefore these layered compounds exist in several modifications. The two most

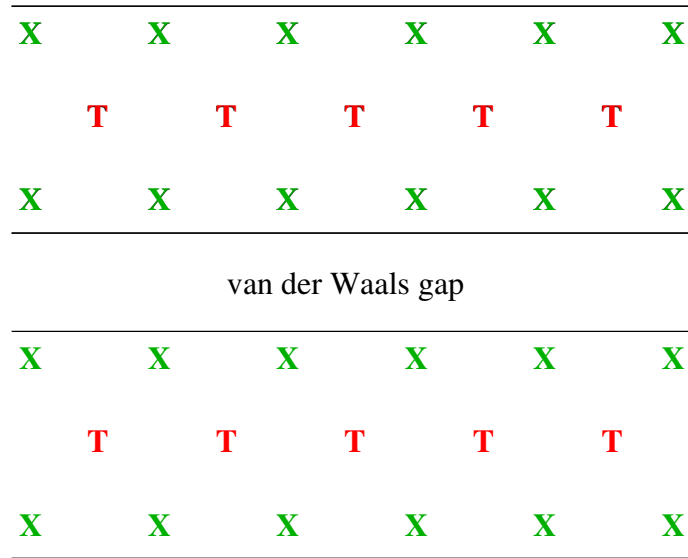


Figure 3.1: Schematic structure of the layered structure

common types of layer packing are shown in Fig. 3.2.

Depending on the relative placement of the layers TMDs can have different polytypes referred as 1T, 2H, 3R, 4H_a, 4H_b. The starting number in this notation denotes the number of X-T-X sandwiches perpendicular to the plain in the unit cell, the T, H, R distinguish the trigonal, hexagonal or rhombohedral symmetry of the structure. Sometimes additional lower case superscript is required to distinguish the otherwise similarly labeled polytypes.

The inter-layer interaction is weak in these materials, therefore the physical properties are largely determined by the two-dimensional structure of the lattice inside the sandwich. But there is an other factor what influences the electronic structure, and therefore many properties of the crystals, the symmetry of the atoms in the layers. Good example is the three modifications of TaS₂ what exhibits a strong dependence of the electronic properties on the type of the structure. The 1T-TaS₂, what is one subject of our study as well, has trigonal packing. It shows clearly non-metallic behavior at room temperature, with a slowly and almost linearly increasing resistivity with decreasing temperature. The 2H polytype with octahedral packing, what has the second biggest unit cell, behaves as

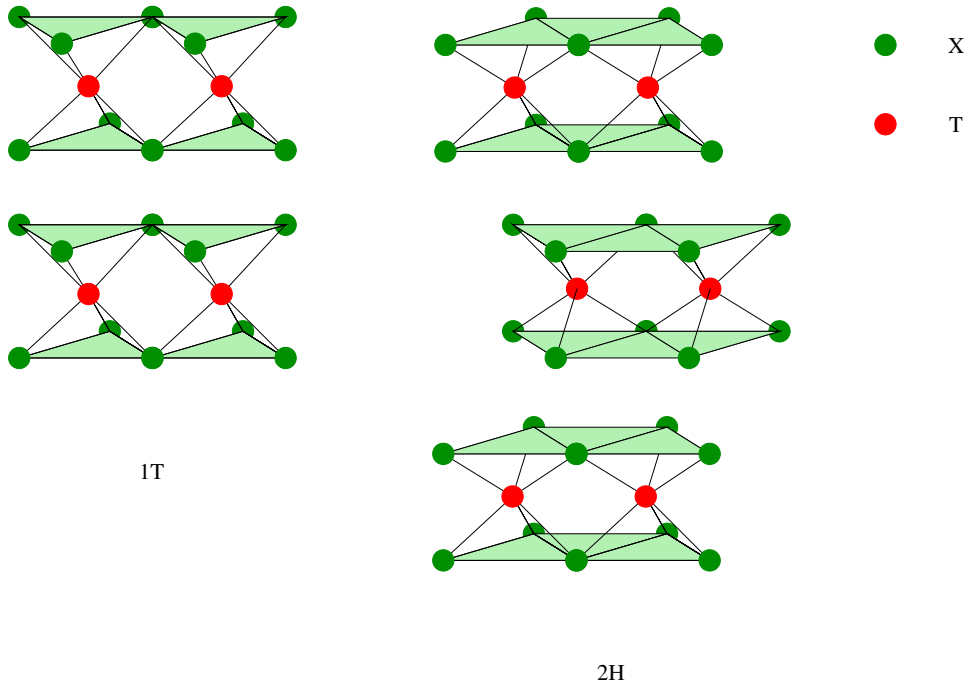


Figure 3.2: The different intra-sandwich coordination of the atoms in the two simplest 1T and 2H polytypes.

an ordinary metal at $T = 300$ K. In the case of $4H_b$ -TaS₂, the trigonal and the octahedral layers are alternating, resulting metallic resistivity along the layers (because of the sandwiches with octahedral coordination), and semimetallic in the perpendicular direction.

Another typical property of layered compounds is the anisotropy of the physical properties. The overlap of the orbitals between the layers is small, because of the van der Waals interlayer interaction, however in the layers the electrons can move more freely.

The anisotropy is mirrored in the electronic resistivity. In example of the 2H-NbSe₂ that anisotropy is 2140 at room temperature and goes up to 7200 at 8 K [1] (Fig. 3.3).

The two dimensionality of the electronic motion is well presented in other electronic (optical) and magnetic properties as well.

But the anisotropy manifests itself not only in the electronic properties. The crystals are easy to cleave between the layers producing good quality atomically

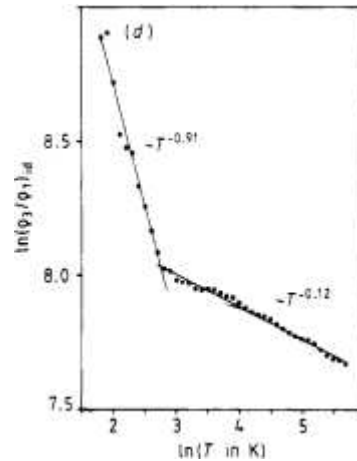


Figure 3.3: The resistivity anisotropy of 2H-NbS₂. (Figure from [1])

flat surfaces. That, and the presence of the charge density wave instability made them a perfect subject to many studies using surface sensitive techniques like AFM, STM or ARPES.

It is also relatively easy to grow thin films of transition metal dichalcogenides by epitaxial methods making them good candidates for industrial applications, or physical studies. One example is the use of NbSe₂ in quantum interferometer devices as a weak coupling element.

3.1.2 Electronic structure

We have seen that the different crystal symmetry, therefore the different coordination of the atoms gives rise to different measured electronic structures. Let's see what electron structure calculation can tell about it TaS₂. That material exist in both 1T and 2H polytype.

The decomposed density of states of 1T-TaS₂ is shown in Figure 3.4(a). We notice that Ta *d* state splits into three lower *t*_{2g} (*d*_{z²}, *d*_{yz}, *d*_{x²-y²}) and two degenerate upper *e*_g (*d*_{xy}, *d*_{yz}) orbitals because of the lattice distortion. There is a strong hybridization between S *p* and Ta *d* bands which appears in valence and conduction bands, which determines the transport properties of 1T-TaS₂. The states in this range consist of three main peaks that are assigned to p *d*_π and

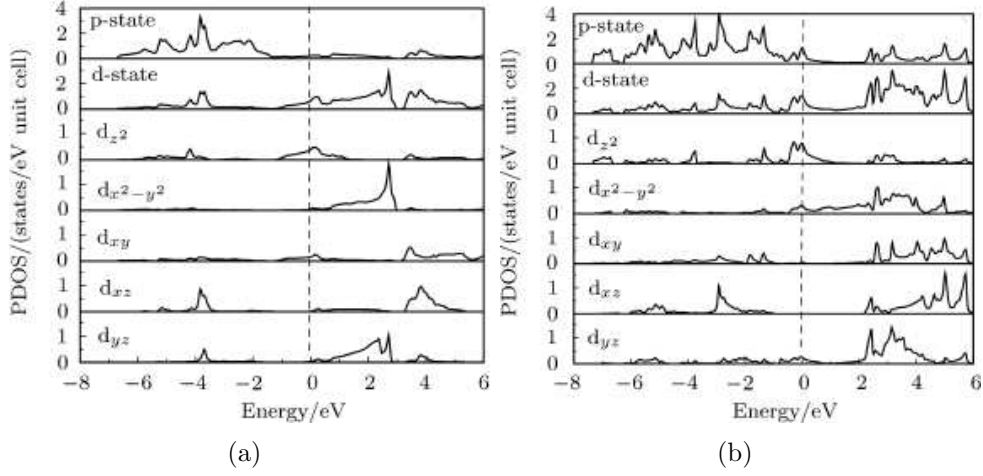


Figure 3.4: Projected density of state of 1T (a) and 2H (b) TaS₂. The calculation was done using full-potential linearized augmented plane wave method. (Figure from [2])

p d_σ bonding, Ta t_{2g} antibonding (-1.2–2.9 eV) and e_g antibonding (3.4–6.0 eV) bands. The value of the density of states at the Fermi level ($N(E_F)$) is 1.512 states/eV per unit cell.

Figure 3.4(b) presents the decomposed density of states of 2H-TaS₂. Owing to the trigonal prismatic coordination of Ta atoms in the 2H phase, there appears a dramatic change in decomposed density of states compared to that of 1T phase. The e_g subband shifts towards lower energies while the t_{2g} subband shifts to higher energies with respect to Fermi level, meanwhile, the band gap between t_{2g} and e_g disappears. In other words, Ta d state splits into upper subband (d_{xy} , d_{yz} , d_{xz}) and lower narrow subband (d_{z^2} , $d_{x^2-y^2}$). A strong hybridization between S 3p and Ta 5d appears in a range from -6.2 to 6 eV. The states in this range are assigned to p d_π and p d_σ bonding (-6.2–0.5 eV), t_{2g} and e_g antibonding (-0.5–6.0 eV) band. The $N(E_F)$ is 4.67 states/eV per unit cell what is about 3.1 times higher than in the 1T phase.

The difference in the electronic structure is also visible on the shape and structure of the Fermi surface (Fig. 3.5). While in 1T-TaS₂ the Fermi surface contains 6 leaves with a small pocket in the middle, in the case of 2H-TaS₂ the pocket in the middle of the Brillouin zone is much larger, comparable in size to

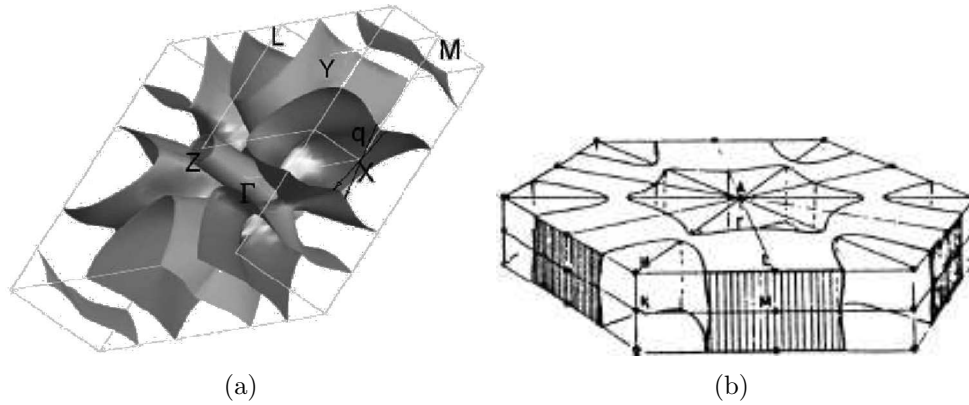


Figure 3.5: The Fermi surface of 1T (a) [3] and 2H (b) [4] TaS₂.

the leave on the side of the BZ. The differences are crucial to understand the structure of the CDW.

3.1.3 Intercalation complexes

The weak van der Waals interlayer coupling allows the introduction of extraneous atoms, or molecules between the layers. They can change the spacing and therefore the band overlap, as well as can donate to or take electrons from the sandwiches. That gives us a unique control over the electronic properties of those materials.

Intercalation has been done on all the important TMD families. Nb and Ta compounds have been modified with organic molecules, ammonia, and metals. Introducing octadecylamin has changed the interlayer spacing of 2H-TaS₂ from 2 Å to 56 Å [5].

It is important to mention that the original aim of the organic molecule intercalation was to modify the relative position of the layers without extrinsically changing the electronic structure. However several studies proved that the N atom present on all the organic molecules used, suffered a partial electron loss, donating them to the TMD layers. That has been seen in photoelectron emission in case of TaS_y(Py)_{1/2} [6], or in the NMR spectrum of the NbS₂(Py)_{1/2} [7].

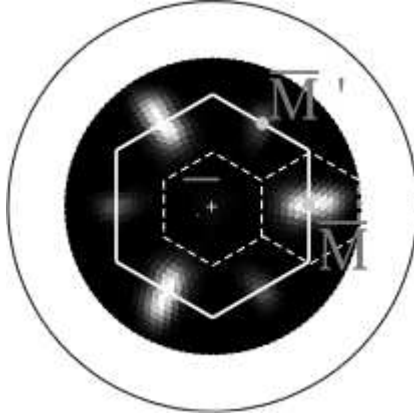


Figure 3.6: The measured Fermi-surface of 1T-TiSe₂. There are pockets around the L-M points, coming from the Ti 3*d* band, and a hole like pocket around the Γ point originating from the Se 4*p* band.

3.2 1T-TiSe₂

3.2.1 Presentation of 1T-TiSe₂

Among the many transition-metal dichalcogenides with charge-density-wave CDW instabilities, 1T-TiSe₂ is particularly interesting because it is the only group IVB transition-metal compound showing a structural transformation. Upon cooling down from room temperature, 1T-TiSe₂ undergoes a second-order phase transition at $T_c = 200$ K into a commensurate CDW phase associated with a $(2 \times 2 \times 2)$ superlattice that forms without the precursor of an incommensurate phase. The three CDW vectors are zone boundary wave vectors connecting the Γ point with the L points of the hexagonal Brillouin zone.

The Fermi-surface contains a hole pocket coming from the Se 4*p*-type valence band, at the Γ point, and electron pockets from the Ti 3*d*-type conduction band around the L points. The overlap between the p and the d-band is 120 meV resulting a relatively small Fermi surface (Fig. 3.6).

The pockets of the Fermi surfaces are relatively small. The estimated volume, relative to the volume of the Brillouin-zone is 1% for the Se 4*p* pockets, and 6% for the Ti 3*d* pockets. That small value is the strongest reason against the Fermi-

surface nesting driven CDW transition, proposed originally by Di Salvo *et al.* [8], based on the similar mechanism found to be important in other low dimensional transition metal dichalcogenides.

One year later White and Lucovsky [9] suggested an antiferroelectric transition mechanism in which the CDW formation is the result of a soft phonon inherent to the lattice system itself. Their model was motivated by the observation that the lattice and electronic polarizabilities, as determined from optical reflectivity spectra, are unusually large for 1T-TiSe₂.

Antiferroelectricity is involved in the recently proposed model of Bussmann-Holder and Büttner [10] as well. According to their calculation the microscopic origin of the CDW is an incipient antiferroelectric state, driven by anharmonic electron-phonon interaction.

Still in 1977 Hughes [11] had different idea. He brought the Jahn-Teller effect in the discussion. According to band structure calculations, the lowest lying *d*-band is slightly lower in the transition metal dichalcogenides of the 2H polytype, then for the 1T materials. That was supported by the atomic displacements, where a transition from octahedral (1T), to trigonal prismatic (2H) structure was observed. In his scenario the movements of the atoms would lower the Ti 3*d* band. Keeping the Jahn-Teller mechanism in mind Whangbo and Canadel [12] pointed out, that the energy lowering which stabilizes the structural transition is not originating from the lowering of the Ti 3*d* band. It should be more associated with the shortening of the Ti-Se bond, which lowers the Se 4*p* band.

Using the band-type Jahn-Teller effect Motizuki [13, 14, 15, 16] and coworkers developed a microscopic theory, involving strong wave-vector-dependent electron-lattice interaction. That was further supported by the ARPES measurement of Rossnagel *et al.* [17], where they have seen the predicted lowering of the 4*p*-type Se band due to the band distortion at the Γ point resulting in a *p-d* gap of about 100 meV (Fig. 3.7).

The fourth big group of the theories to explain the origin of the charge density wave transition in 1T-TiSe₂ is based on an excitonic-insulator mechanism. For

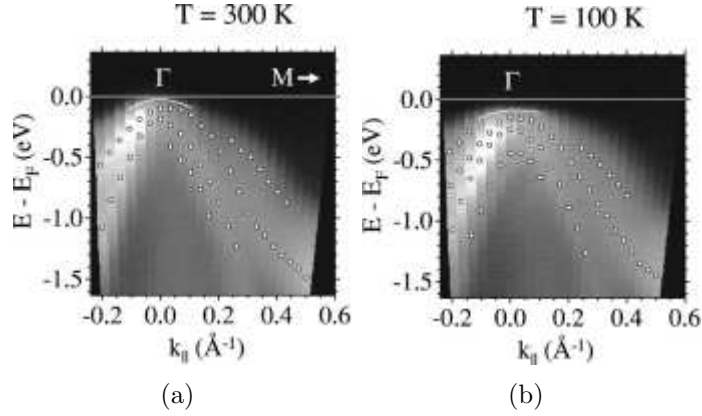


Figure 3.7: Energy distribution curves for the MFAL plane of the Brillouin-zone taken with 13 eV photons at room temperature a) and 100 K b). Se $4p$ emission features are indicated by circles. Solid lines denote the position of the midpoint of the leading edge. Photoemission intensity is represented in a linear gray scale with white corresponding to high intensity. (Figure from [17])

that material it was originally proposed by Wilson in 1977 [18, 19], but the original idea is much older, coming from Kohn from 1960 [20, 21]. If the carrier density in a semimetal is low, the Coulomb interaction between the carriers is weakly screened, and thus the electrons and thermally excited holes can exist in a bound state, mediated by the electrostatic forces. That bound state is called exciton. If the excitonic binding energy is bigger than the gap between the electrons and holes, the system becomes unstable towards the formation of the excitons. This can drive a transition to a condensed ground state of excitons with the periodicity defined by the spanning vector connecting the conduction band maximum with the valence band minimum. In the 1T-TiSe₂ the electron and the hole density around the Γ and L points is relatively small ($< 10^{22} \text{ cm}^{-3}$), making it an ideal candidate to be the first material with excitonic condensed state. Recently a calculation based on a BCS-like theory of the excitonic condensed state, showed a big renormalization of the bands at high symmetry points, and a very large transfer of the spectral weight to the backfolded bands. Those changes of the electronic structure were observed with high resolution ARPES measurement by the same group (Fig. 3.8) [22].

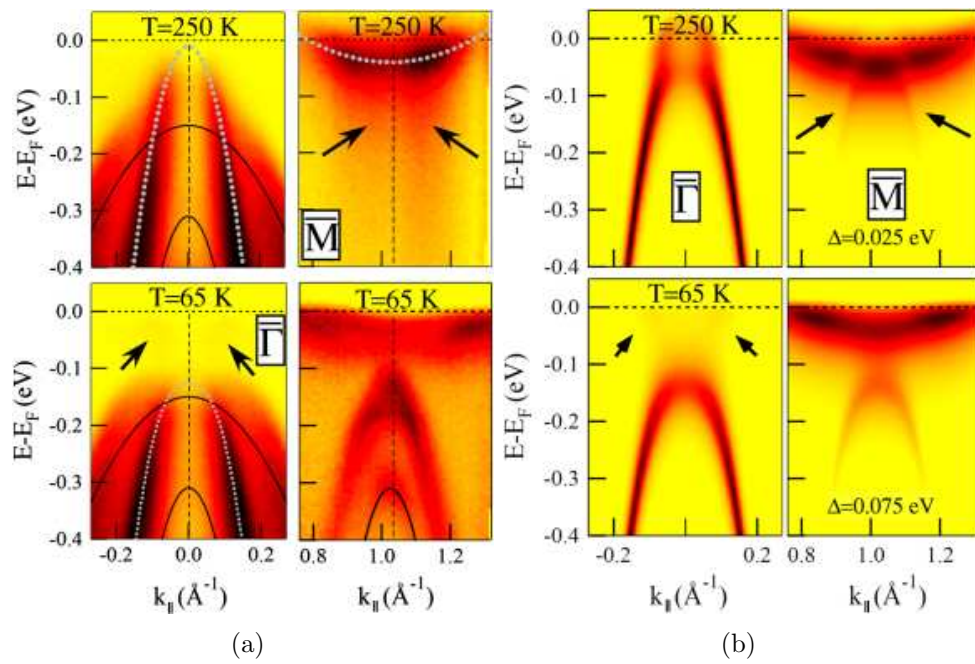


Figure 3.8: Measured a) and calculated b) band structure of the 1T-TiSe₂ above (upper) and below (lower) the charge density wave phase transition, around the Γ and M points. There is good agreement in the large renormalisation of the bands crossing the Fermi surface. (Figure from) [22])

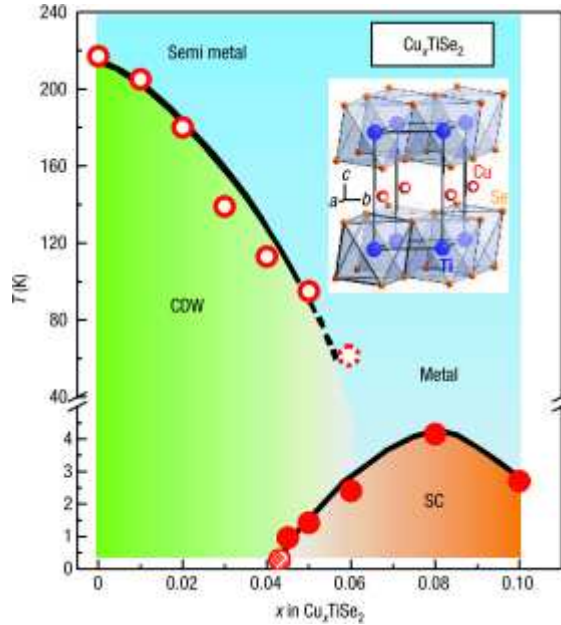


Figure 3.9: The Cu_xTiSe_2 $T - x$ electronic phase diagram. Open circles represents the charge density wave transition, and the filled circles corresponds to the superconducting temperature. Shaded circle at $x = 0.04$ indicates that the transition is just below the accessible temperature range, and the dashed circle at $x = 0.06$ marks the barely visible CDW transition. The inset shows the crystal structure of Cu_xTiSe_2 . (Figure from [23])

1T-TiSe₂ attracted further interest when recently superconductivity was discovered in copper intercalated samples [23] (Fig. 3.9). Right after the publication an innumerable variety of mechanisms have been proposed linking the CDW phase and the superconductivity.

Zhao *et al.* [24] has performed angle resolved photoemission spectroscopy on copper intercalated single crystals and has found that the chemical potential is raised with the Cu content, what makes the charge density wave formation less favorable. Parallel to that, the density of states is raised what destabilizes the electronic system against superconductivity (Fig. 3.10). In their picture the two low temperature phases are not competing, the appearance of the superconductivity at the intercalation where the charge density wave phase is suppressed is just a coincidence.

To reveal the nature of the gap S. I. Li *et al.* performed in plane thermal

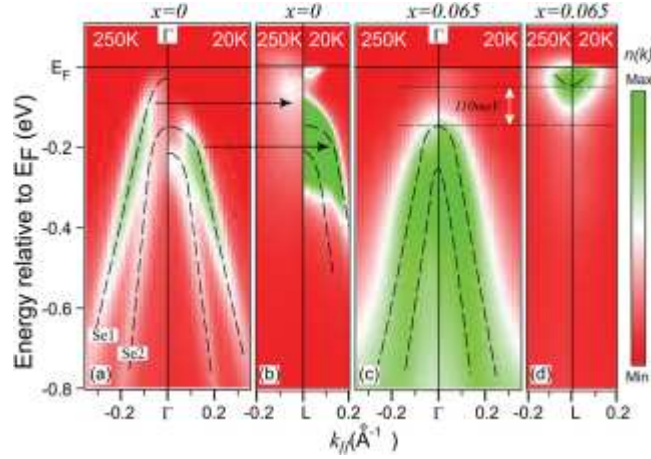


Figure 3.10: Photoemission intensity map for 1T-TiSe₂ (a, b) and 1T-Cu_{0.065}TiSe₂ (c, d) at 250 and 20 K at the Γ and L points. Arrows illustrates the band folding, and Se1 and Se2 labels the two Se 4p band. (Figure from [24])

conductivity κ measurement on Cu_{0.07}TiSe₂. The thermal conductivity of a metal at low temperatures, according to the Wiedemann-Franz law (WF), has the form of

$$\kappa(T) = \sigma LT + \mathcal{O}(T^2), \quad L = \frac{3}{2} \left(\frac{k_B}{e} \right)^2. \quad (3.1)$$

Using the assumption that the WF-law is obeyed by this material, they separated the residual, temperature normalized, linear term of the thermal conductivity κ_0/T , where $\kappa_0 = \kappa(T = 0)$. The assumption was further verified with the measurement under magnetic field, where they found that the material satisfies the WF-law within an error bar of 4%. κ_0/T is a good measure of the gap symmetry. For unconventional superconductors with nodes in the superconducting gap, the nodal quasiparticles will contribute a finite κ_0/T in zero field. They found that $\kappa_0/T = 0$ within the precision of the measurement and conclude that the Cu_{0.07}TiSe₂ is most probably an s-wave superconductor, with a fully gapped excitation spectrum. Furthermore they compared the magnetic field dependence of κ_0/T normalized by its normal state value κ_N/T , with different other superconductors. The very distinct difference from the behavior of

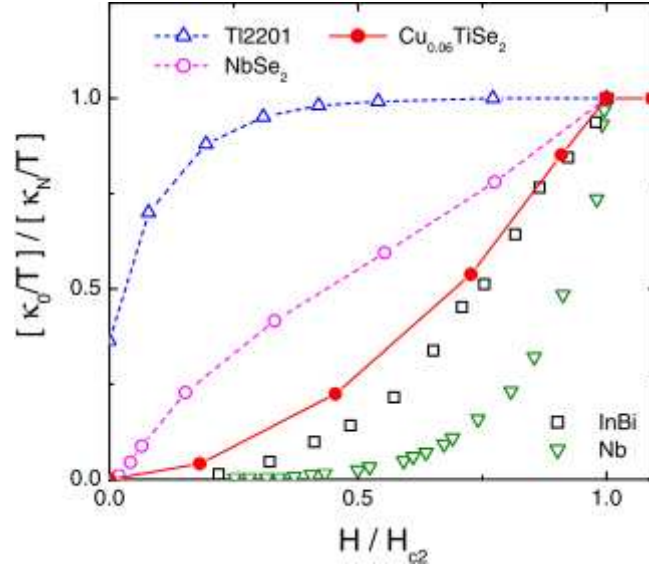
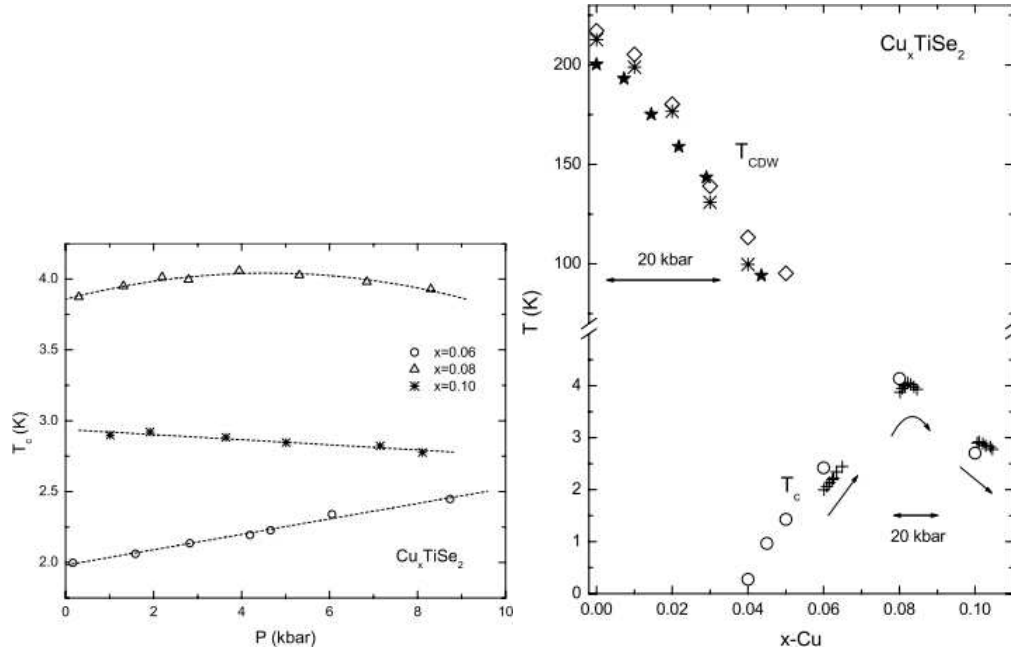


Figure 3.11: Normalized residual linear term κ_0/T of $\text{Cu}_{0.07}\text{TiSe}_2$ plotted as a function of H/H_{c2} . For comparison similar data are shown for the clean s-wave superconductor Nb, The dirty s-wave superconducting alloy InBi, the multiband s-wave superconductor NbSe_2 , and an overdoped sample of the d-wave superconductor Tl-2201. (Figure from [25])

a multiband superconductor NbSe_2 shows that $\text{Cu}_{0.07}\text{TiSe}_2$ is a single gap s-wave superconductor. (Fig. 3.11)

Furthermore, Bud'ko *et al.* performed thermal-expansion and magnetization measurements under pressure on Cu_xTiSe_2 samples in the intercalation range $0 \leq x \leq 0.08$ [26]. They found, by analyzing the ambient pressure thermal-expansion data, a well defined difference in intercalation behavior of the samples below and above 3%. From the magnetization measurement under pressure they found different behavior for the pressure dependence of the T_c at three different x . At $x = 0.06$ the T_c is increasing from 2 K with a rate of 0.05 K/GPa, at the intercalation of $X = 0.1$, the T_c is decreasing from 3 K with the rate of 0.025 K/GPa, and in the middle range $x = 0.08$ T_c has a maximum value of 4 K at the pressure of 0.5 GPa (Fig. 3.12(a)). From these three facts naturally came the question whether the three can be scaled together with the ambient pressure dome as a function of x . It is possible, by using the scaling factor of $5.6 \cdot 10^{-2}$ 1/GPa, the points can be matched. The only thing questioning the



(a) The pressure dependence of the superconducting transition temperature. (b) Pressure dependent T_c and T_{CDW} , scaled on a x - T phase diagram.

Figure 3.12: Measurement of the pressure dependence of the transition temperatures of the 1T- Cu_xTiSe_2 at different intercalation level.

relevance of that scaling is the fact that the scaling factor is different for the CDW transition: in order to match the T_{CDW} points they had to use $1.5 \cdot 10^{-1}$ 1/GPa (Fig. 3.12(b)).

From all those measurements, it is clear, that in that material choice between the two ground states depends on a very subtle balance. With the doping due to the intercalation it is possible to change that balance to favor the superconductivity, but the control on the sample quality is less good. Therefore comparing different measurements, made on different samples coming from different sources is more difficult. Our aim was to change the balance with a parameter what we have more control on, and is ideal for low dimensional materials: pressure. Pressure has the great advantage that can be applied on the very same carefully selected sample. Therefore the comparison of the results between the different measurements, and the tracing of the development of the phases can be more adequately done. It is also important that pressure does not

creates extra defects, what is important when we are dealing with superconducting materials, since impurities can behave as pair breaking centers, and suppress superconductivity.

3.2.2 Results

I measured the transport properties of the pristine 1T-TiSe₂ over a wide pressure range of 0–10 GPa and temperature of 0–300 K. The change of pressure in that material is an ideal tool to change the electronic structure without introducing phase inhomogeneity and disorder. Moreover the subtle balance in the electron density is crucial for the charge density wave formation giving us the hope to be able to suppress it and reveal the low temperature properties of the underlying electronic structure.

The single crystal 1T-TiSe₂ samples used in this investigation were grown by a conventional vapour transport method and the sample stoichiometry was verified by X-ray and resistivity measurements. The RRR of a typical crystal was about 10-20. The resistivity was measured using a standard 4-point technique, with an AC current of 5 mA and a frequency 16.98 Hz. Pressure measurements in the low pressure range 0–2 GPa were obtained in a self-clamped piston cylinder pressure cell. Pressure measurements in the pressure range 2–25 GPa were performed in an opposed anvil Bridgeman-type pressure cell with tungsten carbide or sintered diamond anvils and quasi-liquid steatite medium. A dilution refrigerator was used to achieve base temperatures of 70 mK.

Figure 3.13 shows the temperature-dependence of the resistivity in the pressure range 0–10 GPa. The onset of the charge density wave (CDW) appears as a well-defined broad peak in the resistivity below 200 K. With the application of pressure the peak subsides gradually, until at about 3 GPa there remains no identifiable sign of that feature in the resistivity measurements. The development of the CDW can be followed on the thermoelectric power measurement (Fig. 3.14). Above the CDW transition the resistivity varies linearly with temperature as ex-

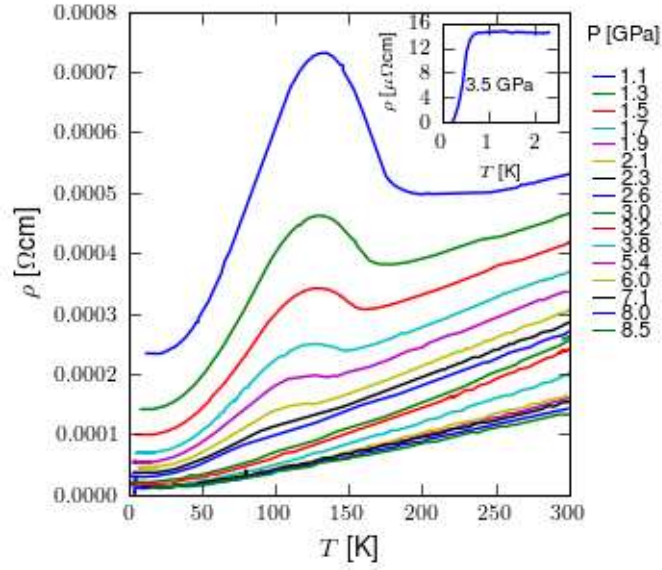


Figure 3.13: Pressure dependent resistivity measurements of 1T-TiSe₂. The transition into the charge density wave (CDW) phase is identified with the broad peak in the resistivity below 200 K. The inset shows the emergent superconducting transition at pressures above 3 GPa. The maximum superconducting transition temperature observed was about 1.8 K at pressures slightly below 3 GPa.

pected of a well-behaved phonon scattering dominated system. On the other hand the TEP increasing with decreasing temperature what is clearly a non metallic behavior. That behavior stays to higher pressure as well. At low temperatures the temperature dependence of the resistivity shows some surprising deviations from the expected model of electron scattering on phonons and static impurities. The precise determination of the temperature exponents will be discussed later.

Let's see somewhat in more details the TEP. If the sample was a simple metal above $T_p = 220$ K at ambient pressure, then one may apply the formula describing the thermopower of a free electron gas with an energy- independent scattering rate:

$$S(T)_{\text{metal}} = \frac{\pi^2 k_B^2 T}{2|e|E_F} \quad (3.2)$$

It shows that it should linearly increase with temperature, and the slope is

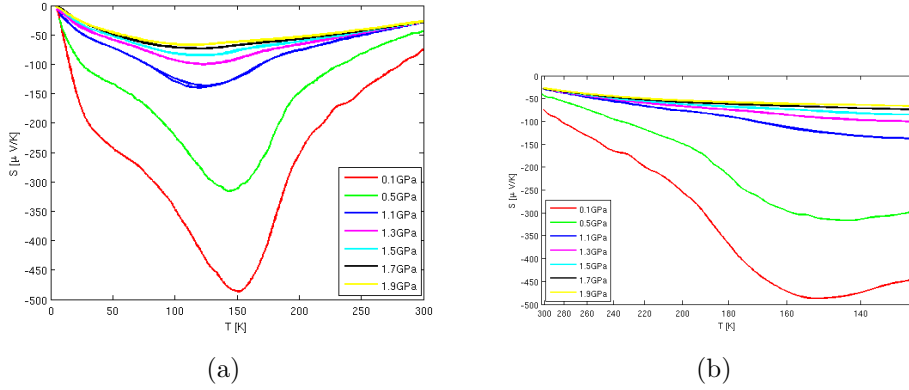


Figure 3.14: (a) Pressure dependent thermoelectric power measurements of 1T-TiSe₂ up to 2.3 GPa, The thermopower is negative in the whole temperature range indicating n type carriers. (b) The thermopower plotted as a function of $1/T$.

inversely proportional with the bandwidth. If it were a semiconductor, TEP would follow the:

$$S(T)_{\text{ins.}} \sim \frac{k_B}{|e|} \frac{\Delta}{2k_B T} \quad (3.3)$$

where Δ is the semiconducting energy gap. In the case of conduction by electrons and holes, this expression contains a prefactor

$$\frac{\mu_e - \mu_h}{\mu_e + \mu_h} \quad (3.4)$$

where μ_e , and μ_h denote electron and hole mobilities.

From figure 3.14, it is clear, that the absolute value of the TEP is decreasing above T_p , therefore does not behave as a metal. If we plot the TEP data as function of $1/T$, one can see that even above 220 K it follows relatively well the semiconducting behavior (Fig 3.14(b)). One could not claim that this is just an apparent semiconducting behavior because of the CDW fluctuations above the Peierls transitions. We should remind ourselves, that even in quasi-1D systems

like $(\text{TaSe}_4)_2\text{I}$, where CDW fluctuations scatter electrons so much that the resistivity is non-metallic, the TEP still gives a metallic-like behavior [27]. If the system is non-metallic, the transition cannot be as of Peierls nature. This puts forward other mechanisms for the CDW formation.

From fig 3.14, one can see that below T_p a second type of carrier appears, which mobility overtakes the TEP behavior, and S starts to decrease below 120-140 K.

In Figure 3.15 I summarize our findings in a pressure-temperature phase diagram. The broad peak in the resistivity associated with the CDW phase transition becomes indistinguishable at pressures above 2.5 GPa. Above that pressure the system is believed to be metallic. Superconductivity persists in the pressure range 2–4 GPa. The residual resistivity or the resistivity in the normal state just above the superconducting transition at 2 K shows dramatic variation with pressure until about 4 GPa with some marginal linear decrease in that quantity at higher pressures. At the critical pressure of about 3 GPa there appears to be a slight local maximum in the residual resistivity coinciding with the maximum transition temperature of the superconducting dome. Incidentally, as can be seen from the lower part of the graph in Fig.3.15 there is a depression in the resistivity temperature exponent n , derived from the standard resistivity equation $\rho = \rho_0 + AT^n$. The resistivity exponent was obtained through a fitting procedure over the low temperature region up to 30 K of the data. More explicitly, everywhere outside the pressure range of 2–4 GPa (where the superconductivity occurs), the exponent of the temperature dependent contribution hovers around the value of $n \sim 3$. In the 2–4 GPa pressure region n drops to a value of $n \sim 2.6$. Although a resistivity thermal exponent of $n \sim 3$ is not entirely unfeasible within a phonon picture, the unusual pressure dependent dip is reminiscent of a quantum critical scenario, especially when coupled to a residual resistivity peak above the superconducting dome. Both of these features may be attributed to the presence of remnant quantum fluctuations in the system at pressures below 4 GPa. The nature of these fluctuations is unclear, but could be linked to the softening of

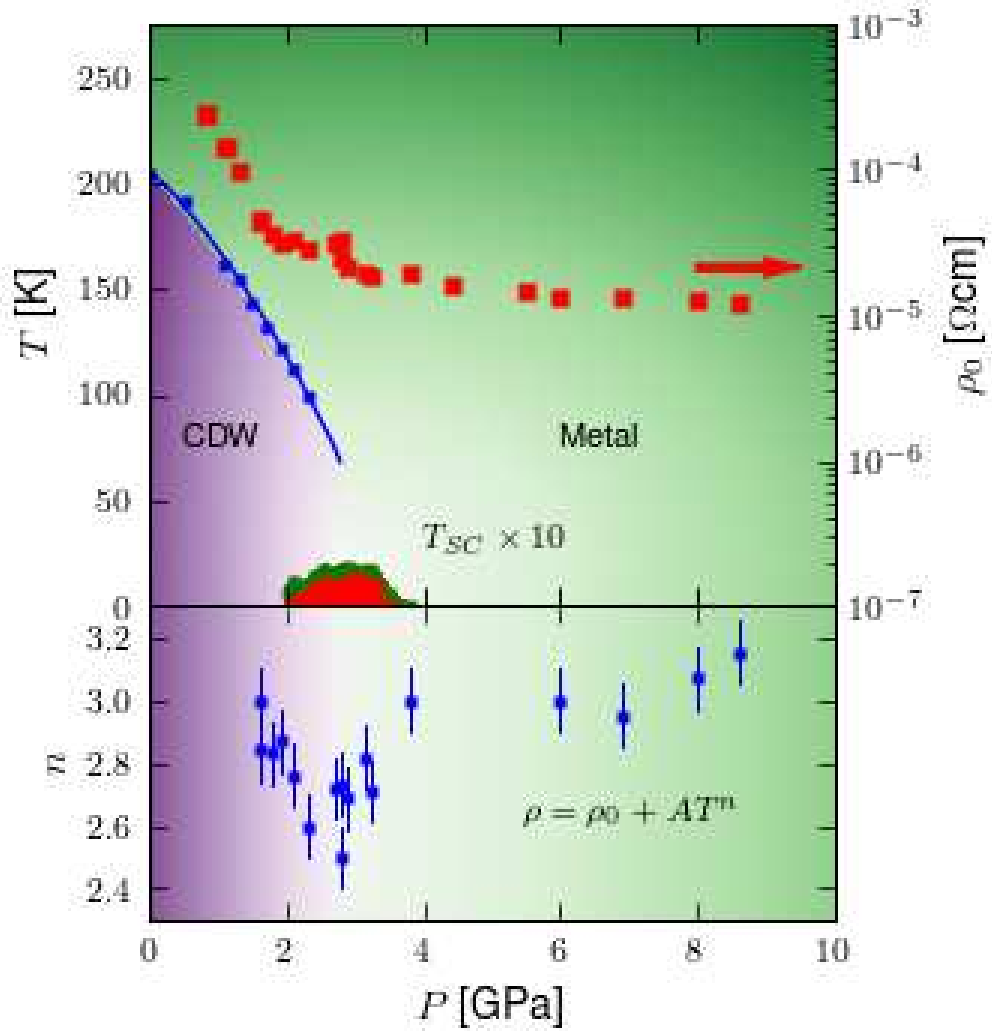


Figure 3.15: Pressure-temperature phase diagram of 1T-TiSe₂. On the left axis we see the evolution of the CDW transition temperature and the superconductivity transition temperature $\times 10$ with pressure. The superconducting dome is constrained to the pressure ranges of 2–4 GPa. On the right axis we see the pressure dependence of the residual resistivity over the entire investigated pressure range.

the possible excitonic CDW state in 1T-TiSe₂. Since the anomaly in the residual resistivity and in the power law exponent happen in the very same pressure window where superconductivity is present, it is reasonable to suppose that they are linked. We think that the fluctuating excitonic interaction (equivalent to the fluctuating short range CDW) is at the origin of the coupling of charges into Cooper pairs.

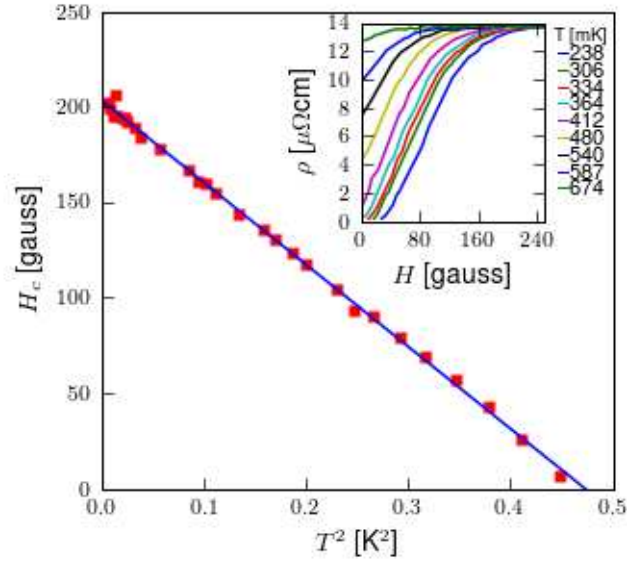


Figure 3.16: Temperature dependence of the magnetic critical field in 1T-TiSe₂ in the temperature range 70–700 mK, shown as a function of $(T/T_C)^2$. Notably, the critical field follows BCS like $H(T) = H(0)(1 - T/T_C^2)$ temperature dependence at low temperatures, as expected for most conventional superconductors. (inset) The resistivity versus magnetic field curves.

A further hint for this conjecture is coming from the measurement of the upper critical field in the superconducting state. It is unusually low for an electron-phonon mediated superconductivity. In Figure 3.16 we present the temperature dependence of the critical fields at a pressure of 3.5 GPa, plotted nominally as a function of T^2 in the temperature range 70–700 mK, the T_c at the investigated pressure was about 480 mK. We have to note that the critical field does depend quadratically on temperature, in agreement with the conventional behavior $H(T) = H(0)(1 - T/T_C^2)$ but there appears to be some slight upward deviation.

That could be compared to the formalism of a positive curvature anomaly (PCA) predicted by Maekawa [28] for dirty 2D systems. The main justification for this effect lies in the enhanced Coulomb repulsion in a soft localisation regime, which is weakened in a perpendicular magnetic field [29]. The upturn signals the presence of weak localisation in the material. The superconductivity in 1T-TiSe₂ is shown to be extremely sensitive to magnetic field, the $H_{C(0)}$ is estimated to be around 200 Gauss.

On the Figure 3.17 I summarize the knowledge about the superconductivity and the melting of the CDW phase in 1T-TiSe₂ on a three dimensional phase diagram. On the right side I plotted the data coming from the intercalated [23] samples, together with the few points published in the paper of Bud'ko [26]. On the left side I plotted my results, as a function of pressure. Looking on those two walls naturally appears the question, what the low temperature phase diagram looks like on the intercalation-pressure plane. Do we have two distinct superconducting bubbles, or a superconducting “tunnel” connects the two discovered phases. In the case of the intercalation it seems clear that partial doping of the material can be accounted for the instability of the charge density wave phase, what gives rise of the superconductivity, and turns the material into a good metal [30]. In the case of pressure it is more difficult to imagine any doping effect, which might be a reason for having two bubbles. That might be further supported by the different behavior of the thermoelectric power in the Cu intercalated samples and the samples under pressure. On the other hand in both cases, the superconductivity appeared at the point where the CDW phase disappears, supporting the idea of quantum-criticality induced superconductivity, where at least partially, the fluctuations of the charge density wave phase play an important role in the formation of superconductivity. That might suggest that the two domes are connected with a superconducting tunnel. Further measurements of Cu intercalated samples under high pressure are needed to discover the physics in that very important part of the parameter-space.

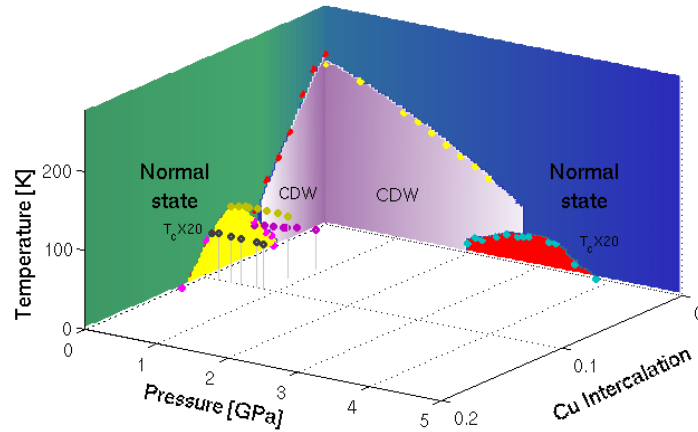


Figure 3.17: The three dimensional phase diagram of 1T-TiSe₂, in the temperature-pressure-intercalation space. The points on the temperature-intercalation plane are coming from the paper of Morosan *et al.* [23], and the pressure dependence of the intercalated samples from the publication of Bud'ko *et al.* [26].

3.3 1T-TaS₂

3.3.1 Presentation of 1T-TaS₂

1T-TaS₂ has a simple crystal structure, composed of planes of tantalum (Ta) atoms, surrounded in an octahedral arrangement by sulphur (S) atoms, see insert on Fig. 3.18. Even at ambient pressure, a variety of phases are present including a metallic phase at high temperatures, an incommensurate charge density wave (ICDW) phase below 550 K, a nearly commensurate charge density wave (NC-CDW) phase below 350 K, and a commensurate charge density wave (CCDW) phase below 180 K. The charge density wave (CDW) state in 1T-TaS₂ is mostly driven by the Fermi surface instability, resembling a Peierls instability in (quasi) one dimension. The Peierls-like instability is, however, substantially more complex in 1T-TaS₂ than in many other systems. That is supported by the measured and calculated Fermi surface shown on the Figure 3.19.

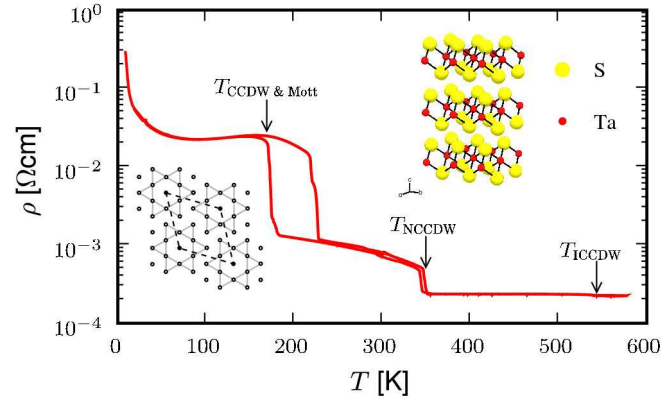


Figure 3.18: Ambient pressure phases of 1T-TaS₂. The phases are: a metallic phase at temperatures above 550 K; a charge density wave phase (ICCDW) above 350 K; a nearly commensurate charge density wave phase (NCCDW) above 190 K; a commensurate charge density wave CCDW Mott phase below 190 K; additionally there is a trigonal phase present solely during the warming up cycle between 200–300 K [31, 32, 33]. Also shown are the Ta atom distortions in the fully commensurate phase (see insert at low temperatures) and the crystal structure of 1T-TaS₂.

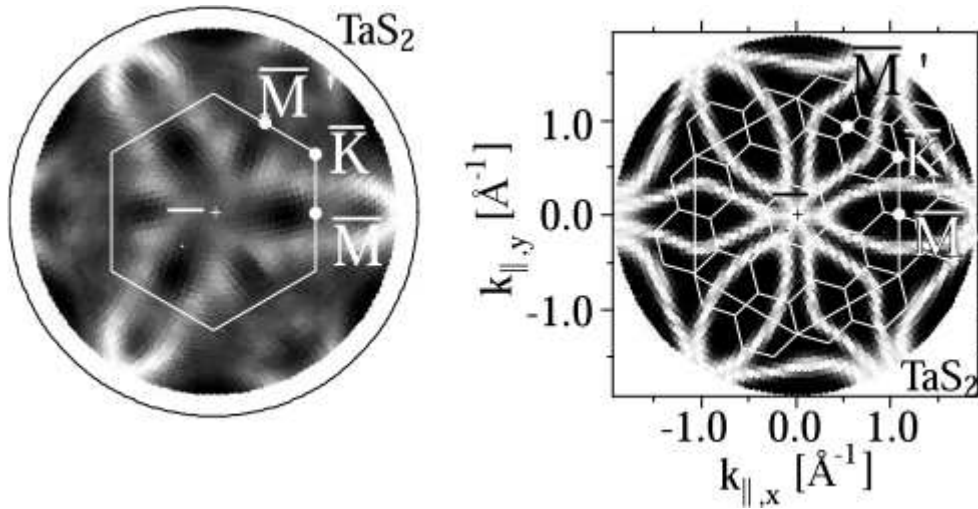


Figure 3.19: The measured and the calculated Fermi-surface of the 1T-TaS₂. The calculation was made using density functional theory. On the left figure, the BZ. in the CDW phase is marked as well.

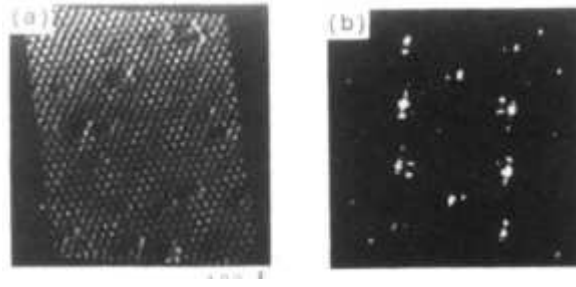


Figure 3.20: (a) Scanning tunneling microscopic image of the incommensurate phase of 1T-TaS₂. (b) Fourier transformation of (a). (Figure from [32])

The incommensurate charge density wave phase

The first modulation of the electronic density occurs below 550 K. In that phase the original lattice parameter $a_0 = 3.346 \text{ \AA}$, and the wavelength of the density wave $a_{\text{ICDW}} = 11.811 \text{ \AA}$ are incommensurate to each other $a_{\text{ICDW}}/a_0 = 3.35$, creating a homogeneous long range ordered CDW state. (Fig. 3.20) The CDW wave vector and the lattice vector are parallel to each other and leads to a partial gapping of the FS.

That phase exhibit metallic behavior. That is in an agreement with the finite electron density seen in angle resolved photoemission spectroscopy (Fig. 3.21) [34], which comes from the non-gapped part of the Fermi-surface.

The nearly-commensurate charge density wave phase

At temperatures below 350 K the structure of the charge modulation changes. Ambient pressure X-ray studies in 1T-TaS₂ reveal, that instead of the long range ordered incommensurate CDW system, the material develops commensurate CDW domains of hexagonal shape [35, 32]. Those islands are separated by regions where the phase of the modulations changes rapidly, connecting the different domains. (Fig. 3.22)

The electrons in the commensurate CDW domains are strongly bound, the carriers responsible for the conduction are coming from the inter-domain space. The decrease of the interdomain space, and the increase of the domain size (Fig.

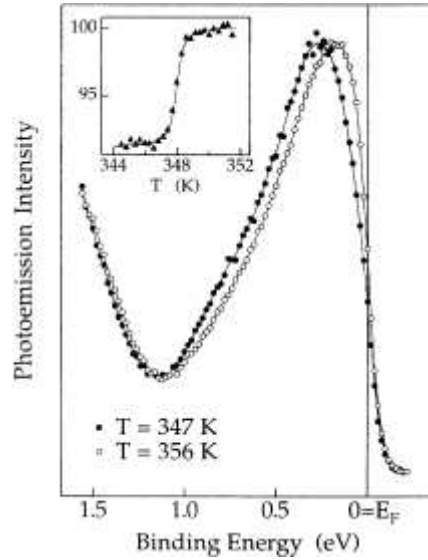


Figure 3.21: Angle resolved photoemission spectra recorded above, and below the ICCDW-NCCDW phase transition. A clear Fermi edge, with finite electron density at the Fermi-level can be seen. The inset shows the photoemission intensity as a function of temperature in arbitrary units at 180 meV (figure from [34]).

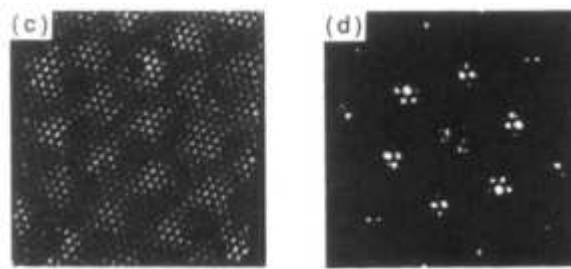


Figure 3.22: (a) Scanning tunneling microscopic image of the nearly-commensurate phase of 1T-TaS₂. The commensurate domains, and the domain walls are clearly present. (b) Fourier transformation of (a). (Figure from [32])

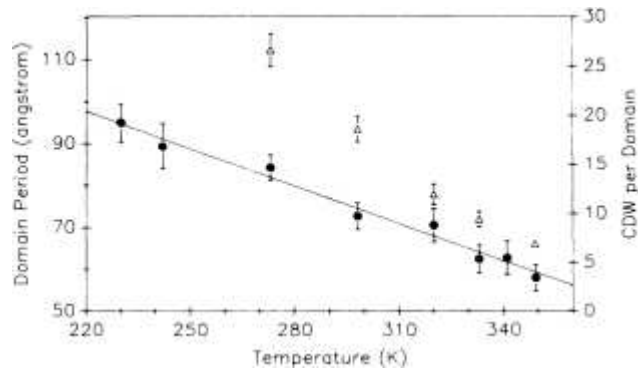


Figure 3.23: The domain size in the nearly-commensurate charge density wave phase of 1T-TaS₂ (Figure from [36])

3.23) is responsible for the clearly non-metallic increasing resistivity.

The removal of the electrons from the Fermi edge can also be seen in ARPES, as shown on Figure 3.24. At the same time, the three Hubbard subbands, which are characteristic signs of the commensurate structure, and therefore will be explained more detailed later, become more pronounced.

The NCCDW phase has been subject of numerous experimental and theoretical investigations at ambient pressure. Previous theoretical approaches invoked mainly phenomenological treatments, based on sophisticated versions of the Landau-type functional, which neglect the microscopic mechanism [37, 38]. However, the main mechanism behind the creation of the textured phase has been established to lie in the tendency of the system to maximize the electronic gap at a given deformation amplitude. This is achieved by (inter)locking the deformations at (three) commensurate wave-vectors, counteracted by the remnant part of the electrons in the states above the gap. This leads to a microscopic mechanism for domain formation, common to many electronic systems with (charge or spin) density waves close to commensurability [39]. Essentially, the discommensuration in the textured phase hosts the electrons that do not fit below the gap that exists in the commensurately ordered domains. Notably, however, the size of the domains in 1T-TaS₂ is substantial, containing several hundred of TaS₂ units within each layer (from 5 to 20 David star structures containing 13 TaS₂

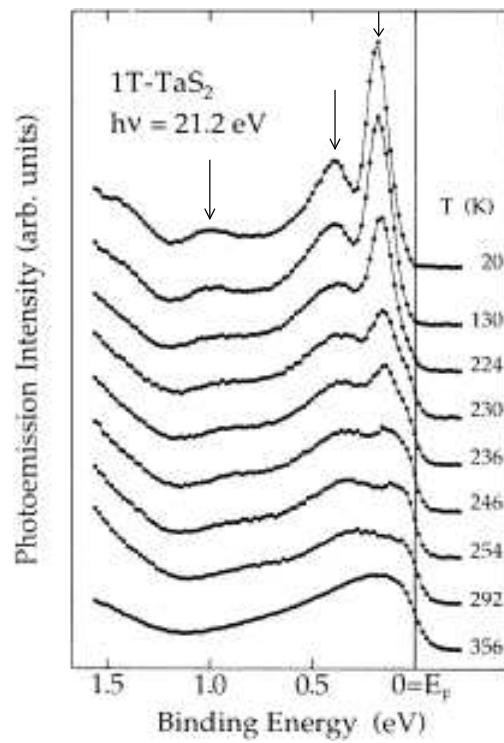


Figure 3.24: Photoelectron intensity of the 1T-TaS₂ at different temperatures. The gradual development of the three Hubbard subbands, and the decrease of the intensity at the Fermi level can be seen (figure from [34]).

unit each). Therefore, long range Coulomb forces are expected to control the charge transfer involved in the domain size and organization as it will be shown later. This important aspect was omitted in former theoretical treatments of the NCCDW phase in 1T-TaS₂.

The commensurate charge density wave phase

The CCDW phase is geometrically the simplest among the CDW phases in this material. The displacement of the atoms leads to the formation of David star clusters, where twelve Ta atoms within the layer move inwards toward a thirteenth central Ta atom. The stars interlock by forming a triangular superlattice (Fig. 3.18, insert). However, this deformation does not fully gap the electronic system, with only twelve out of the thirteen electrons of the new unit cell occupying the electronic states below the energy gap created by the deformation. The “thirteenth” electron resides above the deformation-induced gap [40]. The enigma of high resistivity of this phase was resolved by pointing out that the system stabilizes by simultaneously developing a Mott insulator state from the electrons above the gap [41, 42], latter confirmed by other experiments including spectroscopic methods [43, 44] (Fig. 3.25).

It should be noted that the formation of the David-star clusters also involves displacements perpendicular to the plane, causing a periodic swelling of the TaS₂ layers [45, 46]. This CCDW-Mott phase was found to be sensitive to doping [47, 43], disorder induced by irradiation [48], and pressurization [49].

3.3.2 Goal of the experiment

From the rich phase diagram of the 1T-TaS₂ it is clear that the balance between the different phases is very fragile. Due to the Mott-localization, it is impossible to see what is the reason for be the ground state of the electrons, what gives the semimetallic behavior at intermediate temperature. Pressure is an ideal tool in that case to suppress the localization, and affect the balance between the

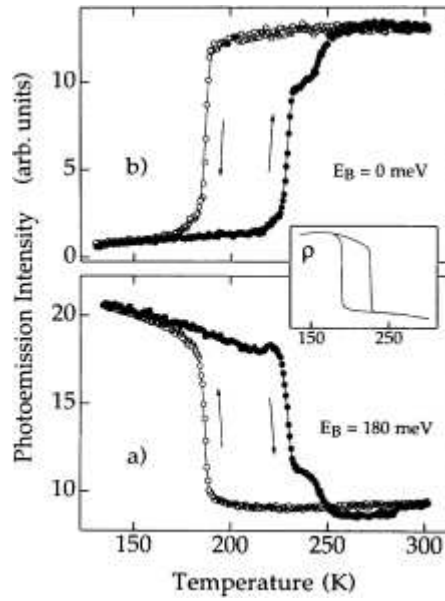


Figure 3.25: Temperature dependent photoelectron intensity of the 1T-TaS₂ at the Fermi-energy, and at the binding energy of 180 meV, collected during a whole cycle of cooling down (open symbols) and warming up (closed symbols). The two steps in the transition are due to the CDW states bound to the impurities on the surface. It is important to notice, that even after the first order phase transition, there is a finite electron density at the Fermi-energy decreasing further with temperature. Those are the 13th electrons localized in the middle of the David-stars.

CDW phases. The c-axes displacement of the atoms in the David-stars can be suppressed by pushing the layers closer to each other. Due to the sandwich structure of the material we could expect that the pressure will mainly reduce the c-axes lattice parameter, and the effect on the a-b plane might be negligible. That is supported by the big difference in the compressibility along the two directions $\alpha_{\parallel} - \alpha_{\perp} = 1.04 \cdot 10^{-3} \text{ kbar}^{-1}$ and $\alpha_V = 2.27 \cdot 10^{-3} \text{ kbar}^{-1}$ [50].

3.3.3 Results

I have carried out resistivity and thermoelectric power measurements on 1T-TaS₂ under pressures ranging from 0–25 GPa and temperatures ranging from 1.3–300 K (Fig. 3.26(a)). At temperatures below 250 K we observe a first order transition from the NCCDW to the CCDW phase at temperatures below 250 K, which melts with a pressure of 0.8 GPa.

This can be followed on change of the thermoelectric power as well. (Fig. 3.27) It shows a distinct behavior from TiSe₂. At high temperatures the TEP starts from a positive value and changes sign showing the two-band nature of conduction, electrons and holes, which is compatible with the complex band structure of the system. Above the nearly commensurate-commensurate phase transition the TEP stays low, showing that there are some free carriers between the commensurate regions which are strongly scattered, resulting in the non-metallic temperature behavior of the resistivity. At the transition the TEP changes sign, becomes positive, and jumps up to huge values. Despite this first order-like phase transition, and despite the semiconducting like behavior of the resistivity, TEP does not show the $1/T$ dependence. It rather flattens out reminiscent of a configurational entropy contribution to TEP which gives a temperature independent contribution $(k_B/e) \ln(\frac{1-c}{c})$ (where c is the density of charge carriers per site). At low temperatures it picks up some T-dependence, presumably because some correlation effects. As we increase the pressure the melting of that Mott phase is even more visible in the TEP, were the hole-like low temperature contribution

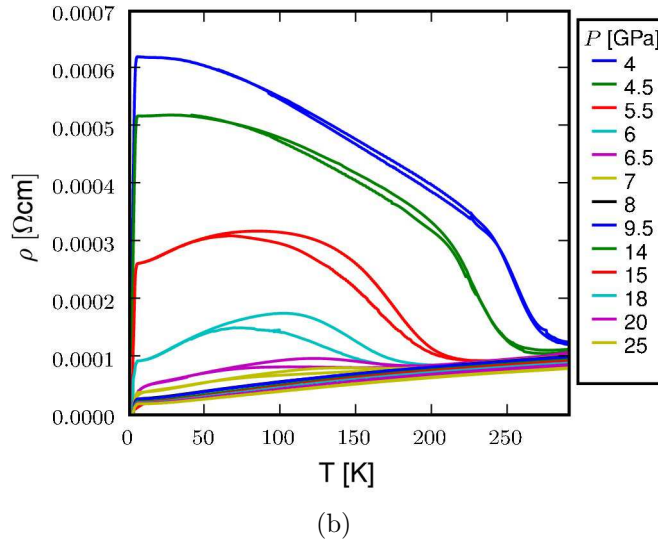
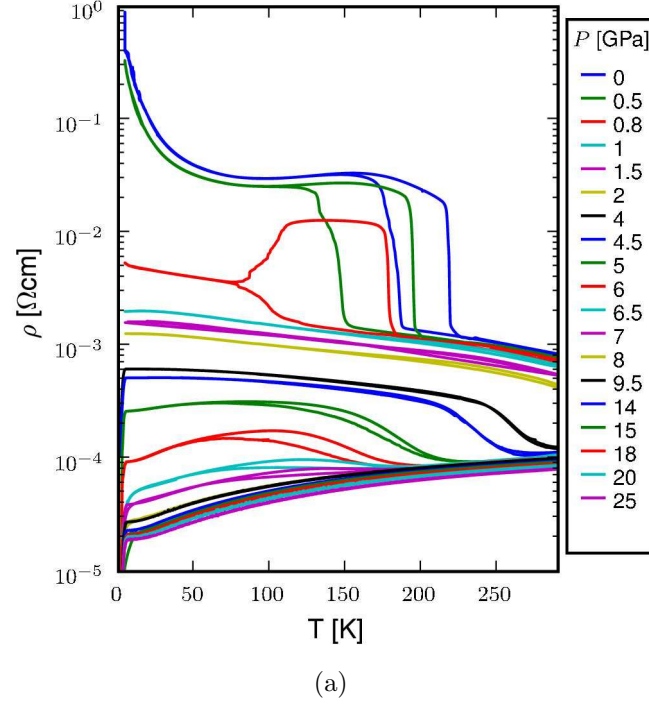


Figure 3.26: Resistivity in the pressure range of 0–25 GPa and temperature range of 1.3–300 K. Figure (a) shows that the temperature dependence of the resistivity is largely non-metallic over the entire temperature range for pressures of 0–4 GPa; the low temperature upturn in the resistivity that relates to the variable-range-hopping conduction in the Mott phase [41, 42] disappears above 0.6 GPa; first traces of the superconductivity are observed at an approximate pressure of 2.5 GPa, with a T_{SC} of 1.5 K; metallic-like behaviour develops for low temperatures at pressures of 4–8 GPa; fully metallic behaviour is present at pressures greater than 8 GPa. Figure (b) clearly demonstrates that the superconductivity first develops with pressure within the non-metallic phase.

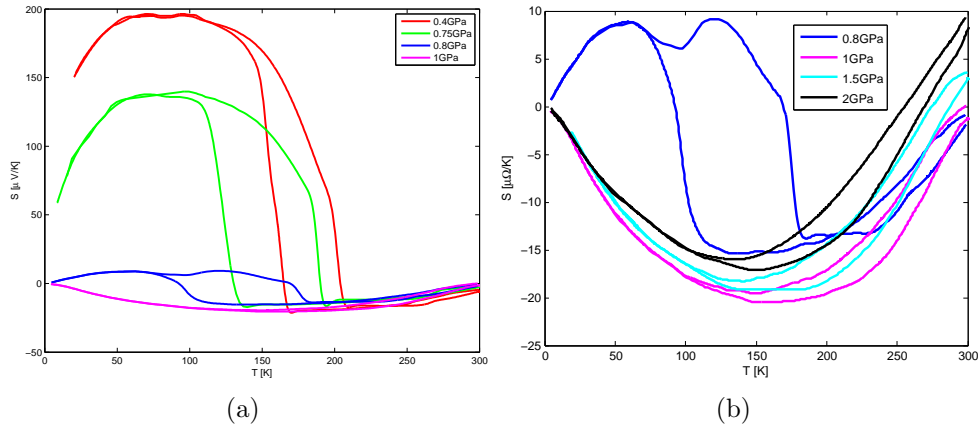


Figure 3.27: Thermoelectric power of the 1T-TaS₂ in two different pressure range. The figure (a) shows a broader pressure scan from 0–0.2 GPa, whereas the (b) is a zoom on the higher (0.8–2 GPa) pressure range

completely disappears.

At low temperatures the resistivity saturates to finite residual values that shift lower and lower as the pressure is increased. The transition from the incommensurate to the nearly commensurate CDW phase appears as an increase in the resistivity in the temperature range of 120–300 K for the whole pressure range. The first confirmed signatures of superconductivity appear at 1.5 K and 2.5 GPa. The superconductivity arises from the *non-metallic* low temperature phase, which continuously evolves from the NCCDW state at ambient pressure.

In addition, at around 4–5 GPa, the resistivity saturates to a plateau-like temperature dependence below 50 K. The value of this low temperature residual resistivity drops as the pressure increases, and a metallic-like signature stabilizes in the low temperature ranges. Above 8 GPa, the resistivity is metallic over the entire investigated temperature range, although the temperature dependence remains unconventional.

Let me summarize my findings in a pressure-temperature phase diagram (Fig. 3.28). The Mott localization and the CCDW phase are fully suppressed at pressures of about 0.8 GPa. The NCCDW phase persists to pressures of 7 GPa and may be visualised as roughly hexagonal CDW domains suspended in

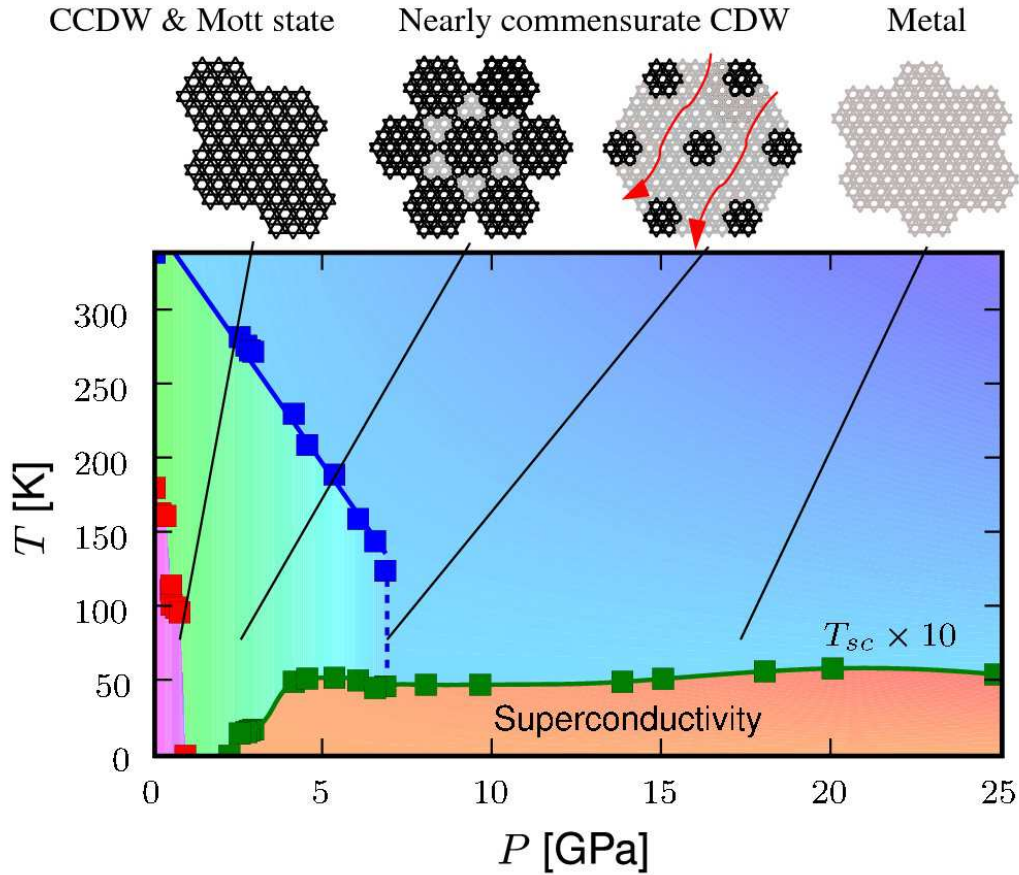


Figure 3.28: The temperature-pressure phase diagram of 1T-TaS₂. The Mott localization is suppressed, closely accompanied by the melting of the commensurate CDW phase at a pressure of 0.8 GPa; the lattice structure in the latter phase is composed of interlocking David stars. The nearly commensurate CDW phase extends over the pressure range of 1–7 GPa, and may be visualised as roughly hexagonal domains suspended in an interdomain phase, indicated in gray. The first signatures of superconductivity appear from the nearly commensurate CDW state, and remain roughly at 5 K throughout the entire pressure range of 3–25 GPa. In the pressure range of 8–25 GPa the system is metallic over the investigated temperature range when above the superconducting transition temperature. The drawing above the phase diagram indicates the probable deformation patterns in the system at low temperature, as discussed in the text.

an interdomain phase [35, 32]. The domains are expected to become progressively smaller as the pressure increases. The first signatures of superconductivity appear in the NCCDW phase and remain roughly at 5 K throughout the entire pressure range of 3–25 GPa. For pressures of 8–25 GPa the system is metallic over the investigated temperature range when above the superconducting transition temperature.

The questions which emerges from this new phase diagram address the melting of the CCDW Mott state, the origin of the textured NCCDW phase in relation to that state, the appearance of superconductivity in a pristine 1T system, which remains apparently insensitive to both pressure and the melting of the charge order.

3.3.4 Discussion

The exceptional assembly of electron-phonon coupling, nesting effects and Coulomb interaction combine to construct the elaborate phase space of 1T-TaS₂. In order to understand the many complexities of this system it is important to consider the microscopics of the different phases at ambient pressure and their possible evolution under pressure. I will address each of the above posed questions separately.

Meltdown of the Mott phase

The standard way of influencing the Mott phase is to affect the ratio between the Coulomb repulsion and the bandwidth. These two relevant energy scales correspond to the parameters U and t of the single-band Hubbard Hamiltonian, usually used to describe the Mott transition (Eq. 2.1). For the special case of the triangular lattice of David stars in 1T-TaS₂, t and U map to the overlap of the electronic wave functions defined by the deformation localized at David stars, and the Coulomb interaction of the electrons above the gap within the same David star, respectively.

The qualitative understanding of the observed phase transition comes from the insight that pressure changes both of the relevant energy scales, by decreasing the swelling of the planes related to the David star deformations in the CDW state. In particular, by reducing the deformation, the pressure diminishes the CDW gap and increases the screening capacity of the electrons below the gap (i.e. the inter-band contribution to the dielectric function)). Similarly, the pressure also weakens the potential that defines the local wavefunction, thereby increasing its extension and the wavefunction overlap integral. Both of these mechanisms simultaneously increase t and decrease U , leading to a decrease in the ratio U/t . The Mott state melting occurs naturally at a critical value of this ratio [51].

Nature of the textured phase

Since the nearly-commensurate phase is created from domains, containing David-star structures, where the Coulomb interaction plays one of the key roles, it is impossible to avoid its effect in the theoretical description of the NCCDW phase.

I fully include this aspect of the charge transfer, when considering the formation of domains in the NCCDW phase in 1T-TaS₂. The two limiting cases of this charge relocation leave the domains either as a lightly (self-)doped Mott state, or fully depleted, where all the extra electrons are in the interdomain space. I compare the Coulomb energy per particle involved in the formation of fully depleted domains, E_c with the electronic energy gap Δ in the domains. The case of $E_c \sim \Delta$ implies a Coulomb controlled textured phase. The alternatives, unrestricted by the long range Coulomb forces, relate to $E_c \ll \Delta$ and $E_c \gg \Delta$ signifying fully depleted and slightly doped Mott phase domains, respectively. Figure 3.29 shows the results of a calculation, for different domain sizes and organization in successive layers. The calculation is performed for a Kagome patchwork with two different stacking alignments. (For the details of the calculation see App. A) Stacking A considers an axial alignment of domains and interdomain triangles in successive layers, and has been experimentally observed in 1T-TaS₂ (see Fig. 3.29, Stacking A). The shifted positions of the domains between adjacent planes resem-

ble a closely packed face centered cubic (FCC) structure [35]. Stacking B refers to a hypothetical case of an exact axial superposition of the domains between the planes, for comparison (see Fig. 3.29, Stacking B). The calculation shows that the deviation from the observed Stacking A structure induces a big change in the Coulomb energy. The calculations demonstrate that the experimentally observed stacking and sizes of the domains support Coulomb controlled texturing and depletion of the domains.

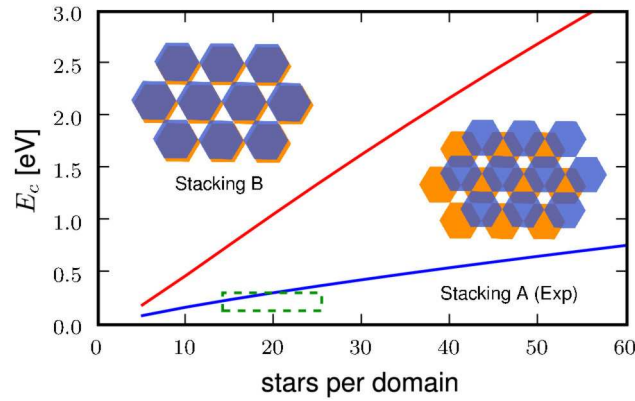


Figure 3.29: The results for the Coulomb energy calculation for two different domain stacking as a function of domain size. The lower line (blue), corresponds to an axial arrangement of domains (hexagonal) and interdomain spaces (triangular) between adjacent layers (stacking A), as deduced from experiment [35]; the upper line (red) shows, for comparison, the Coulomb energy for a hypothetical axial domain stacking between successive layers (stacking B). The green dashed box depicts the values of domain sizes that were experimentally observed in the NCCDW phase at ambient pressure. We note that the Coulomb energies calculated for these values are comparable to the energy of the gap, hinting at a possible Coulomb-controlled phase separation.

We can conclude that the NCCDW phase of 1T-TaS₂ at ambient pressure, is an example of a Coulomb-interaction controlled and commensurability driven electronic phase separation. This state extends to very low temperature upon pressurization, where superconductivity occurs.

Superconductivity in the textured phase

Within the conventional picture, the CDW and superconducting ground states compete against each other, because both result in a gapping of the single-particle electronic spectra at the Fermi level. Indeed, the superconductivity in 1T-TaS₂ appears as soon as the fully commensurate CDW phase is suppressed at low pressures of 0.8-1 GPa, suggesting a mutual exclusion of each other. On the other hand, no notable competition is observed in the pressure range of 1–7 GPa within the NCCDW phase where the CDW and superconductivity coexist.

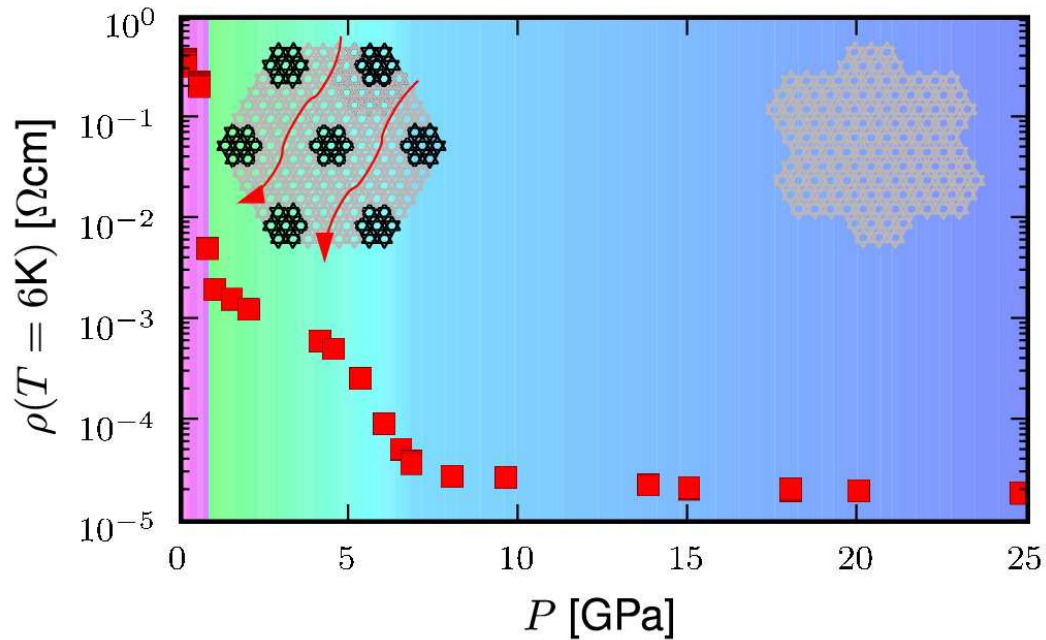


Figure 3.30: Resistivity taken at 6 K as a function of pressure. Sharp decrease in resistivity accompanies the suppression of the Mott-localised phase; linear residual resistivity pressure dependence accompanies the gradual melting of the CDW domains in the nearly commensurate CDW phases; a shoulder-like anomaly in the pressure range 4–7 GPa may be associated with the complete dissociation of the CDW domains with pressure; above 7 GPa the residual resistivity again behaves linearly with pressure. The scattering of electrons on the CCDW islands dominate the resistivity below 7 GPa

To illustrate this point we consider the behaviour of the normal-state resistivity as a function of pressure (Fig. 3.30). Technically, we take the normal-state

or the residual resistivity to be the resistivity at 6 K above 1 GPa. Below that pressure the resistivity is dominated by a variable range-hopping regime in the Mott state, (see Fig. 3.26(a)) and 6 K is just above the superconducting transition temperature in the whole pressure range. The residual resistivity decreases gradually above 1 GPa until approximately 4 GPa. This may be explained by the shrinking of the CDW domains with pressure and an increased fraction of electrons in the interdomain phase. In the pressure range of 4–7 GPa, we see a shoulder-like anomaly in this effective residual resistivity. This probably indicates a complete dissociation of the CDW domains into a uniform, fluctuating background of weak distortions. Above 7 GPa the pressure dependence of the residual resistivity is less significant. It is worthwhile noting that the residual resistivity decreases by 4 orders of magnitude between 0 and 8 GPa.

It is quite normal to assume that the superconductivity forms within the metallic interdomain spaces of the NCCDW phase. Thereby, incidentally, the competition between the CDW and superconductivity is avoided in the NCCDW phase through a phase separation in real space on a microscopic scale. Thus, the superconducting state remains rather insensitive to the size, and even the disappearance of the domains brought on by the pressure change. On the other hand, we may assume that the domains appear as scatterers of the electrons in the normal state, which would explain the manifest sensitivity of the normal-state resistivity to the collapse of the CCDW domains around a pressure of 7 GPa (Fig. 3.30).

I may postulate that the electron-phonon coupling that is inherent in the CDW state vastly helps the superconductivity in undeformed parts of the system. Combined with the phase separation on microscopic level, this would lead to the conclusion that the same parts of the Fermi surface are being affected by the CDW and the superconductivity transitions. This has been recently observed in 2H-NbSe₂ [52] — another member of the TMD compounds, where an analogous indifference of the superconductivity with respect to the CDW transition has been detected [53], with some evidence for a textured phase based on a triple

CDW state [54, 55].

Compete or coexist?

There are several pictures relating charge ordering and superconductivity that exist in the literature; all of them turn out to be inconsistent with our phase diagram. We can rule out the possibility of superconductivity rooted in a manner of a self-doped Mott phase [56, 57]. This scenario is unlikely because of a significant charge transfer from the CCDW domains to the interdomain space within the NC-CDW phase, and the insensitivity of the superconductivity to the disappearance of the CDW state. For that same reason, no sign of charge or spin-ordering fluctuations facilitating superconductivity are established to be present in 1T-TaS₂ contrary to some other low-dimensional materials [58, 59]. On the other hand, our phase diagram of 1T-TaS₂ is remarkably similar to that of some of the organic layered superconductors κ -(BEDT-TTF)₂X [60], although on a different pressure scale. Recent studies have uncovered numerous similarities, especially those revolving around the appearance of the pseudogap, between the layered organics, the superconducting cuprates and several dichalcogenide superconductors, advocating separate origins for the pseudogap and the superconducting gap [61, 62]. 1T-TaS₂ may be sited within this framework by the presence of two types of order presumably accompanied by two distinct gaps in the pressure region between 1 GPa and 7 GPa. In addition, the relation between the electronic phase separation and superconductivity has been extensively considered for the cuprate systems in the form of stripes [63, 63, 64, 65, 66], and recently observed by scanning tunneling microscopy [67].

Conclusion

I have investigated the possibility of pressure induced superconductivity in the transition metal dichalcogenides with 1T structure.

In the case of the 1T-TiSe₂ I found that pressure suppresses the charge density

wave phase, and superconductivity occurs in the pressure range of 2.0–4.0 GPa. This range remarkably coincides with the short range fluctuating CDW before its disappearance at the upper pressure value. By looking the pressure dependence of the thermoelectric power we found further evidence that the mechanism responsible for the CDW formation is excitonic. Those two findings suggest that excitonic interactions can be the origin of the superconductivity as well.

In 1T-TaS₂, the interplay between charge density waves and superconductivity, spanning from the localized CCDW Mott phase to unconventional metallic states is readily and controllably tuneable by the application of external pressure. Although the superconducting phase shares a few common features with the superconductivity in a number of layered superconductors that have been subject to extensive interest in recent years, there are a number of key differences. The remarkable insensitivity of the superconducting phase to the changes in the normal state; the development of a Mott phase at low pressures as well as an exceptional variety of CDW phases, among those the textured non-metallic phase that hosts superconductivity. All combined, they emphasize the importance of this material in the still perplexing field of electronic collective phenomena. In the future 1T-TaS₂ would particularly benefit from further studies of the normal and superconducting states under pressure, by X-ray structural , Raman and infrared measurements.

Bibliography

- [1] B. W. Pfalzgraf and H. Spreckels. The anisotropy of the upper critical field H_{c2} and electrical resistivity in 2H-NbS₂. *Journal of Physics C: Solid State Physics*, 20(27):4359–4367, 1987.
- [2] Qiao Yan-Bin, Li Yan-Ling, Zhong Guo-Hua, Zeng Zhi, and Qin Xiao-Ying. Anisotropic properties of TaS₂. *Chinese Physics*, 16(12):3809–3814, 2007.
- [3] Ray Leslie Withers, Carlos Otero-Diaz, Adrian Gomez-Herrero, A.R. Landa-Canovas, Albert Prodan, Herman J.P. van Midden, and Lasse Norén. Compositionally modulated Fermi surfaces, structured diffuse scattering and ternary derivatives of 1T-TaS₂. *Journal of Solid State Chemistry*, 178(10):3159–3168, October 2005.
- [4] R. H. Friend and A. D. Yoffe. Electronic properties of intercalation complexes of the transition metal dichalcogenides. *Adv. in Phys.*, 36:1, November 1987.
- [5] F. R. Gamble, J. H. Osiecki, M. Cais, R. Pisharody, F. J. DiSalvo, and T. H. Geballe. Intercalation complexes of lewis bases and layered sulfides: A large class of new superconductors. *Science*, 174(4008):493–497, October 1971.
- [6] F. R. Gamble, J. H. Osiecki, and F. J. DiSalvo. Some superconducting intercalation complexes of TaS₂ and substituted pyridines. *J. Chem. Phys.*, 55(7):3525–3530, October 1971.

- [7] E. Ehrenfreund, A. C. Gossard, and F. R. Gamble. Field gradient induced by organic intercalation of superconducting layered dichalcogenides. *Phys. Rev. B*, 5(5):1708–1711, Mar 1972.
- [8] F. J. Di Salvo, D. E. Moncton, and J. V. Waszczak. Electronic properties and superlattice formation in the semimetal TiSe_2 . *Phys. Rev. B*, 14(10):4321–4328, Nov 1976.
- [9] R. M. White and G. Lucovsky. Suppression of anti-ferroelectricity in TiSe_2 by excess carriers. *Nuovo Cimento Della Societa Italiana Di Fisica B-General Physics Relativity Astronomy And Mathematical Physics And Methods*, 38(2):280–289, 1977.
- [10] A. Bussmann-Holder and H. Buttner. Charge-density-wave formation in TiSe_2 driven by an incipient antiferroelectric instability. *Journal Of Physics-Condensed Matter*, 14(34):7973–7979, September 2002.
- [11] H P Hughes and W Y Liang. Vacuum ultraviolet reflectivity spectra of the disulphides and diselenides of titanium, zirconium and hafnium. *Journal of Physics C: Solid State Physics*, 10(7):1079–1087, 1977.
- [12] Myung Hwan Whangbo and Enric Canadell. Analogies between the concepts of molecular chemistry and solid-state physics concerning structural instabilities. electronic origin of the structural modulations in layered transition metal dichalcogenides. *J. Am. Chem. Soc.*, 114(24):9587–9600, November 1992.
- [13] K. Motizuki, N. Suzuki, Y. Yoshida, and Y. Takaoka. Role of electron-lattice interaction in lattice-dynamics and lattice instability of 1T- TiSe_2 . *Solid State Communications*, 40(11):995–998, 1981.
- [14] K. Motizuki, Y. Yoshida, and Y. Takaoka. Lattice instability of 1T- TiSe_2 . *Physica B & C*, 105(1-3):357–360, 1981.

-
- [15] Y. Takaoka and K. Motizuki. Lattice-dynamics of 1T-TiSe₂. *Journal Of The Physical Society Of Japan*, 49(5):1838–1844, 1980.
- [16] N. Suzuki, A. Yamamoto, and K. Motizuki. Microscopic theory of the CDW state of 1T-TiSe₂. *Journal Of The Physical Society Of Japan*, 54(12):4668–4679, 1985.
- [17] K. Rossnagel, L. Kipp, and M. Skibowski. Charge-density-wave phase transition in 1T-TiSe₂ excitonic insulator versus band-type Jahn-Teller mechanism. *Phys. Rev. B*, 65(23):235101, May 2002.
- [18] John A. Wilson. Concerning the semimetallic characters of TiS₂ and TiSe₂. *Solid State Communications*, 22(9):551–553, June 1977.
- [19] J. A. Wilson. Modelling the contrasting semimetallic characters of TiS₂ and TiSe₂. *Physica Status Solidi (b)*, 86(1):11–36, 1978.
- [20] R. S. Knox. *Solid State Phys. Suppl.*, volume 5. Academic Press, New York, 1963.
- [21] W. Kohn. Excitonic phases. *Phys. Rev. Lett.*, 19(8):439–442, Aug 1967.
- [22] H. Cercellier, C. Monney, F. Clerc, C. Battaglia, L. Despont, M. G. Garnier, H. Beck, P. Aebi, L. Patthey, H. Berger, and L. Forro. Evidence for an excitonic insulator phase in 1T-TiSe₂. *Physical Review Letters*, 99(14):146403, 2007.
- [23] E. Morosan, H. W. Zandbergen, B. S. Dennis, J. W. G. Bos, Y. Onose, T. Klimczuk, A. P. Ramirez, N. P. Ong, and R. J. Cava. Superconductivity in Cu_xTiSe₂. *Nat. Phys.*, 2(8):544, August 2006.
- [24] J. F. Zhao, H. W. Ou, G. Wu, B. P. Xie, Y. Zhang, D. W. Shen, J. Wei, L. X. Yang, J. K. Dong, M. Arita, H. Namatame, M. Taniguchi, X. H. Chen, and D. L. Feng. Evolution of the electronic structure of 1t-cuxtise2. *Physical Review Letters*, 99(14):146401, October 2007.

- [25] S. Y. Li, G. Wu, X. H. Chen, and Louis Taillefer. Single-gap s-wave superconductivity near the charge-density-wave quantum critical point in Cu_xTiSe_2 . *Physical Review Letters*, 99(10):107001, 2007.
- [26] S. L. Bud'ko, P. C. Canfield, E. Morosan, R. J. Cava, and G. M. Schmiedeshoff. Thermal expansion and effect of pressure on superconductivity in Cu_xTiSe_2 . *Journal of Physics: Condensed Matter*, 19(17):176230–, 2007.
- [27] C. Bansal and K. Surendranath. Thermopower behaviour of incommensurate charge density wave systems – (nbse4)10/3 i and (tase4)2i. *Solid State Communications*, 76(2):209–212, October 1990.
- [28] S. Maekawa, H. Ebisawa, and H. Fukuyama. Upper critical-field in two-dimensional superconductors. *Journal Of The Physical Society Of Japan*, 52(4):1352–1360, 1983.
- [29] M. Ikebe, H. Fujishiro, Y. Obi, H. Fujimori, and S. Morohashi. On anomalous temperature dependence of $h_{C_2}^\perp$ in natural and artificial layer superconductors. *Physica C: Superconductivity*, 317-318:142–148, May 1999.
- [30] G. Wu, H. X. Yang, L. Zhao, X. G. Luo, T. Wu, G. Y. Wang, and X. H. Chen. Transport properties of single-crystalline Cu_xTiSe_2 (0.015 $\leq x \leq$ 0.110). *Phys. Rev. B*, 76(2):024513–5, July 2007.
- [31] T. Isa, M. Sasaki, G.R. Wu, Y. Isobe, W.X. Gao, and H. Ozaki. Charge density wave domain originated Altshuler-Aronov-Spivak effect in 1T-TaS₂ single crystal. *Physica Status Solidi (b)*, 229(3):1111, 2002.
- [32] R. E. Thomson, B. Burk, A. Zettl, and John Clarke. Scanning tunneling microscopy of the charge-density-wave structure in 1T-TaS₂. *Phys. Rev. B*, 49(24):16899–16916, Jun 1994.

-
- [33] J. A. Wilson, F. J. Di Salvo, and S. Mahajan. Charge density waves and superlattices in metallic layered transition-metal dichalcogenides. *Adv. in Phys.*, 24(2):117, 1975.
- [34] B. Dardel, M. Grioni, D. Malterre, P. Weibel, Y. Baer, and F. Lévy. Spectroscopic signatures of phase transitions in a charge-density-wave system: 1T-TaS₂. *Phys. Rev. B*, 46(12):7407–7412, Sep 1992.
- [35] A. Spijkerman, J. L. de Boer, A. Meetsma, G. A. Wiegers, and S. van Smaalen. X-ray crystal-structure refinement of the nearly commensurate phase of 1T-TaS₂ in (3 + 2)-dimensional superspace. *Phys. Rev. B*, 56(21):13757, Dec 1997.
- [36] Xian Liang Wu and Charles M. Lieber. Direct observation of growth and melting of the hexagonal-domain charge-density-wave phase in 1T-TaS₂ by scanning tunneling microscopy. *Phys. Rev. Lett.*, 64(10):1150–1153, Mar 1990.
- [37] W. L. McMillan. Theory of discommensurations and the commensurate-incommensurate charge density wave phase transition. *Phys. Rev. B*, 14(4):1496, Aug 1976.
- [38] K. Nakanishi and H. Shiba. Theory of 3-dimensional orderings of charge density waves in 1T-TaS₂. *J. Phys. Soc. Jpn.*, 53(3):1103, 1984.
- [39] S. Brazovskii. Solitons and their arrays: From quasi 1D conductors to stripes. *Jour. Of Sup. Cond. And Nov. Mag.*, 20:489, 2007.
- [40] K. Rossnagel and N. V. Smith. Spin-orbit coupling in the band structure of reconstructed 1T-TaS₂. *Phys. Rev. B*, 73(7):073106, 2006.
- [41] P. Fazekas and E. Tosatti. Charge carrier localization in pure and doped 1T-TaS₂. *Physica B & C*, 99(1-4):183, 1980.

- [42] P. Fazekas and E. Tosatti. Electrical, structural and magnetic-properties of pure and doped 1T-TaS₂. *Philos. Mag. B*, 39(3):229, 1979.
- [43] F. Zwick, H. Berger, I. Vobornik, G. Margaritondo, L. Forró, C. Beeli, M. Onellion, G. Panaccione, A. Taleb-Ibrahimi, and M. Grioni. Spectral consequences of broken phase coherence in 1T-TaS₂. *Phys. Rev. Lett.*, 81(5):1058, Aug 1998.
- [44] Th. Pillo, J. Hayoz, H. Berger, R. Fasel, L. Schlapbach, and P. Aebi. Interplay between electron-electron interaction and electron-phonon coupling near the Fermi surface of 1T-TaS₂. *Phys. Rev. B*, 62(7):4277, Aug 2000.
- [45] J. A. Wilson. Questions concerning the form taken by the charge density wave and the accompanying periodic-structural distortions in 2H-TaSe₂, and closely related materials. *Phys. Rev. B*, 17(10):3880, May 1978.
- [46] M. Bovet, S. van Smaalen, H. Berger, R. Gaal, L. Forró, L. Schlapbach, and P. Aebi. Interplane coupling in the quasi-two-dimensional 1T-TaS₂. *Phys. Rev. B*, 67(12):125105, Mar 2003.
- [47] F. J. Di Salvo, J. A. Wilson, B. G. Bagley, and J. V. Waszczak. Effects of doping on charge density waves in layer compounds. *Phys. Rev. B*, 12(6):2220, Sep 1975.
- [48] H. Mutka, L. Zuppiroli, P. Molinié, and J. C. Bourgoin. Charge-density waves and localization in electron-irradiated 1T-TaS₂. *Phys. Rev. B*, 23(10):5030, May 1981.
- [49] T. Tani, T. Osada, and S. Tanaka. The pressure effect on the CDW-transition temperatures in 1T-TaS₂. *Solid State Commun.*, 22(4):269, April 1977.
- [50] T. Butz, A. Vasquez, H. Saitovitch, G. M. Kalvius, and A. Lerf. Charge density wave effects, structural effects and charge transfer in the layered compound TaS₂. *Hyperfine Interactions*, 4(1):798–802, January 1978.

-
- [51] M. Capone, L. Capriotti, F. Becca, and S. Caprara. Mott metal-insulator transition in the half-filled Hubbard model on the triangular lattice. *Phys. Rev. B*, 63(8):085104, Feb 2001.
- [52] T. Kiss, T. Yokoya, A. Chainani, S. Shin, T. Hanaguri, M. Nohara, and H. Takagi. Charge-order-maximized momentum-dependent superconductivity. *Nat. Phys.*, 3(10):720, October 2007.
- [53] A. M. Gabovich, A. I. Voitenko, J. F. Annett, and M. Ausloos. Charge- and spin-density wave superconductors. *Sup. Sci. and Tech.*, 14(4):R1, 2001.
- [54] D. E. Moncton, J. D. Axe, and F. J. Di Salvo. Study of superlattice formation in 2H-NbSe₂ and 2H-TaSe₂ by neutron scattering. *Phys. Rev. Lett.*, 34(12):734, Mar 1975.
- [55] W. Sacks, D. Roditchev, and J. Klein. Voltage-dependent STM image of a charge density wave. *Phys. Rev. B*, 57(20):13118, May 1998.
- [56] P. A. Lee, N. Naoto, and W. Xiao-Gang. Doping a Mott insulator: Physics of high-temperature superconductivity. *Rev. Mod. Phys.*, 78(1):17, 2006.
- [57] G. Baskaran. Mott insulator to high T_c superconductor via pressure: resonating valence bond theory and prediction of new systems. *Phys. Rev. Lett.*, 90(19):197007, May 2003.
- [58] J. Merino and R. H. McKenzie. Superconductivity mediated by charge fluctuations in layered molecular crystals. *Phys. Rev. Lett.*, 87(23):237002, Nov 2001.
- [59] D. Jérôme. The physics of organic superconductors. *Science*, 252(5012):1509, 1991.
- [60] M.-S. Nam, A. Ardavan, S. J. Blundell, and J. A. Schlueter. Fluctuating superconductivity in organic molecular metals close to the Mott transition. *Nature*, 449(7162):584, October 2007.

- [61] R. A. Klemm. Striking similarities between the pseudogap phenomena in cuprates and in layered organic and dichalcogenide superconductors. *Physica C*, 341-348(Part 2):839, November 2000.
- [62] R. H. McKenzie. Similarities between organic and cuprate superconductors. *Science*, 278(5339):820, 1997.
- [63] V. J. Emery and S. A. Kivelson. Frustrated electronic phase separation and high-temperature superconductors. *Physica C: Superconductivity*, 209(4):597, May 1993.
- [64] EW Carlson, VJ Emery, SA Kiveslon, and D. Ograd. *The Physics Of Conventional And Unconventional Superconductors*. Springer-Verlag, Berlin, 2003.
- [65] K. A. Müller and G. Benedek, editors. *Phase Separation In Cuprate Superconductors*. World Scientific, Singapore, 1993.
- [66] S. A. Kivelson, I. P. Bindloss, E. Fradkin, V. Oganesyan, J. M. Tranquada, A. Kapitulnik, and C. Howald. How to detect fluctuating stripes in the high-temperature superconductors. *Rev. Mod. Phys.*, 75(4):1201, Oct 2003.
- [67] Y. Kohsaka, C. Taylor, K. Fujita, A. Schmidt, C. Lupien, T. Hanaguri, M. Azuma, M. Takano, H. Eisaki, H. Takagi, S. Uchida, and J. C. Davis. An intrinsic bond-centered electronic glass with unidirectional domains in underdoped cuprates. *Science*, 315(5817):1380, 2007.

Chapter 4

Underdoped $\text{Bi}_2\text{Sr}_2\text{CaCu}_2\text{O}_{8-\delta}$ high T_c superconductor

The high temperature superconductivity in a copper-oxide family has been discovered in 1986 by Bednorz and Müller. This discovery by all means has revolutionized solid state physics, at least the sub-field of strongly correlated materials. Despite the more than two decades elapsed, the solution of the high T_c is still missing. This is due to difficulties both in theoretical description of a doped Mott insulator and the complexity of the materials showing this phenomenon. Some theoretical models, e.g. $t - J$ model, rely on the importance of magnetic interaction in the coupling of charges into Cooper pairs, since the parent compound is an antiferromagnetic Mott insulator which doping with charges shows the zero resistance state. Recently, ARPES measurements have shown the presence of strong electron-phonon coupling in these materials, which have revitalized models which put this interaction in the first plan. From the experimental point of view one of the greatest challenge is the sample quality. Most of these materials consist of 4-5 different elements. It is difficult to achieve a high chemical and structural order in single crystals. This is especially true for the samples in which underdoping is required by substituting one element for another (e.g. Ca or Pr) or by oxygen depletion. Nevertheless, it is a general opinion that in-depth study of underdoped

cuprates is primordial for the unraveling of the high- T_c phenomenon.

One of the claims in this field is that the ground state of the underdoped cuprates is insulating. This notion was based on the observations that one superconductivity is suppressed by high magnetic field, the temperature dependence of the resistivity is that of a semiconductor and not that of a metal. Our conjecture was that the origin of this observation is sample inhomogeneity. After suppressing the superconducting state, the non-metallic part of the sample is dominating the overall response.

Since in our Institute we have an excellent single crystal growing facility, where high quality underdoped crystals have been made, we have decided to address this issue in this thesis. Magnetic fields up to 16 Tesla were applied in our laboratory for certain samples, but the major part of the measurements was carried out in the 50 T pulsed field facility of the Laboratory of Pulsed Magnetic Fields in Toulouse.

4.1 Introduction

High- T_c cuprates are quasi two dimensional materials. In their structure the central part is the conducting copper-oxygen plain (bi-layer or tri-layer in certain families) which is separated by several other insulating oxide planes. A copper oxygen plane is represented in figure 4.1. by the sketch of the atomic orbitals which determine the electronic structure of these materials. 4.1. Among the cuprates $\text{Bi}_2\text{Sr}_2\text{CaCu}_2\text{O}_8$ and its derivatives have the strongest anisotropy in their transport properties between in-plane and out-of-plane behaviors [1] (of the order of $10^5 - 10^6$) and therefore are the most 2D conductors among the high- T_c cuprates. The idealized crystal structure of $\text{Bi}_2\text{Sr}_2\text{CaCu}_2\text{O}_8$ is shown in Figure 4.2. It should be noted, however, that excess oxygen atoms are incorporated in the BiO plane, resulting in a clear superstructure modulations [2] which is believed not to have a major influence on T_c . The T_c of $\text{Bi}_2\text{Sr}_2\text{CaCu}_2\text{O}_8$ can be controlled by changing the oxygen stoichiometry (annealing in oxygen or in a vac-

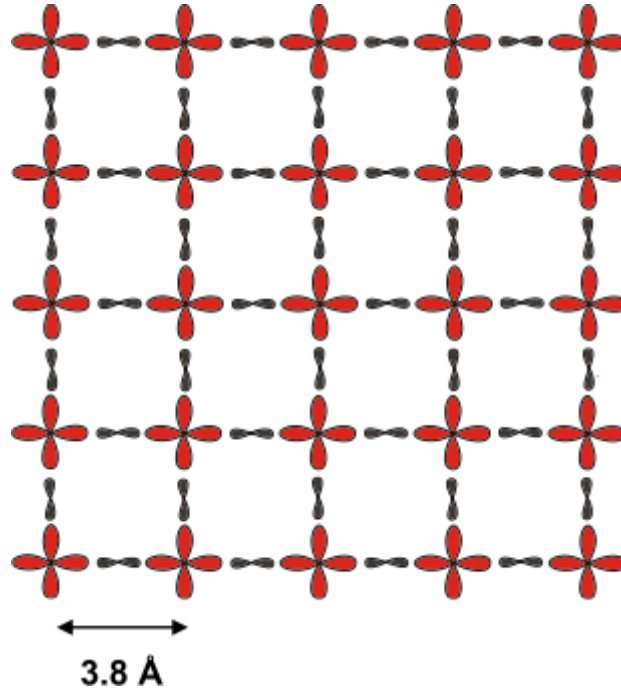


Figure 4.1: The structure of the copper oxygen plane. Copper (red) is represented with the $3d^9$ $d_{x^2-y^2}$ orbital, and oxygen (black) with the closed 2p shell.

uum) or by substituting Y, Pr or other rare-earth elements for Ca. The highest T_c for this compound is 95 K. To the carrier concentration of 0.16 hole/Cu corresponding to this T_c the name of optimum doping is attributed. Below and above this carrier concentration we are speaking of underdoped and overdoped cuprates. As-grown $\text{Bi}_2\text{Sr}_2\text{CaCu}_2\text{O}_8$ samples are close to the optimum doping ($T_c \sim 90$ K). Holes are depleted in the Y or Pr substituted samples $\text{Bi}_2\text{Sr}_2\text{Ca}_{1-x}\text{Y}_x\text{Cu}_2\text{O}_8$, and they become insulating ($T_c = 0$ at around $x \sim 0.5$).

The electronic structure of $\text{Bi}_2\text{Sr}_2\text{CaCu}_2\text{O}_8$ has been extensively studied by various electron spectroscopic techniques, including angle-resolved photoemission spectroscopy (ARPES) [3, 4, 5] because of the high quality and stability of cleaved surfaces. One of the latest issues coming from these measurements, in the notion of the two energy gaps in the superconducting state. The superconducting gap – an energy scale tied to the superconducting phenomena – opens on the Fermi surface at the superconducting transition temperature in conventional BCS su-

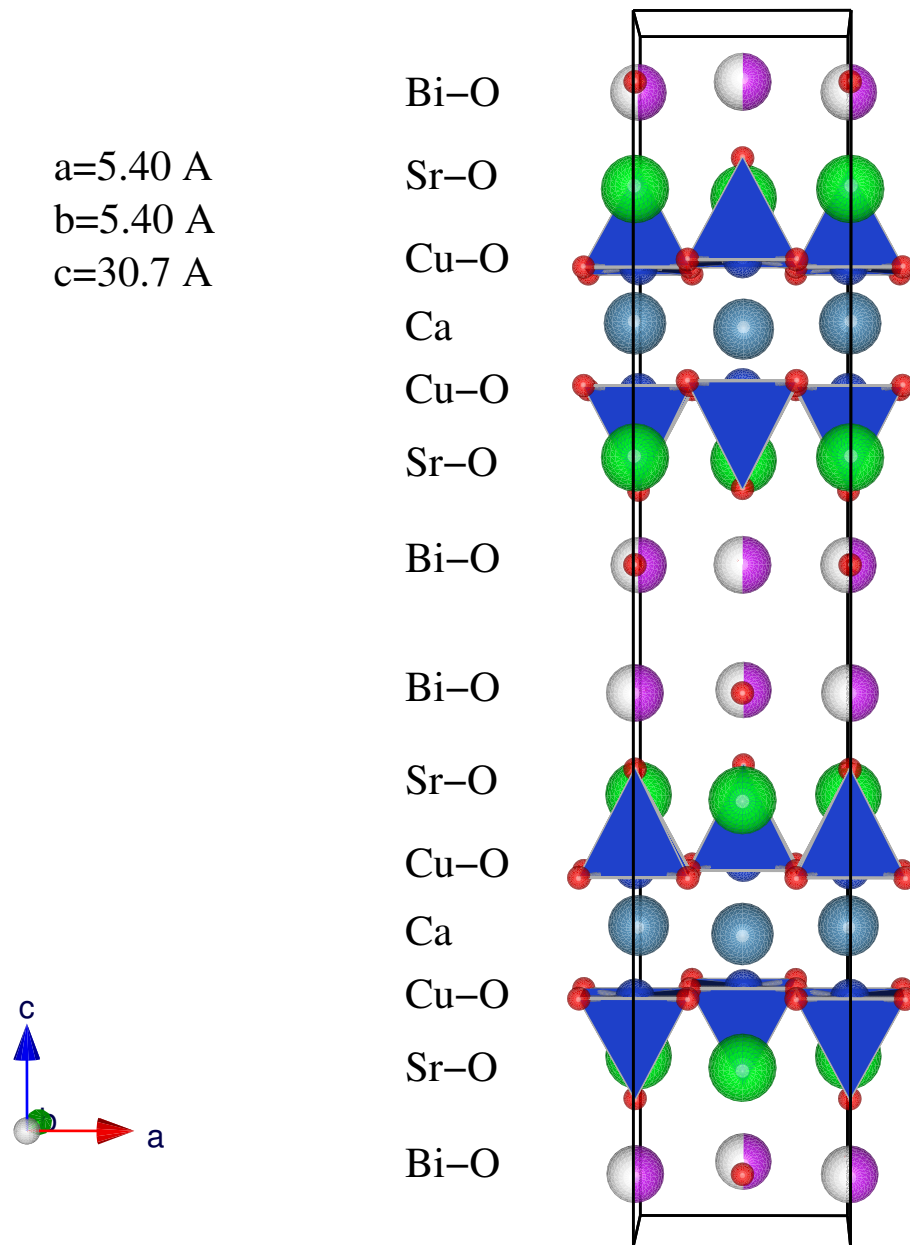


Figure 4.2: The unit cell of the $\text{Bi}_2\text{Sr}_2\text{CaCu}_2\text{O}_8$ with the lattice parameters.

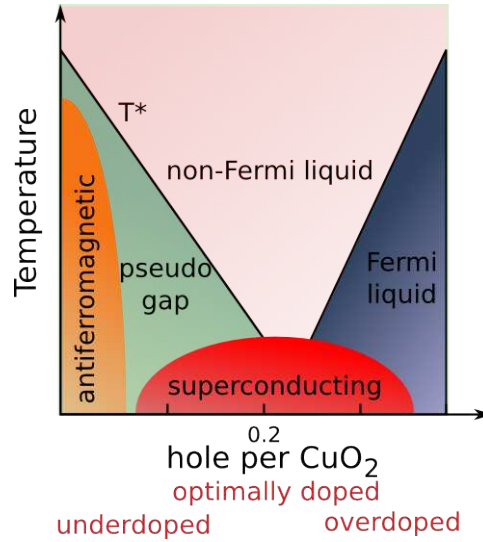


Figure 4.3: The phase diagram of $\text{Bi}_2\text{Sr}_2\text{CaCu}_2\text{O}_8$, as a function of hole doping p . Below the maximum T_c is the underdoped region, and above is the overdoped.

perconductors. In the high- T_c cuprates going towards the underdoped side an additional gap opening was observed, called pseudogap (opens at T^* well above T_c) which relation to the superconducting gap remains open.

Whether the pseudogap is a distinct phenomenon or coming from Cooper pairs without macroscopic phase coherence above T_c is one of the central questions in high- T_c research. Although some experimental evidence suggests that the two gaps are distinct, this issue is still under intense debate. The crucial piece of evidence to firmly establish this two-gap picture is still missing.

As mentioned above one major difficulty in the study of High- T_c superconductors is the sample quality. Due to the complex structure, cuprates tends to develop inhomogeneity, what can appear on very different length-scales. Recent high resolution scanning tunneling microscopy study showed that microscopic electronic inhomogeneity might be an intrinsic property of the High- T_c superconductors [6].

According to these measurements the local electronic density (LDOS), even in a good quality single crystal, is very inhomogeneous. In the interpretation of these measurements, due to strong Coulomb repulsion electronic phase separation

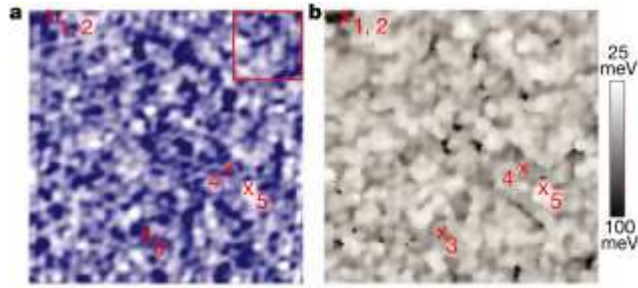


Figure 4.4: A comparison of an integrated LDOS map, and its corresponding superconducting gap map of a pure single crystal $\text{Bi}_2\text{Sr}_2\text{CaCu}_2\text{O}_8$. a) $600 \times 600 \text{ \AA}$ LDOS map measured in a constant current mode. To remove the modulation due to the well ordered topological atomic structures, Fourier filtering was used. b) Superconducting gap map, obtained simultaneously with the LDOS map on the same location, showing the spatial variation of the superconducting energy gap. The energy gap values are extracted from the corresponding local differential conductance spectra. (Figure from [6])

occurs even on a perfect lattice. The measured LDOS shows high correlation with the local superconducting properties, like the superconducting gap, what shows that even very localized changes in the electronic structure can have impact on macroscopic properties. That is very important when we look the doping dependence of any parameter of the cuprates. Alternatively to the phase separation picture, reorganization of the doping atoms can locally change the behavior of the material, and the measured average property will not be the same as it would be in the homogeneous case.

One way to follow the doping (and the inhomogeneities) is by measuring the electrical resistivity in the normal state. The resistivity of the cuprates is very sensitive to the hole concentration. Near optimal doping the material is a reasonably good metal. As one reduces the number of carriers, the resistivity increases monotonously until it reaches the metal–Mott insulator phase boundary, and becomes an insulator (Figure 4.5). One of the key question is, at what carrier concentration this transition occurs and what happens at T^* (Fig. 4.5(b)).

The overall accepted phase diagram of the cuprates, T_c versus hole/Cu (d) is established largely based on resistivity and thermopower (S) measurements. Re-

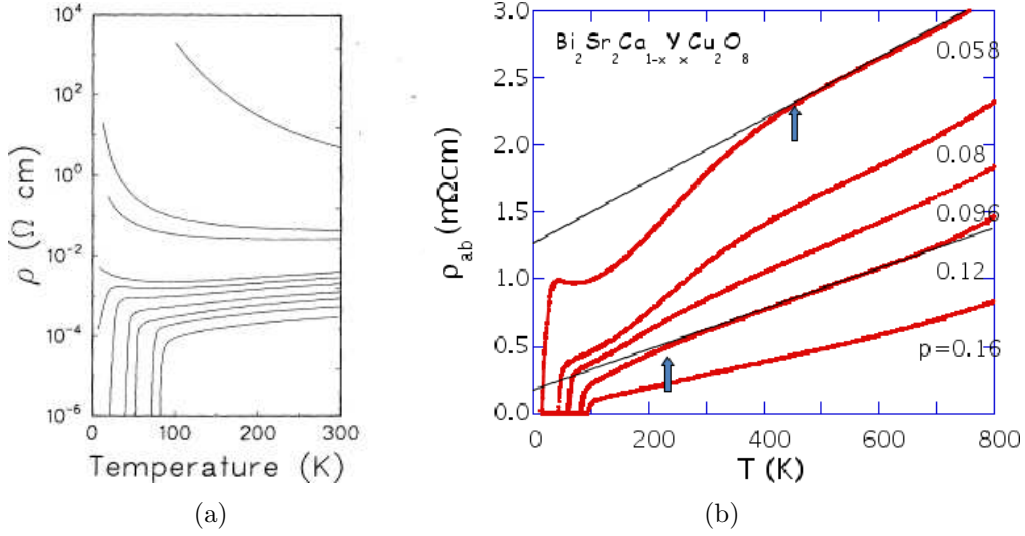


Figure 4.5: Temperature dependence of resistivity of $\text{Bi}_2\text{Sr}_2\text{Y}_x\text{Ca}_{1-x}\text{Cu}_2\text{O}_y$ samples in two different doping range. The arrow on (b) shows the opening of the pseudogap T^* . (Figure (a) from [7])

sistivity can measure precisely T_c , and there is a well accepted relation between S (300 K) and d established by Tallon and co [8, 9]. Eventually, a.c. susceptibility is also used since the appearance of shielding currents coincide with T_c . But already these measurements show the serious problem of sample homogeneity (absence of single T_c with narrow transition region) when one goes to the underdoped region. It already announces the difficulty in determining the ground state of the underdoped cuprates, that is which is the state from which superconductivity emerges.

Several research groups have addressed this question, but the clear answer is still missing. Of course, a difficulty is coming from the fact that ground state is hidden by the superconductivity. In order to have access to it, one should suppress superconductivity. There are several ways to achieve it. One is to introduce defects by irradiation with electrons [10], protons [11], or heavy ions [12]. Defects introduce pair braking (in cuprates even non-magnetic defects break up the pairs due to the d-wave symmetry) and with high enough defect concentration it is possible to suppress completely superconductivity. However, in High- T_c superconductors the carrier density is low, and there are not enough free elec-

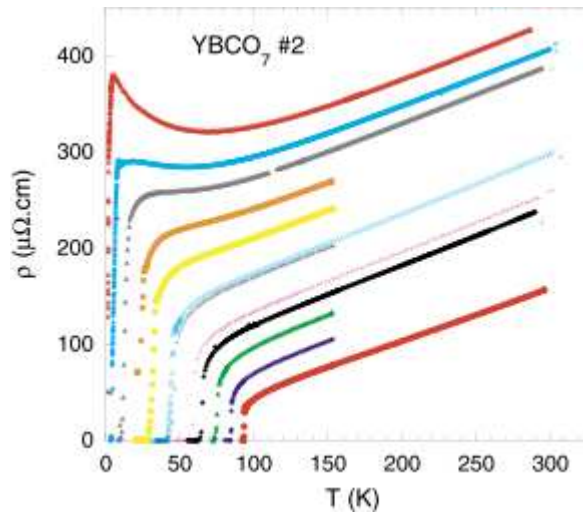


Figure 4.6: The resistivity plotted versus temperature for YBCO_7 at different impurity concentration created by irradiation with 2.5 MeV electrons. At high temperature the resistivity lines are parallel, showing that the Matthiessen's rule is well verified. (Figure from [10])

trons to screen out efficiently the disorder potential created by the impurities. They manifest as if the size of the scattering centers would grow with decreasing temperature and they introduce a non-metallic temperature dependence like in Kondo systems. This can be seen as an upturn at low temperatures in the electron irradiated YBa_2CuO_7 . (Fig. 4.6) This effect is even more important in the underdoped samples.

A better way to suppress superconductivity is to put the sample in magnetic field. High enough magnetic field brakes up the cooper pair singlets, and the material regains it's normal state. This happens at a characteristic field H_{C2} . This method is the most straightforward for bulk, low temperature BCS superconductors, where the H_{C2} is moderate and can be accessed by conventional superconducting magnets. But in the case of High- T_c superconductors the H_{C2} can be as high as 100 T, so very often pulsed magnetic fields are employed which can reach fields of 60 T.

One of the earliest measurements was performed on $\text{La}_{2-x}\text{Sr}_x\text{CuO}_4$ [13], where a logarithmic divergences of the resistivity as observed as a function of temper-

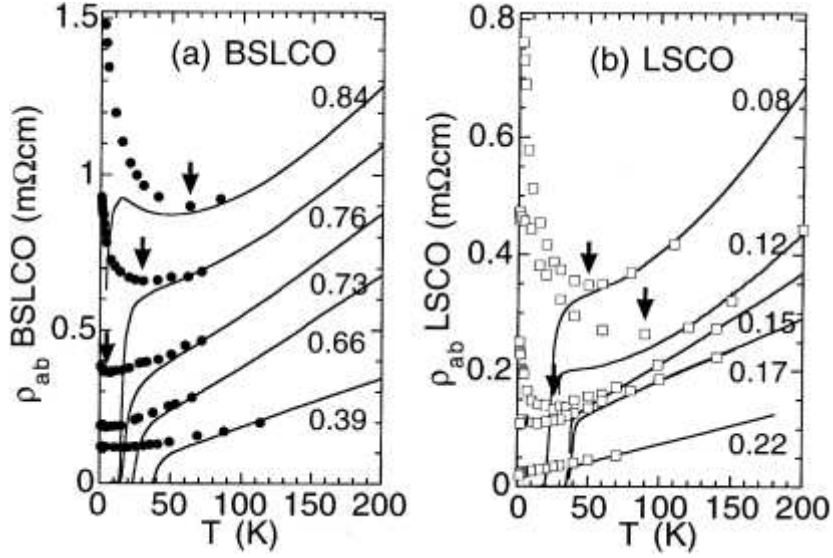


Figure 4.7: In plane resistivity versus temperature plots from samples of $\text{Ln}_2 - x\text{Sr}_x\text{CuO}_4$ and $\text{Bi}_2\text{Sr}_{2-x}\text{La}_x\text{CuO}_{7-\delta}$. Open squares denote the data taken at 60 T. The thick line is the zero field curve. The lines are labeled with the Sr content. Arrow shows the minimum of the resistivity. (Figure from [16])

ature in high magnetic fields. That measurement was followed later on with the study of $\text{Bi}_2\text{Sr}_{2-x}\text{La}_x\text{CuO}_{7-\delta}$ crystals [14, 15], where the same low temperature resistivity behavior was present (Fig. 4.7).

Based on these findings they have suggested an intriguing phase diagram for the two families of cuprate superconductors. (Fig 4.8).

The strangest thing in Fig. 4.8(a) is not the peak of T_{min} at 1/8 of hole concentration per Cu site (it is explained by commensurability effect of stripes), but the proximity of the insulating and superconducting phases in the $\sim 0.05-0.1$ hole concentration range. This suggests that the Cooper pairing happens in a non-metallic phase. The same model is proposed for BISCO in a different hole concentration range.

It is worth to mention that a follow up investigation of the magnetoresistance revealed an interesting behavior [17]. From the measurement on LSCO crystals, it looks like the magnetoresistance is saturating at high magnetic fields. Similar behavior of the magnetoresistance has been seen in the case of granu-

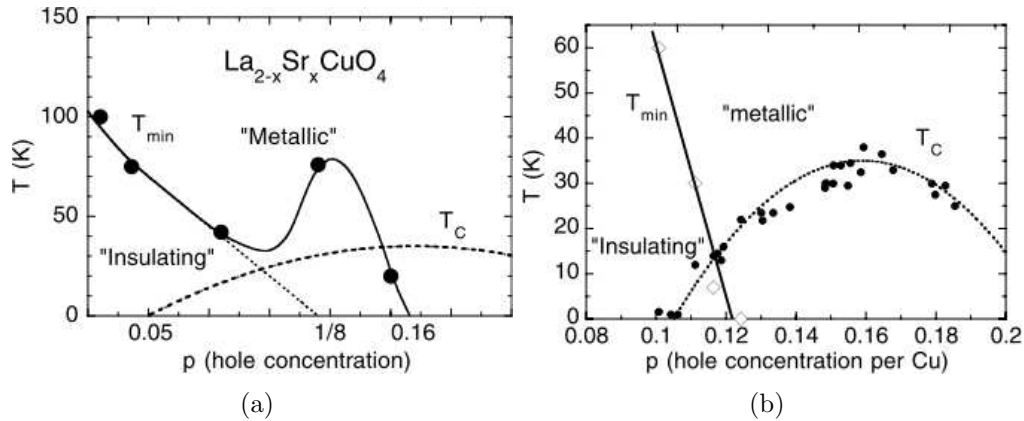


Figure 4.8: Phase diagram of $\text{La}_{2-x}\text{Sr}_x\text{CuO}_4$ (a), and $\text{Bi}_2\text{Sr}_{2-x}\text{La}_x\text{CuO}_{7-\delta}$ (b) as a function of hole concentration in high magnetic field ($B=60$ T). Solid line shows the minimum of the resistivity, dashed line follows the T_c at zero field. (Figure from [16])

lar superconducting systems, where the grains are connected by the Josephson phase-coupling. The phase what was denoted earlier as normal phase is more likely a Bose-insulator phase, where the electrons are scattered on the fluctuating Cooper-pairs. Once the magnetic field is high enough to suppress even the Cooper pairs without phase coherence the real ground state of the material appears. In the explanation of the authors the magnetic field first increases the phase fluctuations, driving the system further in the Bose-insulating phase, and then brakes the Cooper-pairs what brings the system closer to it's normal state. The competition of those two effect gives rise to a peak in the magnetoresistance. Since the fluctuations are enhanced by the small grains, or in the case of high- T_c materials domain size, one would expect that the effect will be less pronounced, or non existing in high quality samples.

4.2 Sample and measurements

My goal was to check whether the same phase boundary occurs in the case of high quality $\text{Bi}_2\text{Sr}_2\text{Pr}_x\text{Ca}_{1-x}\text{Cu}_{8-\delta}$ single crystals. In our Institute we are enjoying an in house crystal growing facility. In our attempt to underdoped the

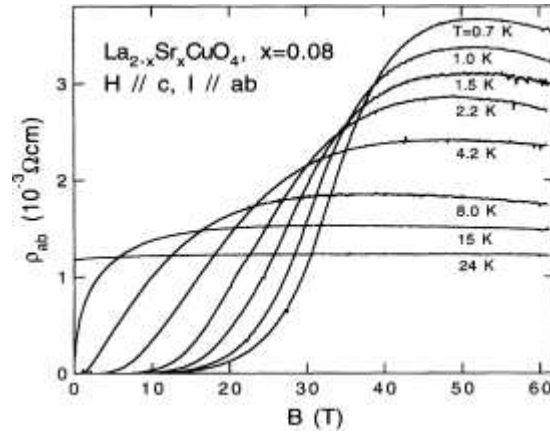


Figure 4.9: In plane resistivity ρ_{ab} versus magnetic field for the $x = 0.08$ $\text{La}_{2-x}\text{Sr}_x\text{CuO}_4$, at various temperatures (Figure from [13]).

samples we focused on lowering the T_c and keeping the crystal structure as close as possible to the optimally doped one. From large batches of single crystals with variable Pr content samples were selected with the following criteria: 1. lowest room temperature resistivity and metallic temperature dependence in the whole temperature range; 2. low residual resistivity; 3. single and relatively sharp superconducting transition. Even when extreme precautions were taken in the single crystal synthesis by the self flux method (choosing pure starting materials, crucibles, very low cooling rate of the melt) within the same batch there were considerable dispersion of T_c s. Out of 150 resistivity runs 10 crystals were selected obeying the above criteria. The lowest T_c (the highest underdoping) was 15 K, and the highest T_c in the underdoped side was 50 K. Two typical resistivity versus temperature curves are shown in magnetic field up to 16 T in figures 4.10(a) and 4.10(b). These runs clearly show the absence of upturn in resistivity but also show the need to go to higher magnetic fields. The H_{c2} is well above of 16 T for these T_c s. Most of the measurements were performed in the National Pulsed Magnetic Field Laboratory in Toulouse up to fields of 60 T.

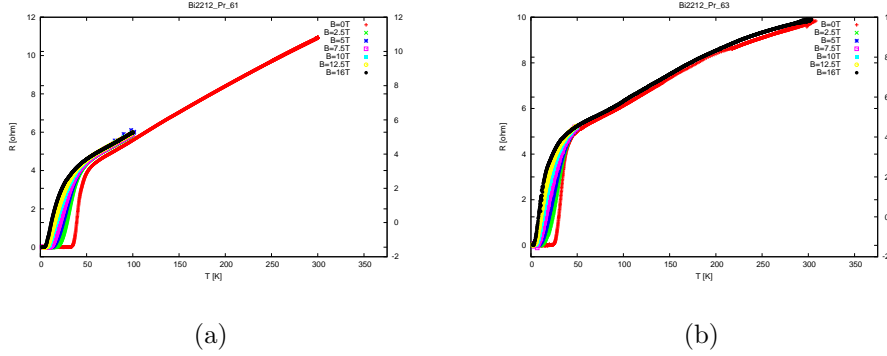


Figure 4.10: Two typical, resistivity versus temperature curves of $\text{Bi}_2\text{Sr}_2\text{Pr}_x\text{Ca}_{1-x}\text{Cu}_{8-\delta}$ under magnetic fields up to 16 T. $T_c^{(0)} = 41$ K (a) and $T_c^{(0)} = 33$ K

4.2.1 Results

From the set of measurements 3 characteristic results are shown below. To see the normal state behavior of our samples with relatively good homogeneity, I selected three of them for high magnetic field measurement. For all samples the size was chosen to be very small ($0.004 \times 0.05 \times 0.2 \text{ mm}^3$) in order to reduce further the possibility of inhomogeneities. The samples were characterized with a temperature dependent resistivity measurement (Fig. 4.11). One sample had $T_c = 50$ K (corresponding to $p = 0.085$ hole/Cu) the second had $T_c = 35$ K (corresponding to $p = 0.075$ hole/Cu) and the last one with $T_c = 15$ K (corresponding to $p = 0.058$ hole/Cu). The last sample had T_c low enough to suppress the superconducting state with 16 T of field available in our laboratory as shown in figure 4.11(a). The samples with higher T_c were measured in pulsed magnetic field. Figure 4.11(b) depicts the temperature dependence of the resistivity in several magnetic fields for T_c of 50 K. For $H = 50$ T the sample stays in the normal state in the entire temperature range.

From both of the graphs it is clear, that we can suppress superconductivity in those samples, and that the resistivity stays metallic, down to the lowest temperature reached in our experiment ($T_{min} = 1.2$ K), even if the sample is strongly underdoped and the zero field transition temperature is as low as $T = 15$ K.

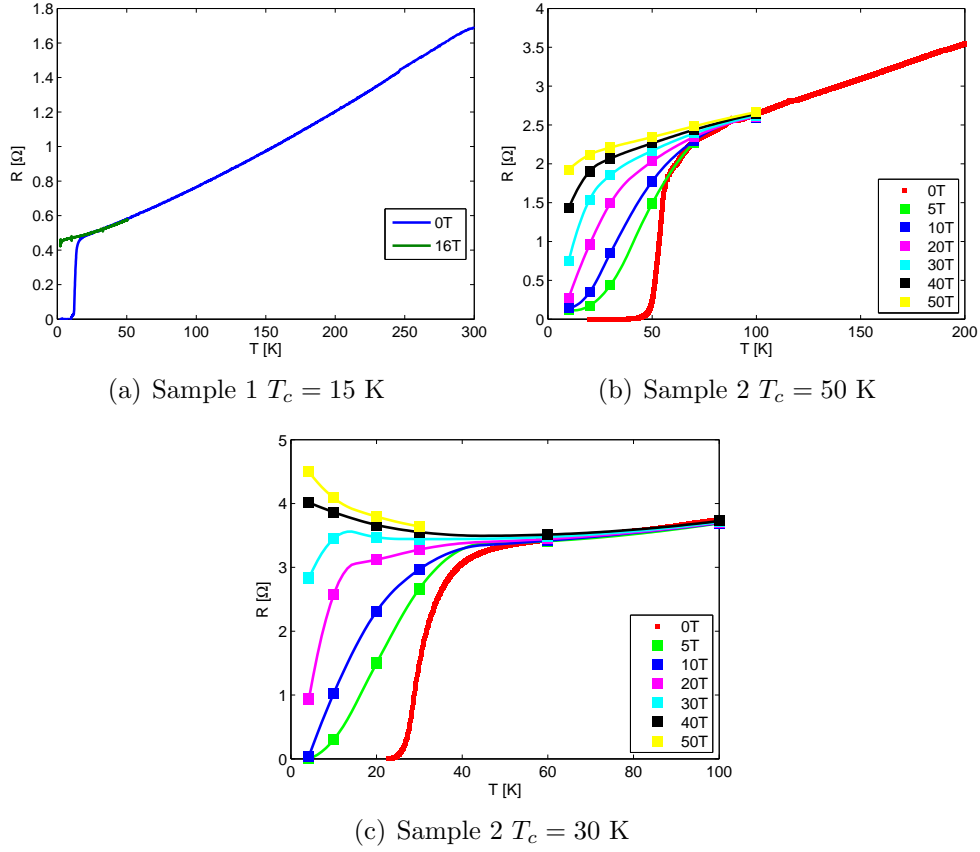


Figure 4.11: Resistivity versus temperature measurements of a Pr doped $\text{Bi}_2\text{Sr}_2\text{CaCu}_2\text{O}_{8-\delta}$ samples at different magnetic field. The zero field transition temperature of the first samples are $T_c^{(0)} = 50$ K (a), $T_c^{(0)} = 30$ K (b) $T_c^{(0)} = 15$ K (c).

These observations do not support the claims of Boebinger and co. [18] based on the high magnetic field data obtained on various underdoped cuprate families that the low temperature ground state of these samples is non-metallic. This notion is reported in Figure 4.8 as an insulator-superconductor phase boundary in the underdoped region.

What could be the origin of this discrepancy between those and our measurements. In our opinion it comes from different sample quality. It stresses the difficulty of making a good quality underdoped single crystalline cuprate superconductor.

Figure 4.11(c) shows well the difficulty in the selection of good underdoped sample. The third crystal, which has similar T_c to the second one, which has satisfied the selection criteria for a “good sample” shows a behavior close to that reported by Ono *et al.* [15]. Before giving a tentative description for this behavior lets discuss in more details samples 1 and 2.

4.2.2 Magnetoresistance in the normal state

The temperature and field dependence of the magnetoresistance of many metals can be analyzed in terms of Köhler’s rule. [19] Semiclassical transport theory based on the Boltzmann equation predicts Köhler’s rule to hold if there is a single species of charge carrier and the scattering time τ is the same at all points on the Fermi surface. The dependence of the resistance on the field is then contained in the quantity $(\omega_c\tau)$, where ω_c is the frequency at which the magnetic field H causes the charge carriers to sweep across the Fermi surface. Since the resistance in zero field is proportional to the scattering rate, the field dependence of the magnetoresistance of samples with different scattering times either due to different purity or temperature (T) can be related by rescaling the field by the zero-field resistance $\rho(0, T)$:

$$\frac{\Delta\rho}{\rho_0} = f\left(\frac{H}{\rho_0}\right) = f(\omega_c\tau) \quad (4.1)$$

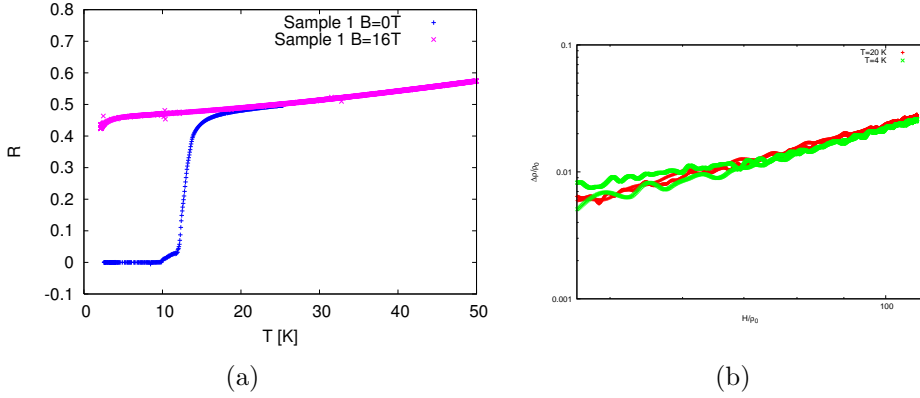


Figure 4.12: (a) A zoom on the transition of sample 1 with $T_c = 15$ K. (b) The scaled results of $\frac{\Delta\rho}{\rho_0}$ versus $\frac{H}{\rho_0}$ (Köhler plot) for the same sample. The Köhler's rule surprisingly obeys in the entire scanned magnetic field range.

where $\Delta\rho = \rho(H) - \rho_0$, ρ_0 is the zero-field resistivity, and f is a function that depends upon the geometrical configuration and on the kind of metal. This is Köhler's rule and the corresponding plots are known as Köhler plots. It holds regardless of the topology and geometry of the Fermi surface.

The scaled results of $\frac{\Delta\rho}{\rho_0}$ versus $\frac{H}{\rho_0}$ for the underdoped sample with $T_c = 15$ K are shown in Fig. 4.12 at the fixed temperatures of $T = 20$ K and varying field and at fixed field of 16 T and varying temperature. It is not only that the ground state of this underdoped sample of exceptional quality is metallic down to the lowest temperatures, but surprisingly obeys the Köhler's rule, at these low temperatures. It is surprising, because it is expected to be violated, for example due to two relaxation rates, one for spinons and the other for holons as proposed in some theories. Actually Kimura *et al.* [20] report some data where Köhler is satisfied above T_c only in the overdoped samples, which are supposed to resemble an ordinary metal.

If we extend our magnetoresistance measurements to high temperature (unfortunately sample 1 broke during the measurements) on sample 2 ($T_c = 50$ K) we obtain also the violation of the Köhler's rule (see Figure 4.13), in accordance with Kimura *et al.*

On theoretical basis there are several possible explanations for the violation

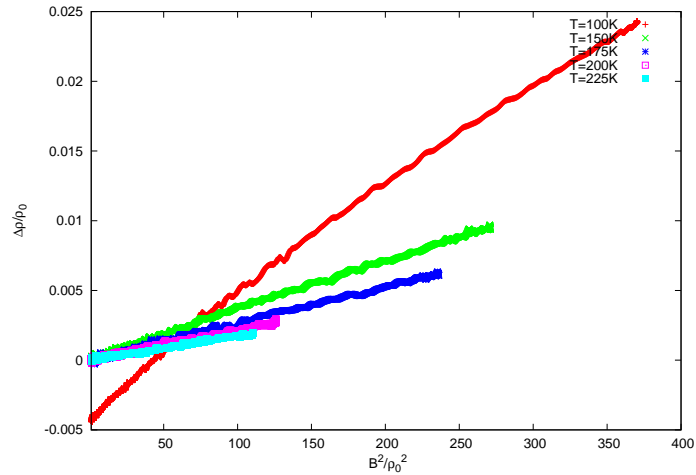


Figure 4.13: The Köhler plot of an underdoped $\text{Bi}_2\text{Sr}_2\text{CaCu}_2\text{O}_{8-y}$ with $T_c = 50$ K (Sample 2)

of Köhler's rule, within the framework of a semiclassical description. i) The electronic structure varies with temperature due to the formation of the density wave, or pseudogap formation. In this case the carrier density will change in temperature. ii) There is more than one type of carrier and their mobilities have different temperature dependences. In the cuprates it was always considered that the charge carriers are hole-like. However, recently

Proust *et al.* [21] reported the presence of electron-like charge carriers on the Fermi surface, as well. iii) The temperature dependence of the scattering rate varies significantly at different points on the Fermi surface. This possibility was also evoked for the explanation of the temperature dependence of the Hall coefficient [22, 23, 24] iv) The scattering time τ is field dependent in a way that $\tau(H, T)/\tau(0, T)$ is temperature dependent. If the scattering is due (or even partially) to local magnetic moments which develop with underdoping, then that will vary τ with field.

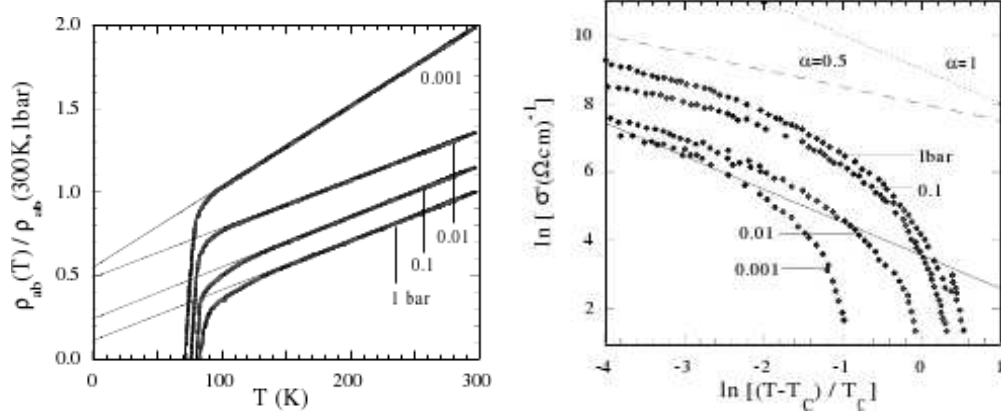
Since the magnetoresistance measurements were done in the pseudogap phase, all this scenarios might have some role in the violation of Köhler's rule. Neverthe-

less, the greatest challenge is to join the satisfaction at very low temperatures and the violation at high ones. For the time being the major effort would be to perform MR measurements on the very same sample from low to high temperatures and to record the gradual departure from the universal behavior.

4.2.3 Superconducting fluctuations near T_c

Another intensively discussed issue related to high- T_c superconductors is the superconducting fluctuations above T_c . The strength of these fluctuations is due to the facts that cuprate superconductors have much smaller values of the coherence length and lower carrier densities than most conventional superconductors, and in addition they have anisotropic layer structure. Because of these properties, fluctuation effects [25, 26] are more important and have been studied both above and below T_c and in applied magnetic fields by many research groups [27, 28]. Over the last few years [29] it has become clear that several families of cuprate superconductors exhibit a parabolic curve of T_c versus hole concentration (p) similar to that originally established for $\text{La}_{2-x}\text{Sr}_x\text{CuO}_{8-\delta}$. Superconductivity only exists over a rather limited range of p and disappears both for underdoped and overdoped samples. This behavior may provide a critical test for different theoretical mechanisms and it is clearly of interest to understand how the fluctuation effects change with doping.

Some time ago Forró *et al.* [30] have reported a detailed study of superconducting fluctuations in $\text{Bi}_2\text{Sr}_2\text{CaCu}_2\text{O}_{8-y}$ both on the overdoped and underdoped side. They claimed that the contribution to the electrical conductivity from superconducting fluctuations above T_c falls off drastically as oxygen concentration deviates from the optimum, both on the underdoped and overdoped sides (see Fig. 4.14(a) for the underdoped samples). Furthermore, the range of these fluctuations is also decreasing with the departure from the optimally doped situation. The doping was done with oxygen depletion and insertion in a limited range. The underdoping was limited to T_c of ~ 70 K. Since we have underdoping in a much



(a) Normalized resistivity measured in the ab plane for the same single crystal of $\text{Bi}_2\text{Sr}_2\text{CaCu}_2\text{O}_{8-y}$ at various oxygen content y . The numbers on the curve refer to the oxygen partial pressure (in bars) at the annealing temperature [30]

(b) Fluctuation analysis of the data in (a). σ' is the excess conductivity. The dashed lines show the slope expected (-0.5 and -1) in the 3D and 2D limits of Eq. 4.2 using $S = 1.5$ nm and room temperature resistivity of $150 \mu\Omega\text{m}$ [30]

Figure 4.14:

broader range, we could test those ideas.

As it is shown on Figure 4.14(b) [30] the fluctuating contribution to the conductivity is deduced as the difference between the measured conductivity ($\frac{1}{\rho}$) and the extrapolated one from the region where one does not expect this contribution ($\frac{1}{\rho_{extra}}$). A simplistic picture is that Cooper pairs are preformed well above T_c , but macroscopic phase coherence cannot be established to give the zero resistance state, but they diminish the resistivity. The functional dependence on the dimensionality of these fluctuations and of the different microscopic contributions have a huge literature. A detailed discussion of it would go beyond the scope of this section. Nevertheless, σ' depends on the reduced temperature $\tau = (T - T_c)/T_c$ in the following way:mozilla

$$\sigma' = \left(\frac{e^2}{16\hbar S} \right) \tau^{-1/2} (\tau + 4K)^{-1/2} \quad (4.2)$$

in the 2D case, S is the interlayer spacing between CuO_2 layers, $K = (\xi_c/S)^2$, where ξ_c is the zero temperature coherence length perpendicular to the CuO_2

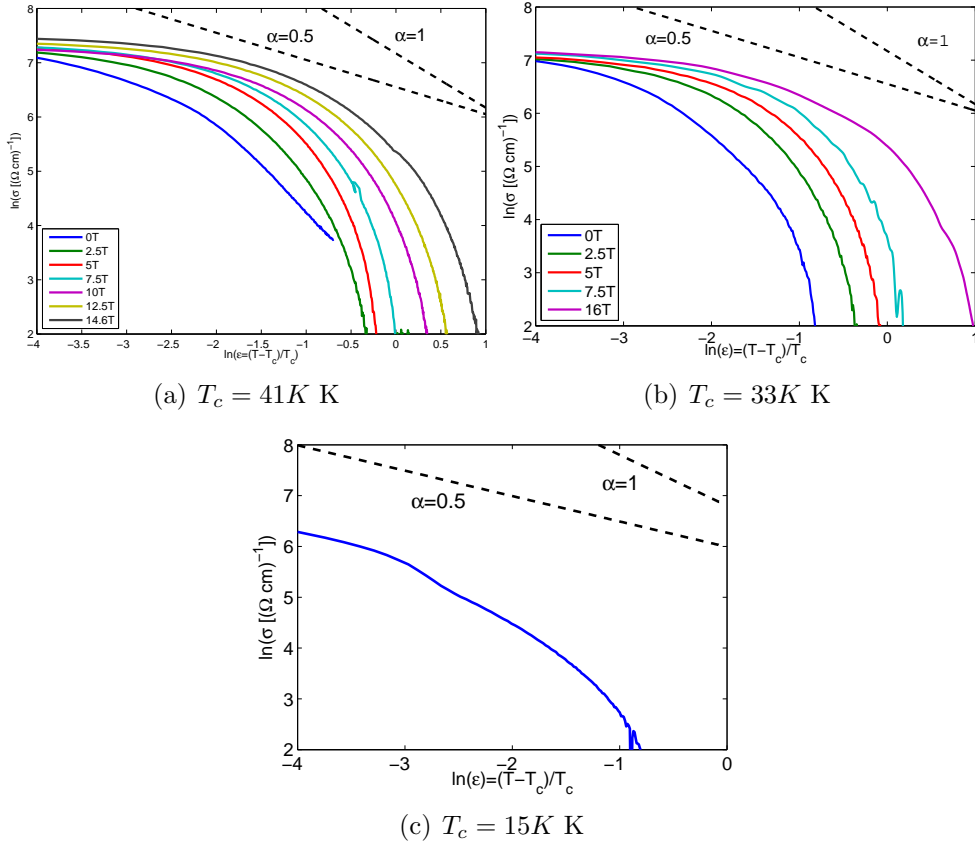


Figure 4.15: Fluctuation analysis of the data of three samples. σ' is the excess conductivity. The dashed lines show the slope expected (-0.5 and -1) in the 3D and 2D limits of Eq. 4.2

planes. From Fig. 4.14(b) one can read that both σ' and the τ region where these fluctuations appear shrinks with underdoping.

We have checked these claims in three of our samples (Fig. 4.15). Since our MR data are not continuous in temperature (but they are recorded at few fixed temperatures) the interpolation necessarily brings in some uncertainty. Nevertheless, from Fig. 4.15 one can read, that for all the three samples ($T_c = 41 \text{ K}$ for the resistivity see 4.10(a), $T_c = 33 \text{ K}$ for the resistivity see 4.10(a), $T_c = 15 \text{ K}$ for the resistivity see 4.11(a)) underdoped sample, the fluctuating conductivity has very similar behavior as in the case of Forró *et al.* What is very interesting and puzzling is that apparently with magnetic field the extent and the range of superconducting fluctuations is extended. The confirmation of these effects is the

subject of future works.

It shows as well, together with the simple model presented in the last subsection, that the careful choice of the sample regarding the sample quality is crucial in the field of cuprates.

4.2.4 A minimal model for the resistivity of inhomogeneous superconductor.

Now lets turn back to our main finding, which needs no more confirmation, which stands firmly as an experimental fact. In good samples after the suppression of T_c with high magnetic field, the sample stays metallic. In many cases in the literature, and occasionally in some of our measurements, the resistivity turns to be non-metallic after the disappearance of the superconducting state. How should we understand it?

To achieve low enough transition temperature, the doping content (achieved by substitution of Ca for Y or Pr) has to be high, and the material is close to the metal insulator transition already at zero field. Therefore, just a small fluctuation in the distribution of the doping atoms can turn a big part of the sample insulator, and change the overall behavior which shows up in resistivity measurement. The inhomogeneous distribution of Y atoms in $\text{Bi}_2\text{Sr}_2\text{CaCu}_2\text{O}_8$ was observed for example in the work of Stoto *et al.* [31] where they have observed the lack of periodicity along the c axes. They attributed this kind of disorder to the coexistence along c direction of regions with the normal arrangement, and low Y content, and regions which have shifted due to an antiphase boundary, with high Y content. $\text{Bi}_2\text{Sr}_2\text{Y}_x\text{Ca}_{1-x}\text{Cu}_{8-\delta}$

In order to check whether the resistivity changes due to the reorganization of the doping atoms, I calculated the lower bound of the resistivity of an inhomogeneous sample. I assumed that on one half of the sample the concentration of the doping atoms is higher, and therefore the hole concentration is smaller. I neglected the change in the region with higher doping concentration. I did that

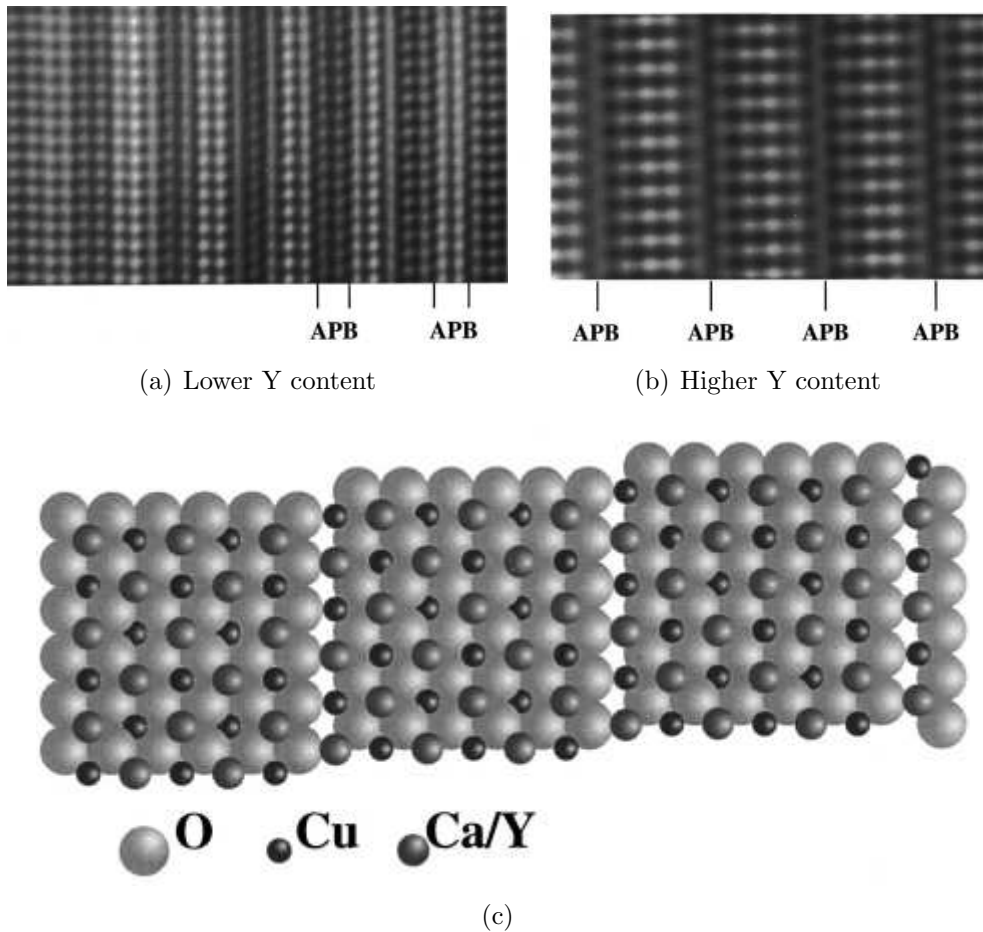


Figure 4.16: (a,b)High Resolution Electron Microscopic image of the crystal structure of Y-substituted $\text{Bi}_2\text{Sr}_2\text{CaCu}_{8-\delta}$ with two different Y content in the projection down to the c axes. With increasing Y content an antiphase domain structure appears. A few antiphase boundaries (APB) are already present in the weakly substituted crystal. (c) Schematic representation of the domains structure of the CuO_2 planes of Y-rich crystals due to the presence of translation interfaces (Figure from [31])

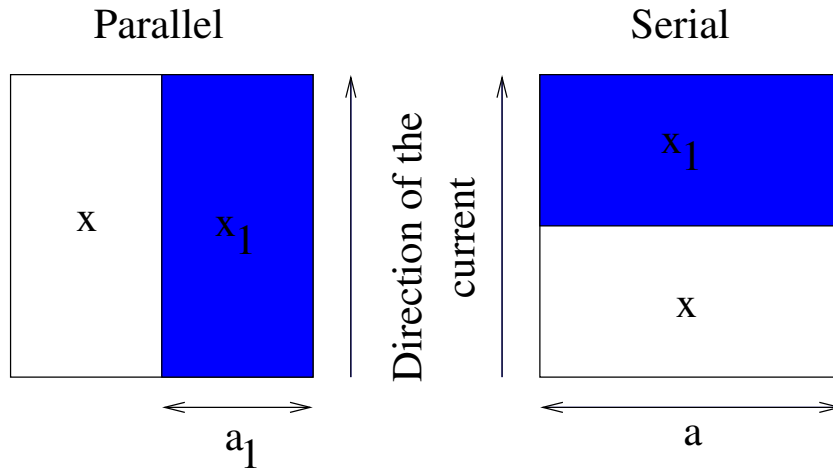


Figure 4.17: The geometry and parameters used in the calculation of the resistivity of an inhomogeneous superconductor.

so, because neither during the annealation of the samples in different oxygen atmospheres, nor during the chemical substitution the control over the amount of the dopant is perfect. The most direct way to characterize the samples is by measuring the transition temperature, and using the general formula for T_c versus hole concentration to get the doping level. The transition temperature is determined, by the superconducting regions, therefore in the case of an inhomogeneous sample, where non-superconducting regions are in the superconducting background, the doping content will be determined by the hole concentration of the SC part of the sample. To compare samples with the same T_c I kept the doping level constant on one part of the sample.

To calculate the lower bound of the resistivity, I used the geometric configuration what is the “best case” (Fig. 4.17).

The resistivity is the most enhanced if the two regions are serially connected to each other, and the least if they are parallel. Although in a real sample the islands are rather randomly distributed, the model is not that far from the reality. Generally the distribution of the dopant atoms in the material is such that in some of the layers the concentration is lower, while other layers it’s higher. Since the current is parallel to the layers, we can consider the material as several parallel

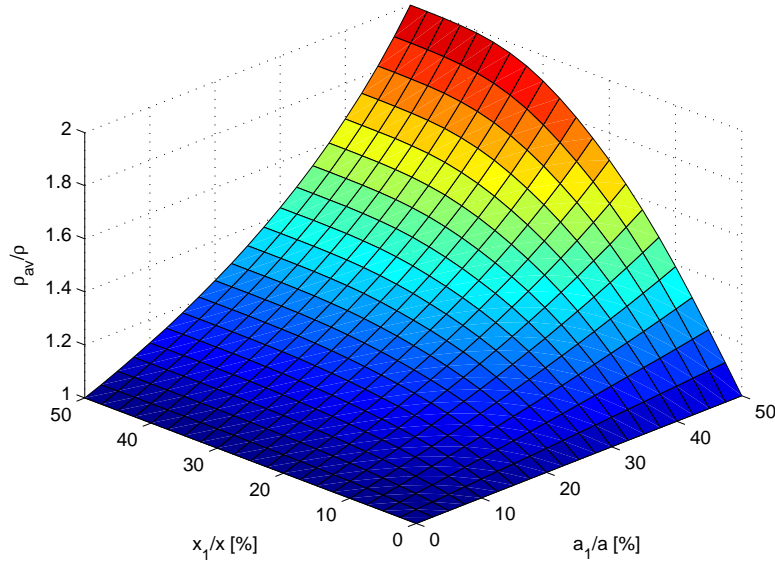


Figure 4.18: The change of the resistivity of a $\text{Bi}_2\text{Sr}_2\text{Pr}_x\text{Ca}_{1-x}\text{Cu}_2\text{O}_{8-\delta}$ as a function of spacial and doping variation in the sample.

connected layers with different hole concentrations. The resistivity in that case, has the following form

$$\rho_{par}(x_1, a_1) = \rho(x) \frac{1}{\frac{a_1}{a} a_1 \left(\frac{\rho(x)}{\rho(x_1)} - 1 \right) + 1}, \quad (4.3)$$

where x is the Pr content of the metallic part, x_1 and a_1 are the Pr content and the size of the insulator half and a is the size for the sample. For the calculation I used $x = 0.6$, and I obtained the $\rho(x)$ function from the residual resistivity published in a systematic study of the Pr doped $\text{Bi}_2\text{Sr}_2\text{CaCu}_2\text{O}_8$ [32]. The result is shown on the Figure 4.18

To see how much the result depends on the geometry, I did the same calculation for serially connected two parts, and plotted the ratio of the two results (Fig. 4.19).

The outcome of the calculation shows two things. First that even in the most optimistic case, the resistivity can change with a factor of two relative to the part of the sample which gives superconductivity. And that is just a very optimistic lower bound calculation, because changing the geometry the value can increase

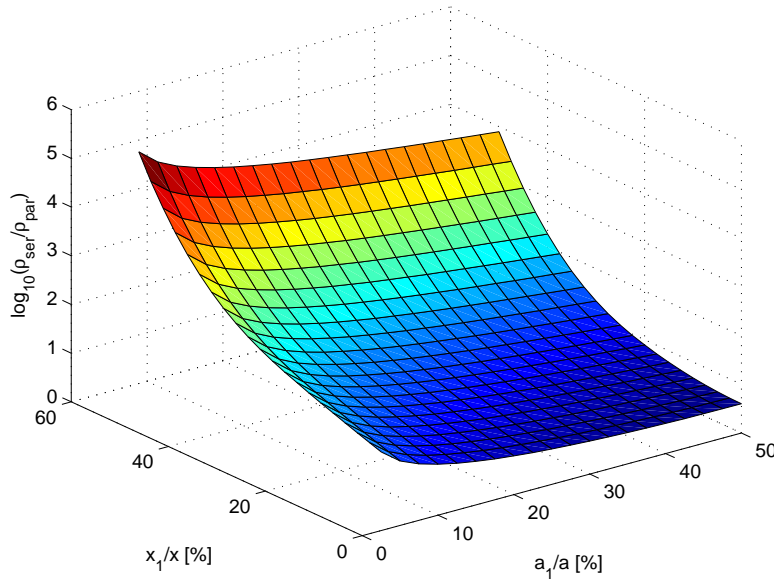


Figure 4.19: The ratio of the resistivity of a $\text{Bi}_2\text{Sr}_2\text{Pr}_x\text{Ca}_{1-x}\text{Cu}_2\text{O}_{8-\delta}$ calculated in a serial and a parallel geometry (ρ_{ser}/ρ_{par}) as a function of spacial and doping variation in the sample. The z-axis is plotted in a logarithmic scale.

further as much as a few orders of magnitude. To obtain more precise value of the expected resistivity increase, more accurate finite element calculations are needed for randomly distributed insulating islands.

4.3 Conclusion

We can conclude that the sample quality in high- T_c cuprates is primordial. By carefully selecting high quality samples I showed that the ground state of the $\text{Bi}_2\text{Sr}_2\text{Ca}_x\text{Cu}_2\text{O}_{8-\delta}$ is metallic even in the highly underdoped, low T_c range. To explain the discrepancy between my and earlier reported measurements, I created a minimalistic model for resistivity of inhomogeneous samples and showed that already a small reorganization of the doping atoms, can have a drastic impact on the overall behavior of the samples, and turn a metal to an insulator.

I also performed magnetoresistivity measurement up to 60 T, and fluctuation analysis. From the magnetoresistance I could read that the Köhler's rule is violated in the sample with higher T_c in accordance with other measurement, but

surprisingly it is obeyed in a sample with $T_c = 15$ K. By comparing the fluctuations with an earlier measurement of Forró *et al* [30], I found the puzzling result that with increasing magnetic field the amplitude and the range of superconducting fluctuations is extended. Both of the latter findings ask for further works and shows the way for future experiments.

Bibliography

- [1] T. Ito, H. Takagi, S. Ishibashi, T. Ido, and S. Uchida. Normal-state conductivity between CuO_2 planes in copper oxide superconductors. *Nature*, 350(6319):596–598, April 1991.

- [2] Akiji Yamamoto, Mitsuko Onoda, Eiji Takayama-Muromachi, Fujio Izumi, Toru Ishigaki, and Hajime Asano. Rietveld analysis of the modulated structure in the superconducting oxide $\text{Bi}_2(\text{Sr,Ca})_3\text{Cu}_2\text{O}_{8+x}$. *Phys. Rev. B*, 42(7):4228–4239, Sep 1990.

- [3] T. Takahashi, H. Matsuyama, H. Katayama-Yoshida, Y. Okabe, S. Hosoya, K. Seki, H. Fujimoto, M. Sato, and H. Inokuchi. Band structure of $\text{Bi}_2\text{Sr}_2\text{CaCu}_2\text{O}_8$ studied by angle-resolved photoemission. *Phys. Rev. B*, 39(10):6636–6639, Apr 1989.

- [4] W. S. Lee, I. M. Vishik, K. Tanaka, D. H. Lu, T. Sasagawa, N. Nagaosa, T. P. Devereaux, Z. Hussain, and Z.-X. Shen. Abrupt onset of a second energy gap at the superconducting transition of underdoped Bi2212. *Nature*, 450(7166):81–84, November 2007.

- [5] W Zhang, G Liu, J Meng, L Zhao, H Liu, X Dong, W Lu, JS Wen, ZJ Xu, and GD Gu. High energy dispersion relations for the high temperature $\text{Bi}_2\text{Sr}_2\text{CaCu}_2\text{O}_8$ superconductor from laser-based angle-resolved photoemission spectroscopy. *Physical Review Letters*, 101(1):17002, 2008.

- [6] S. H. Pan, J. P. O'Neal, R. L. Badzey, C. Chamon, H. Ding, J. R. Engelbrecht, Z. Wang, H. Eisaki, S. Uchida, A. K. Gupta, K.-W. Ng, E. W. Hudson, K. M. Lang, and J. C. Davis. Microscopic electronic inhomogeneity in the high- T_c superconductor $\text{Bi}_2\text{Sr}_2\text{CaCu}_2\text{O}_{8+x}$. *Nature*, 413(6853):282–285, September 2001.
- [7] D. Mandrus, L. Forro, C. Kendziora, and L. Mihaly. Two-dimensional electron localization in bulk single crystals of $\text{Bi}_2\text{Sr}_2\text{Y}_x\text{Ca}_{1-x}\text{Cu}_2\text{O}_8$. *Phys. Rev. B*, 44(5):2418–2421, Aug 1991.
- [8] J. L. Tallon, C. Bernhard, H. Shaked, R. L. Hitterman, and J. D. Jorgensen. Generic superconducting phase behavior in high- T_c cuprates: T_c variation with hole concentration in $\text{YBa}_2\text{Cu}_3\text{O}_{7-\delta}$. *Phys. Rev. B*, 51(18):12911–12914, May 1995.
- [9] S. D. Obertelli, J. R. Cooper, and J. L. Tallon. Systematics in the thermoelectric power of high- T_c oxides. *Phys. Rev. B*, 46(22):14928–14931, Dec 1992.
- [10] F. Rullier-Albenque, H. Alloul, and R. Tourbot. Influence of pair breaking and phase fluctuations on disordered high T_c cuprate superconductors. *Phys. Rev. Lett.*, 91(4):047001, Jul 2003.
- [11] AA Gapud, JR Liu, JZ Wu, WN Kang, BW Kang, SH Yun, and WK Chu. Effects of 1-MeV proton irradiation in hg-based cuprate thin films. *Physical Review B*, 56(2):862–867, 1997.
- [12] Y Zhu, ZX Cai, RC Budhani, M Suenaga, and DO Welch. Structures and effects of radiation damage in cuprate superconductors irradiated with several-hundred-mev heavy ions. *Physical Review B*, 48(9):6436–6450, 1993.
- [13] Y. Ando, G. S. Boebinger, A. Passner, T. Kimura, and K. Kishio. Logarithmic divergence of both inplane and out-of-plane normal-state resistivities

- of superconducting $\text{La}_{2-x}\text{Sr}_x\text{CuO}_4$ in the zero-temperature limit. *Physical Review Letters*, 75(25):4662–4665, December 1995.
- [14] S. Ono, Y. Ando, T. Murayama, F. F. Balakirev, J. B. Betts, and G. S. Boebinger. Low-temperature normal state of Bi-2201 in a wide doping range: Where does the metal to insulator crossover take place? *Physica C*, 341:641–642, November 2000.
- [15] S. Ono, Y. Ando, T. Murayama, F. F. Balakirev, J. B. Betts, and G. S. Boebinger. Metal-to-insulator crossover in the low-temperature normal state of $\text{Bi}_2\text{Sr}_{2-x}\text{La}_x\text{CuO}_{6+\delta}$. *Physical Review Letters*, 85(3):638–641, July 2000.
- [16] S. Ono, Y. Ando, T. Murayama, F. F. Balakirev, J. B. Betts, and G. S. Boebinger. Low-temperature normal state of $\text{Bi}_2\text{Sr}_{2-x}\text{La}_x\text{CuO}_{6+\delta}$: comparison with $\text{La}_{2-x}\text{Sr}_x\text{CuO}_4$. *Physica C*, 357:138–141, August 2001.
- [17] M. A. Steiner, G. Boebinger, and A. Kapitulnik. Possible field-tuned superconductor-insulator transition in high- T_c superconductors: Implications for pairing at high magnetic fields. *Physical Review Letters*, 94(10):107008, March 2005.
- [18] G. S. Boebinger, Y. Ando, A. Passner, T. Kimura, M. Okuya, J. Shimoyama, K. Kishio, K. Tamasaku, N. Ichikawa, and S. Uchida. Insulator-to-metal crossover in the normal state of $\text{La}_{2-x}\text{Sr}_x\text{CuO}_4$ near optimum doping. *Physical Review Letters*, 77(27):5417–5420, December 1996.
- [19] A.B. Pippard. *Magnetoresistance in metals*. Cambridge University Press Cambridge (England), 1989.
- [20] T. Kimura, S. Miyasaka, H. Takagi, K. Tamasaku, H. Eisaki, S. Uchida, K. Kitazawa, M. Hiroi, M. Sera, and N. Kobayashi. In-plane and out-of-plane magnetoresistance in $\text{La}_{2-x}\text{Sr}_x\text{CuO}_4$ single crystals. *Phys. Rev. B*, 53(13):8733–8742, Apr 1996.

- [21] N. Doiron-Leyraud, C. Proust, D. LeBoeuf, J. Levallois, J.B. Bonnemaïson, R. Liang, DA Bonn, WN Hardy, and L. Taillefer. Quantum oscillations and the Fermi surface in an underdoped high- T_c superconductor. *NATURE-LONDON-*, 447(7144):565, 2007.
- [22] L. Forro, D. Mandrus, C. Kendziora, L. Mihaly, and R. Reeder. Hall-effect measurements on superconducting and nonsuperconducting copper-oxide-based metals. *Phys. Rev. B*, 42(13):8704–8706, Nov 1990.
- [23] Chris Kendziora, David Mandrus, Laszlo Mihaly, and Laszlo Forro. Single-band model for the temperature-dependent hall coefficient of high- T_c superconductors. *Phys. Rev. B*, 46(21):14297–14300, Dec 1992.
- [24] A. Carrington, A. P. Mackenzie, C. T. Lin, and J. R. Cooper. Temperature dependence of the Hall angle in single-crystal $\text{YBa}_2(\text{Cu}_{1-x}\text{Co}_x)_3\text{O}_{7-\delta}$. *Phys. Rev. Lett.*, 69(19):2855–2858, Nov 1992.
- [25] M. B. Salamon. *Physical Properties of High Temperature Superconductors I*, volume I. World Scientific, Singapore, 1989.
- [26] L. N. Bulaevskii, V. L. Ginzburg, and A. A. Sobianin. The macroscopic theory of superconductors with a short coherence length. *Zhurnal Eksperimentalnoi i Teoreticheskoi Fiziki*, 94:355–375, July 1988.
- [27] P. P. Freitas, C. C. Tsuei, and T. S. Plaskett. Thermodynamic fluctuations in the superconductor $\text{Y}_1\text{Ba}_2\text{Cu}_3\text{O}_{9-\delta}$: Evidence for three-dimensional superconductivity. *Phys. Rev. B*, 36(1):833–835, Jul 1987.
- [28] Andrea Gauzzi and Davor Pavuna. Evidence for nonuniversal behavior of paraconductivity caused by predominant short-wavelength Gaussian fluctuations in $\text{yba}_2\text{cu}_3\text{o}_{6.9}$. *Phys. Rev. B*, 51(21):15420–15428, Jun 1995.
- [29] M. R. Presland, J. L. Tallon, R. G. Buckley, R. S. Liu, and N. E. Flower. General trends in oxygen stoichiometry effects on t_c in bi and tl superconductors. *Physica C: Superconductivity*, 176(1-3):95–105, May 1991.

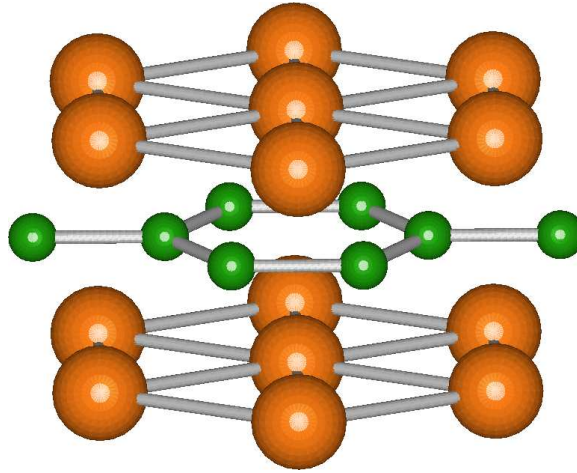
-
- [30] L. Forro. Suppression of superconducting fluctuations in the electrical conductivity in oxygen underdoped and oxygen overdoped $\text{Bi}_2\text{Sr}_2\text{Cu}_2\text{O}_8$. *FIZIKA A*, 8:267–274, 1999.
- [31] T. Stoto, D. Pooke, L. Forro, and K. Kishio. Oxygen distribution, incommensurate modulation, and structural disorder in $\text{Bi}_2\text{Sr}_2\text{Ca}_{1-y}\text{Y}_y\text{Cu}_2\text{O}_{8+\delta}$ and $\text{Bi}_{10}\text{Sr}_{15}\text{Fe}_{10}\text{O}_{46}$ single crystals. *Phys. Rev. B*, 54(22):16147–16159, Dec 1996.
- [32] B. Beschoten, C. Quitmann, R. J. Kelley, M. Onellion, and G. Güntherodt. Metal-insulator transition and electronic structure in Pr-doped $\text{Bi}_2\text{Sr}_2(\text{Ca}_z, \text{Pr}_{1-z})\text{Cu}_2\text{O}_{8+y}$. *Physica B: Condensed Matter*, 223-224:519–521, June 1996.

Chapter 5

MgB₂

5.1 Introduction

The idea of superconductivity in metal borides, carbides and nitrides is old. [1, 2]. Many ternary transition metal diborides have been found to superconduct with transition temperatures of 2–6 K (YRe₂B₂, LuB₂C₂) [3], and even a few with higher T_c s like LuRuB₄ [4] and YNi₄B [5] $T_c \sim 12$ K. Some quaternary compounds were even more promising: LnNi₂B₂C $T_c = 6.6$ K [6] and YPb₅B₃C_{0.3} $T_c = 23$ K [7]. In 1970, transition temperatures above 11 K were found in the diboride Zr_{0.13}Mo_{0.87}B₂ by Cooper *et al* [8]. Later on Leyarowska *et al* [9] examined diborides and discovered NbB₂ with $T_c \sim 0.062$ K, but the majority of the materials didn't superconduct down to 0.42 K. After all these efforts, the discovery in 2001 of MgB₂ with $T_c \sim 39$ K [10], came as a large surprise. This led to another wave of research, dedicated to find higher temperature superconductors among other diborides, but so far no new materials have been found. There is a simple evidence that the superconductivity in MgB₂ can be described by the BCS theory, assuming two different superconducting gaps opening in two different bands. In the light of this, it is quite surprising to have such a high T_c since interband scattering acts as pair-breaker. Thus one would expect samples with very much varying transition temperatures. This is not the case. Furthermore,

Figure 5.1: The crystal structure of the MgB₂

the normal state resistivity seems anomalous in the sense that Matthiessen's rule does not seem to be followed when comparing different samples. This is a point, that merits further attention.

5.1.1 Crystal structure

MgB₂ has a hexagonal crystal structure with space group $p6/mmm$, which is common among diborides (Fig. 5.1). The boron atoms form a graphite-like honeycomb network and the Mg atoms are located at the interstices of these hexagons. In the unit cell the atomic positions are $(0, 0, 0)$ for Mg (Weizkoff symbol 1a) and $(1/3, 2/3, 1/2)$ and $(2/3, 1/3, 1/2)$ for the B (Weizkoff symbol 2d) atoms. Lattice parameters are $a = 0.3084$ nm and $c = 0.3524$ nm. The intralayer interatomic distances are B–B 0.1780 nm and Mg–Mg 0.3084 nm, whilst the interlayer interatomic distances are Mg–Mg 0.3524 nm and Mg–B 0.25 nm. The reciprocal space primitive translations are $A = 2\pi/a(2/\sqrt{3}, 0, 0)$, $B = 2\pi/a(-1/\sqrt{3}, 1, 0)$ and $C = 2\pi/c(0, 0, 1)$.

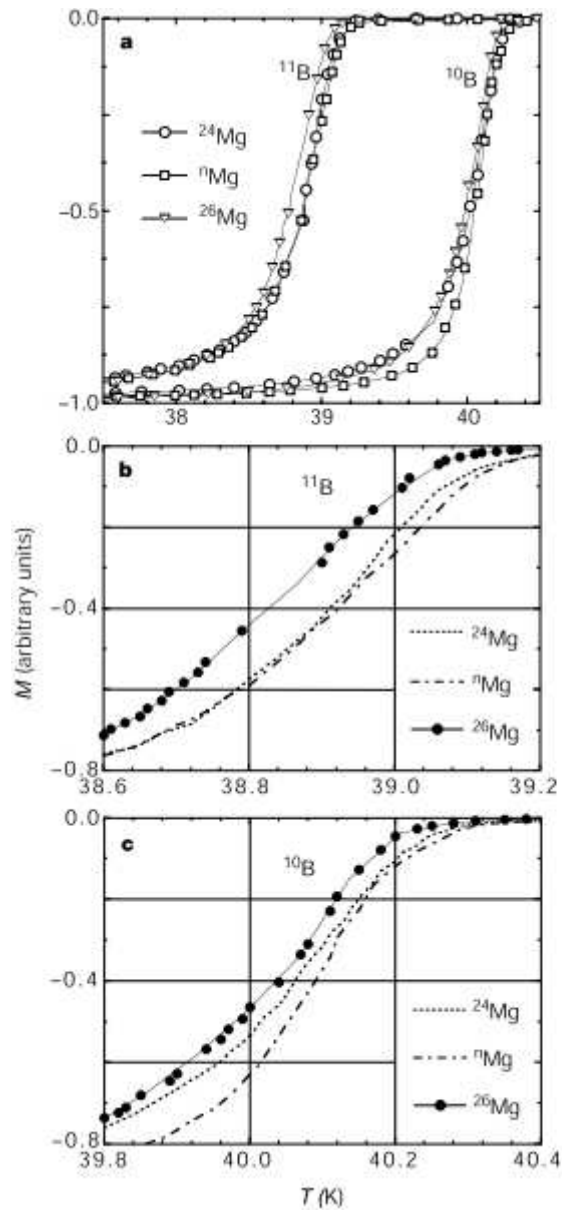


Figure 5.2: Isotope effect of MgB₂. Magnetization curves measured with SQUID. The sample was cooled down to 20 K and warmed up above the transition temperature in 1 mT (Figure from [11])

5.1.2 Isotope effect

One might ask the question if a superconductor with such a high T_c behaves according to the BCS theory or not. One of the most common proofs of its applicability is the presence of the isotope effect. From the BCS theory $T_c \sim M^{-\alpha}$ where M is the isotope mass and $\alpha = 1/2$ in the weak coupling limit. This proves the presence of phonons in the mechanism of the attractive interaction as well.

An isotopic substitution study has been performed by Hinks *et al.* in 2001 [11], where both the Mg and the B atoms were exchanged. Pure ¹⁰B and ¹¹B were combined with ²⁴Mg, ²⁶Mg and with the natural isotopic mixture. The T_c was determined from the magnetization curves measured with a SQUID.

Using the standard definition of the isotope effect coefficient for multicomponent systems $\alpha_i = d \ln T_c / d \ln M_i$, they found that $\alpha_B = 0.30 \pm 0.01$ and $\alpha_{Mg} = 0.02 \pm 0.01$. This pronounced effect shows that the phonons are indeed involved in the superconducting pairing mechanism. From the fact that α_B is one order of magnitude bigger than α_{Mg} it is clear that those phonons are due to the movements of the B atoms. The deviation from the weak coupling value of $\alpha_{w.c.} = 0.5$ comes from the strong anharmonicity of the B E_{2g} mode, where the boron atoms are moving out of phase.

5.1.3 Specific heat measurement

The low temperature specific heat of a metal can be described as a sum of two terms, $C_n = \gamma T + AT^3$. The first term is electronic, and the second from phonons. From BCS theory, the specific heat jumps at the superconducting transition temperature, and in the superconducting state the electronic contribution can be described as $C_s \sim e^{\frac{\delta}{k_b T}}$. The size of the jump is given by the Rutgers-formula, $(C_s - C_n)|_{T_c} = T_c \mu_0 \left[\frac{dH}{dT} \Big|_{T_c} \right]^2$.

Bouquet *et al.* [12] performed specific heat measurements on Mg¹¹B₂ powder samples (Fig. 5.3). The results show the predicted jump, and a temperature dependent electronic specific heat coefficient (γ), but it is clearly different from

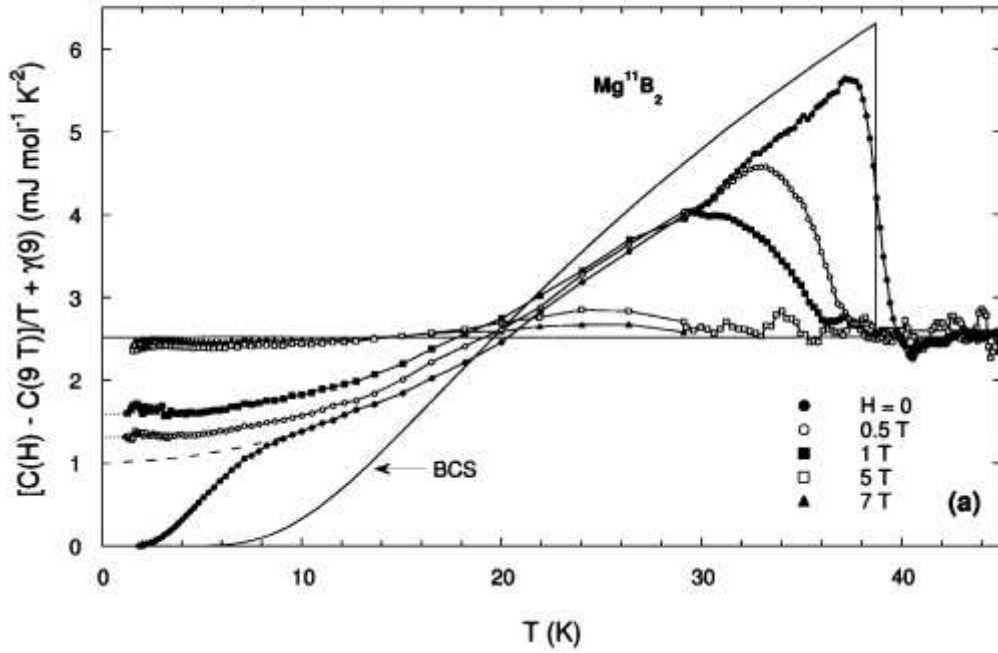


Figure 5.3: Electronic specific heat coefficient (γ) of MgB_2 at different magnetic field. (Figure from [12])

the theoretical curve coming from isotropic BCS theory: there is a little shoulder below 5 K which doesn't exist in the one band BCS-theory. The shoulder disappears upon applying 0.5 T. This will be explained in the following section with an anisotropic two gap model.

5.1.4 Point contact spectroscopy

A direct way to see the two gaps is point contact spectroscopy, where the fine structure of the gap can reveal the presence as well as the size of the second gap. It also gives direct access to the eDOS of the material. The measurement was performed by Gonelli *et al.*, on high quality single crystals [13]. The result (Fig. 5.4(a) shows the double gap in the *ab*-plane, at ± 2.7 mV and at ± 7.2 mV. By changing the temperature it is possible to follow the disappearance of the gaps. This is presented in Fig. 5.4(b). It is interesting to remark that the second, smaller gap, is much less pronounced in the *c* direction, than in the *ab* plane.

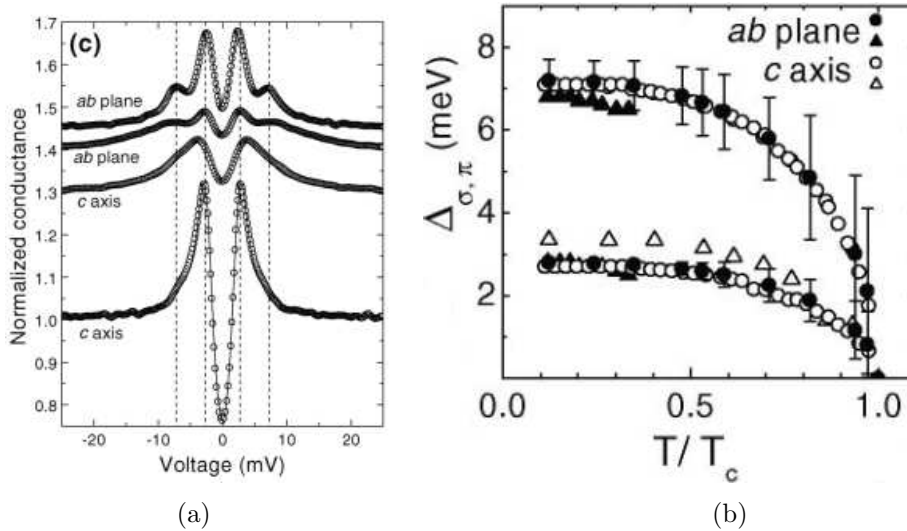


Figure 5.4: (a) Point contact spectroscopy curves of MgB₂. The dashed lines shows the position of the two gaps. (b) the temperature dependence of the two gaps. It can be seen that they disappear at the same temperature. (Figures from [13])

5.1.5 Electronic structure calculation and the proof of the two gap model

In MgB₂, the Mg atom forms ionic bonds with the boron atoms, giving its valence electrons to the boron planes. The boron atoms are held together by 2D covalent σ bonds formed by the sp^2 orbitals, which arise from hybridization of the boron 2s and $p_{x,y}$ levels, and a 3D metallic π band from the boron p_z orbitals. The p_z band contains both holes and electrons as charge carriers. The energies of the σ and π bands are almost the same at the zone center allowing charge transfer between them. The eDOS at the Fermi level and the normal state conductivity has a contribution from both bands, however the 2D σ band is responsible for the superconductivity.

The aforementioned bands can be seen in the band structure calculation of Choi *et al.* [14]. The calculation was made using ab initio pseudopotentials using density functional theory (DFT) in the local density approximation (LDA). From the electronic band structure (Fig. 5.5(a) (top)), it is clear that the Fermi surface

of MgB₂ has two parts: 2 dimensional hole-like coaxial σ bands along the Γ to A line, a holelike tubular network of π bands connecting the K and M points, and an electron like network around the H and L points.

The phonon dispersion was calculated using the frozen phonon method (Fig. 5.5(a)(bottom)). It is important to remark the large anharmonicity of the E_{2g} phonons, as these are the phonons coupled to electrons in the superconducting state.

Using the above results, Choi *et al.* presented ab initio calculations of the superconducting properties of MgB₂. The anisotropic Eliashberg formalism was used for the calculation, which is a generalized form of the isotropic theory and is more suitable for materials with strongly momentum dependent gap. In agreement with the earlier proposition, they found that the superconducting gap has s-wave symmetry. Plotting the energy gap distribution ($\rho(\Delta) = \int d\mathbf{r} \sum_{\mathbf{k}} |\Psi_{\mathbf{k}}(\mathbf{r})|^2 \delta(\Delta - \Delta(\mathbf{k}))$ where $\Psi_{\mathbf{k}}(\mathbf{r})$ is the electron wave function with crystal momentum \mathbf{k}), two typical gap values can be clearly defined. From 6.4 meV to 7.2 meV on the σ sheets and from 1.2 to 3.7 meV on the π sheets. These results are in agreement with the values coming from experiment, such as point contact spectroscopy or specific heat. The temperature dependence of the two gaps also gave similar results to the experiment. It was possible to prove that the anomalous isotope effect coefficient is due to the large anharmonicity of the E_{2g} mode involved in the superconductivity. The calculation of the temperature dependence of the specific heat is in good agreement with experiment as well.

5.2 The goal of our experiment

In the last section we have seen that there is good agreement between theory and experiment on several points describing the superconductivity of MgB₂. It has been shown that it has an anisotropic s-wave gap, where the gap has two well defined branches corresponding to the σ and π bands, which are well separated in both real and momentum space. The question then arises how the existence of

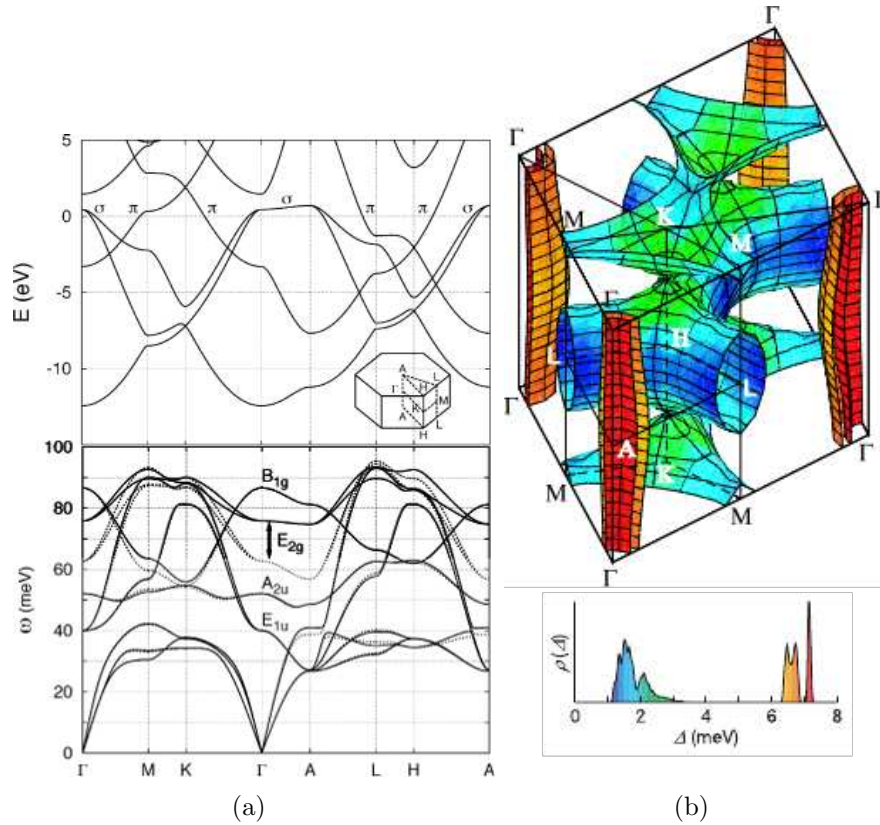


Figure 5.5: (a) Calculated electron (top) and phonon (bottom) band structures of MgB₂. The solid lines are the anharmonic phonon frequencies, and the dashed lines represent the standard harmonic phonon frequencies. Inset: the BZ of a standard hexagonal crystal. (b) top) The superconducting energy gap on the the Fermi surface of the MgB₂ at 4K. The Fermi surface consist of four sheets. Two σ (“cylinders”) where the superconducting gap is ~ 7.2 meV, and two π (“webbed tunnels”) where the gap ranges from 6.4 to 6.8 meV. The lower part shows the distribution of the energy gap, using the same color code as on the upper part of the figure (Figure from [14])

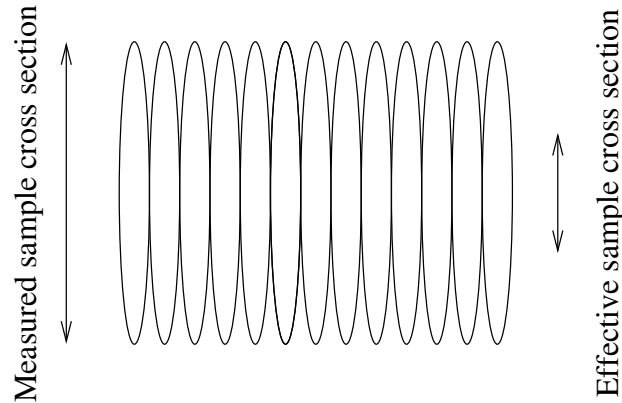


Figure 5.6: Reduction of the current-carrying cross-section in polycrystalline samples

those two bands and two gaps changes the transport properties of the material. Is the scattering in the two Fermi-surface sheets comparable and is the scattering between the bands important?

If the two band description is valid we can conclude that the relation for the inter- and intralayer scattering rates is $\gamma_{intra} \gg \gamma_{inter}$. This is due to several reasons, one of which is the σ π disparity. The σ and π bands are formed from different local orbitals, and therefore orthogonal on the atomic scale. Moreover the disparity between the two bands is relatively large due to the compactness of the B 2s and 2p orbitals. This can be understood if we observe that while the p_z orbital has odd parity, the bond orbitals have even parity with respect to the B layer. Therefore, the only possible way to the hybridization involve interlayer hopping from a p_z orbital on one layer to a bond orbital in the other layer. However, the relative scattering within the two layers is unaccounted for.

In order to address the problem of inter and intraband scattering the resistivity curves from crystals of different sample quality were compared by I. I. Mazin *et al.* [15]. In this study two conclusions were made based on the findings: (i) The high-temperature slope of the resistivity is clearly correlated with the residual resistivity in other words Matthiessen's rule is not followed and

Although those two statements are valid based on the results of the analysis,

there is one questionable point; the sample quality. In order to compare samples with different impurity concentration polycrystalline samples, thin films, single crystals, and substituted materials from different synthesis routes were used. As such, a non-negligible contribution can arise from extrinsic effects. Indeed, other authors [16], have concluded based on another set of samples that the main influence on the sample resistivity in non-single crystals comes from the reduced current-carrying cross-section. This reduction arises from the fact that the only place where the current can travel from one grain to the other is the point, or reduced area where they touch each other – this is illustrated in Fig. 5.6.

Another common method for determining the in-plane scattering is atomic substitution. Both Mg and B can be substituted with elements like Zn, Si, Ni, Fe, Al, C, Co and Mn [17, 18, 19]. Although in this case homogeneous distribution of defects can be guaranteed, doping of the material can't be avoided.

More recently several authors have performed measurements on irradiated samples from the same source in order to obviate the problem of comparing distinct samples. Wang *et al.* [20], and later Putti *et al.* [21] have used neutron irradiation to create point defects in polycrystalline samples. It is known that neutron irradiation produces cascades of atomic displacements resulting in clustering of defects. This has induced almost a factor of 100 change in the residual resistivity and the authors found a linear variation of T_c with defect level. Specific heat measurements indicate a change from two-gap to single-gap superconductivity as T_c is suppressed below 20 K [21].

Our goal was to check the validity of the first statement using a well defined, systematic study, measuring the relation between residual resistivity, temperature dependent resistivity, critical temperature and defect concentration.

5.3 Experimental setup

In our measurement we used high-quality single crystal samples grown by the group of J. Karpinski in Zürich with the high pressure cubic anvil technique [17].

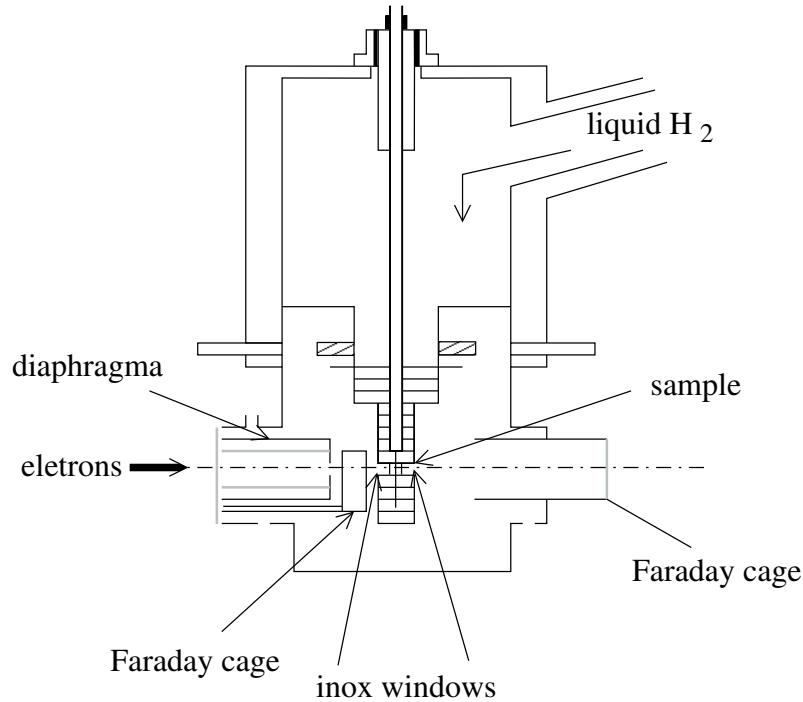


Figure 5.7: The setup for electron irradiation in the Laboratoire des Solides Irradiés, Ecole Polytechnique in Palaiseau, France.

The resistivity was measured using the 4-point method. To reduce the contact resistivity coming from the oxidized surface layer, we sputtered gold patches on the crystal. Gold wires were glued later on these patches with silver epoxy.

To introduce homogeneously distributed point defects we chose electron irradiation. The irradiation was performed in the Laboratoire des Solides Irradiés, Ecole Polytechnique in Palaiseau. The setup is shown in Fig. 5.7.

This method has the advantage that the 2.5 MeV electrons only interact weakly with the material. They mostly create interstitial/vacancy pairs by head-on collisions with the nuclei. These defects are considered to not carry a magnetic moment. In order to minimize defect recombination and clustering, during the irradiation the sample was as far as possible kept at a temperature of 20 K in liquid H_2 . This insured that the defect level is a linear function of the electron dose.

To avoid heating during irradiation, the electron flux was limited to $3 \cdot 10^{14} \text{ e/cm}^2$.

The irradiation was interrupted regularly and the resistivity measured between 20 and 50 K. This range is wide enough to allow determination of the T_c and the residual resistivity, and the temperature is low enough to avoid considerable defect recombination. After a few such cycles the sample was heated up to room temperature and cooled down again. This has allowed for comparison in the whole temperature range between 20 – 290 K. This way, the same single crystal sample with increasing defect concentration could be used, avoiding any artifacts which are inevitable if measurements on different samples are compared.

5.4 Results

Fig 5.8 shows $\rho(T)$ curves in the 20–50 K range. Already at the lowest applied fluence, one can observe a doubling of the superconducting transition. Both observed transitions are sharp. It is very likely that the phase with higher T_c is due to areas near the contacts, partially protected from radiation. Both transitions vary linearly with the applied fluence, thus we used the lower temperature transition to determine T_c . The residual resistivity was found to vary linearly with electron fluence (see insert on Fig. 5.9), which is a proof that defects are created independently and that they do not interact. The main panel of Figure 5.9 shows T_c as a function of the residual resistivity. This again is a linear function of the electron fluence, the slope of which can give information about the nature of the defects, and when compared to superconductors with known pairing symmetry, can also give a hint of the pairing symmetry of the gap. In order to put this result into context, in fig.5.10 we plot the scaled transition temperature and the scaled residual resistivity together with similar curves of superconductors with various order parameters (V₃Si – s-wave [22]; Sr₂RuO₄ – [23] p-wave; YBa₂Cu₃O₇ - d-wave [24]). In all these compounds it is considered that the residual resistivity is increased by non-magnetic defects. The decrease of T_c with increasing residual resistivity indicates pair breaking by induced scattering centers. According to the theorem of Anderson [25], in a dirty superconductor with s-wave symmetry

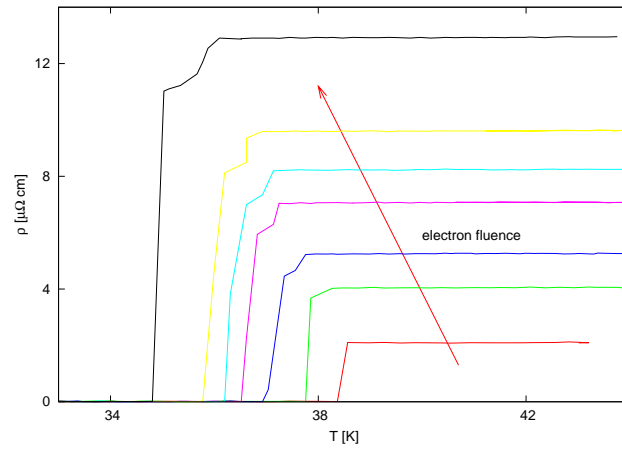


Figure 5.8: Resistivity of MgB_2 versus temperature at different electron fluences.

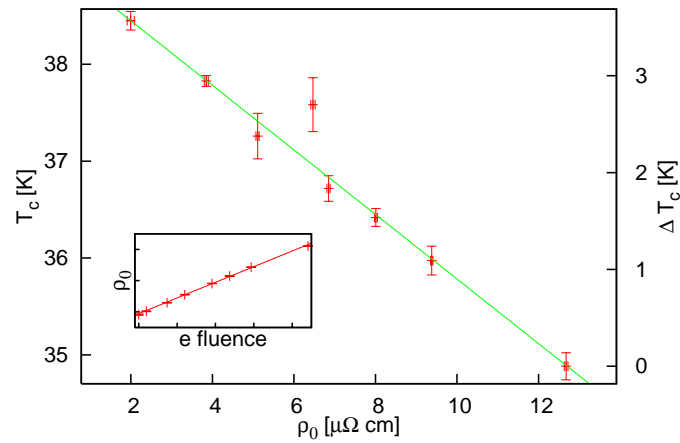


Figure 5.9: The critical temperature versus residual resistivity in MgB_2 . The inset shows the variation of the residual resistance with electron fluence.

non-magnetic impurities do not reduce the transition temperature, as they do not introduce time reversal symmetry breaking. In a two-band superconductor the situation, however, is different: interband scattering breaks the time reversal symmetry, and should result in a decrease of T_c [26].

One can see that despite the 2-band nature of the superconductivity, the decrease of T_c in MgB₂ is less steep than that observed in, for instance, V₃Si, a conventional s-wave superconductor; this hints to s-wave pairing in MgB₂. It also seems to rule out the possibility that, at these defect concentrations, increased interband scattering could be responsible for the decrease of T_c .

Anderson's [25] theorem states that for s-wave pairing non-magnetic impurities do not change the T_C . This is because Cooper pairs are formed from time reversed states and although non-magnetic impurities may change for example the phonon spectrum, they do not break the time reversal symmetry (TRS). However, magnetic impurities strongly reduce T_c for all singlet states because they do break TRS. This behaviour is described by the Abrikosov-Gorkov formula [27, 28, 29]:

$$\ln\left(\frac{T_{c0}}{T_c}\right) = \Psi\left(\frac{1}{2} + \frac{\hbar}{4\pi k_B T_c \tau_M}\right) - \Psi\left(\frac{1}{2}\right) \quad (5.1)$$

where T_{c0} is the superconducting critical temperature in the pure system, $\Psi(x)$ is the digamma function and τ_M is the quasiparticle lifetime due to scattering from magnetic impurities. The finite decrease of T_c on defect concentration means that some of them carry a spin – being magnetic.

In order to check the stability of the electron irradiation induced defects, we warmed our sample to room temperature (Fig. 5.11), then cooled it down again. This allowed us to compare the temperature dependence of the resistivity in the whole temperature range, as well as to check Matthiessen's rule, which states that resistivities coming from different mechanisms are superadditive, that is: $\rho \geq \rho_1 + \rho_2$. The equality is only satisfied for certain special cases, but in reality

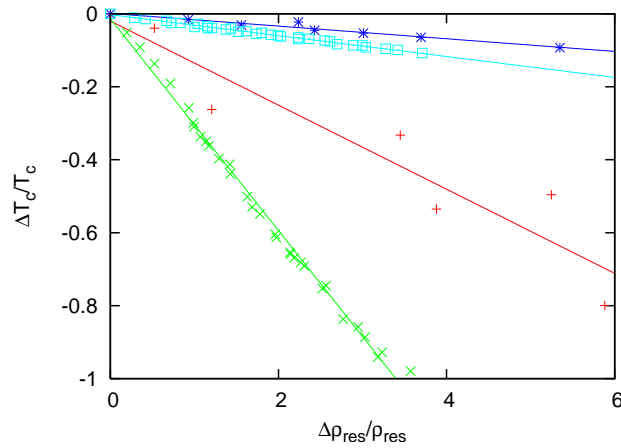


Figure 5.10: Normalized critical temperature versus normalized residual resistivity of superconductors with different order parameter symmetries (In order of steepness of the curve MgB_2 *, V_3Si \square , Sr_2RuO_4 +, $\text{YBa}_2\text{Cu}_3\text{O}_7$, \times) Lines are guide to the eye

it holds with sufficient precision for simple metals.

It is also well known that impurity scattering is essentially temperature independent. This means that resistivity curves $\rho(T)$ of a simple metal which differ only by impurity scattering are parallel lines. Magnesium diboride is not a simple metal however; it has two bands, with very little scattering between the two, which results in two almost independent conducting channels [15]. In this case the resistivity can be written as

$$\frac{1}{\rho} = \frac{1}{\rho_0^{(\pi)} + \rho^{(\pi)}(T)} + \frac{1}{\rho_0^{(\sigma)} + \rho^{(\sigma)}(T)} \quad (5.2)$$

This form does not allow the separation of a temperature independent term unless one of the temperature dependent terms is very large, in which case that particular channel is switched off. This can happen if the electron-phonon coupling is much stronger in one of the two bands.

The upper part of Figure 5.11 shows the $\rho(T)$ curves. It is clear that some of the defects are annealed at room temperature, presumably in the Mg sublattice. The lower part of the figure shows the difference between the partly annealed and the non-irradiated $\rho(T)$ curve. Despite a factor of 3 change in the residual resis-

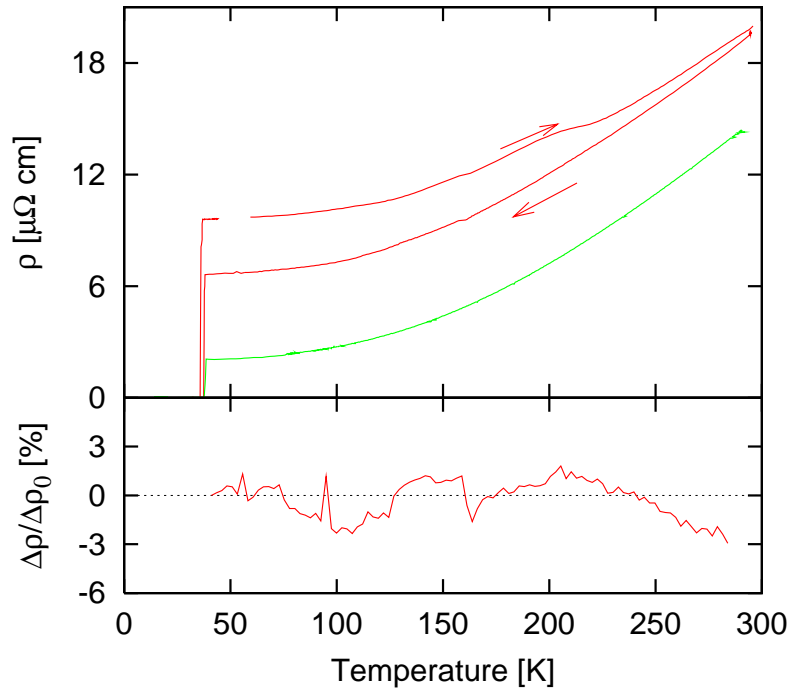


Figure 5.11: (upper) Resistivity versus temperature before and after irradiation. The arrows show the direction of the temperature sweep, (lower) The difference between the irradiated and the non-irradiated curve as a function of temperature.

tivity, within the precision of the measurement, the difference between the two curves is temperature independent, thus Matthiessen's rule seems to be followed. These two findings can be reconciled with two-band conduction if we assume that point defects do not increase interband scattering, and intraband scattering in the two bands is very different, independently of the impurity concentration.

5.5 Conclusion

In conclusion, we have measured the resistivity of a single crystal MgB₂ sample as a function of point defect concentration. We have found linear variation of the residual resistivity with electron fluence, showing the creation of homogeneously distributed point defects. T_c decreased linearly, but very weakly with electron fluence, suggesting s-wave pairing. A partly annealed irradiated sample, when

compared to a non-irradiated one has an $\rho(T)$ curve which is only shifted by a temperature-independent constant, in agreement with Matthiessen's rule. This confirms that interband scattering does not play an important role at these levels of irradiation.

Bibliography

- [1] B. T. Matthias and J. K. Hulm. A search for new superconducting compounds. *Physical Review*, 87(5):799–806, 1952.
- [2] W. T. Ziegler and R. A. Young. Studies of compounds for superconductivity. *Physical Review*, 90(1):115–119, 1953.
- [3] Aravind D. Chinchure, R. Nagarajan, and L. C. Gupta. New superconducting quaternary borocarbide system R-Re-B-C (R=Sc, Y, Gd, Tb and Lu). *Physica B: Condensed Matter*, 281-282:894–895, June 2000.
- [4] D. C. Johnston. Superconductivity in a new ternary structure class of boride compounds. *Solid State Communications*, 24(10):699–702, December 1977.
- [5] Chandan Mazumdar, R. Nagarajan, C. Godart, L. C. Gupta, M. Latroche, S. K. Dhar, C. Levy-Clement, B. D. Padalia, and R. Vijayaraghavan. Superconductivity at 12 K in Y—Ni—B system. *Solid State Communications*, 87(5):413–416, August 1993.
- [6] R. J. Cava, H. Takagi, H. W. Zandbergen, J. J. Krajewski, W. F. Peck, T. Siegrist, B. Batlogg, R. B. van Dover, R. J. Felder, K. Mizuhashi, J. O. Lee, H. Eisaki, and S. Uchida. Superconductivity in the quaternary intermetallic compounds $\text{LnNi}_2\text{B}_2\text{C}$. *Nature*, 367(6460):252–253, January 1994.
- [7] R. J. Cava, H. Takagi, B. Batlogg, H. W. Zandbergen, J. J. Krajewski, W. F. Peck, R. B. van Dover, R. J. Felder, T. Siegrist, K. Mizuhashi, J. O. Lee,

- H. Eisaki, S. A. Carter, and S. Uchida. Superconductivity at 23 K in yttrium palladium boride carbide. *Nature*, 367(6459):146–148, January 1994.
- [8] A. S. COOPER, CORENZWIE, LONGINOT.LD, B. T. MATTHIAS, and ZACHARIA.WH. Superconductivity - transition temperature peak below 4 electrons per atom. *Proceedings Of The National Academy Of Sciences Of The United States Of America*, 67(1):313–&, 1970.
- [9] L. Leyarovska and E. Leyarovski. Search for superconductivity below 1 K in transition-metal borides. *Journal Of The Less-Common Metals*, 67(1):249–255, 1979.
- [10] Jun Nagamatsu, Norimasa Nakagawa, Takahiro Muranaka, Yuji Zenitani, and Jun Akimitsu. Superconductivity at 39 K in magnesium diboride. *Nature*, 410(6824):63–64, March 2001.
- [11] D. G. Hinks, H. Claus, and J. D. Jorgensen. The complex nature of superconductivity in MgB_2 as revealed by the reduced total isotope effect. *Nature*, 411(6836):457–460, May 2001.
- [12] F. Bouquet, R. A. Fisher, N. E. Phillips, D. G. Hinks, and J. D. Jorgensen. Specific heat of (MgB_2) -B-11: Evidence for a second energy cap. *Physical Review Letters*, 8704(4):047001, July 2001.
- [13] R. S. Gonnelli, D. Daghero, G. A. Ummarino, V. A. Stepanov, J. Jun, S. M. Kazakov, and J. Karpinski. Direct evidence for two-band superconductivity in MgB_2 single crystals from directional point-contact spectroscopy in magnetic fields. *Physical Review Letters*, 89(24):247004, December 2002.
- [14] H. J. Choi, D. Roundy, H. Sun, M. L. Cohen, and S. G. Louie. The origin of the anomalous superconducting properties of MgB_2 . *Nature*, 418(6899):758–760, August 2002.

-
- [15] I. I. Mazin, O. K. Andersen, O. Jepsen, O. V. Dolgov, J. Kortus, A. A. Golubov, A. B. Kuzmenko, and D. van der Marel. Superconductivity in MgB_2 : Clean or dirty? *Phys. Rev. Lett.*, 89(10):107002, Aug 2002.
- [16] J. M. Rowell. The widely variable resistivity of MgB_2 samples. *Superconductor Science and Technology*, 16(6):R17–R27, 2003.
- [17] J. Karpinski, S. M. Kazakov, J. Jun, N. D. Zhigadlo, M. Angst, R. Puzniak, and A. Wisniewski. MgB_2 and $\text{Mg}_{1-x}\text{Al}_x\text{B}_2$ single crystals: high pressure growth and physical properties. *Physica C: Superconductivity*, 408-410:81–82, August 2004.
- [18] Sergey Lee, Takahiko Masui, Ayako Yamamoto, Hiroshi Uchiyama, and Setsuko Tajima. Carbon-substituted MgB_2 single crystals. *Physica C: Superconductivity*, 397(1-2):7–13, October 2003.
- [19] C. Buzea and T. Yamashita. Review of the superconducting properties of MgB_2 . *Superconductor Science and Technology*, 14(11):R115–R146, 2001.
- [20] Yuxing Wang, Frederic Bouquet, Ilya Sheikin, Pierre Toulemonde, Bernard Revaz, Michael Eisterer, Harald W. Weber, Joerg Hinderer, and Alain Junod. Specific heat of MgB_2 after irradiation. *Journal of Physics: Condensed Matter*, 15(6):883–893, 2003.
- [21] M. Putti, M. Affronte, C. Ferdeghini, P. Manfrinetti, C. Tarantini, and E. Lehmann. Observation of the crossover from two-gap to single-gap superconductivity through specific heat measurements in neutron-irradiated MgB_2 . *Phys. Rev. Lett.*, 96(7):077003–4, February 2006.
- [22] F Rullier-Albenque. PhD thesis.
- [23] A. P. Mackenzie, R. K. W. Haselwimmer, A. W. Tyler, G. G. Lonzarich, Y. Mori, S. Nishizaki, and Y. Maeno. Extremely strong dependence of superconductivity on disorder in Sr_2RuO_4 . *Phys. Rev. Lett.*, 80(1):161–164, Jan 1998.

- [24] F. Rullier-Albenque, H. Alloul, and R. Tourbot. Influence of pair breaking and phase fluctuations on disordered high- T_c cuprate superconductors. *Phys. Rev. Lett.*, 91(4):047001, Jul 2003.
- [25] P.W. Anderson. Theory of dirty superconductors. *Journal of Physics and Chemistry of Solids*, 11(1-2):26–30, September 1959.
- [26] A. A. Golubov and I. I. Mazin. Effect of magnetic and nonmagnetic impurities on highly anisotropic superconductivity. *Phys. Rev. B*, 55(22):15146–15152, Jun 1997.
- [27] A. A. Abrikosov and L. P. Gorkov. Contribution to the theory of superconducting alloys with paramagnetic impurities. *Soviet Physics JETP-USSR*, 12(6):1243–1253, 1961.
- [28] A. A. Abrikosov and L. P. Gorkov. On the theory of superconducting alloys .1. the electrodynamics of alloys at absolute zero. *Soviet Physics JETP-USSR*, 8(6):1090–1098, 1959.
- [29] A. A. Abrikosov and L. P. Gorkov. Superconducting alloys at finite temperatures. *Soviet Physics JETP-USSR*, 9(1):220–221, 1959.

Chapter 6

Conclusion

Despite its advanced age, superconductivity is one of the hottest topics in the strongly correlated materials. High- T_c superconductors might look like an ever-green theme. The reason for that is the number of opened questions concerning the pairing mechanism which is strongly related to the materials' qualities. There are also superconductors, like MgB₂ which are promising for applications, but there are features which should be clarified. Beside those we shouldn't forget about the possibility to discover new superconductors. They can be interesting by themselves, and by their investigation they can provide valuable contribution to understand other, more complicated systems, like that of cuprates superconductors.

In my research I focused on three major question. The role of inhomogeneity in the low temperature transport properties of the underdoped cuprates, the validity of the Matthiessen's rule in the case of MgB₂ and the possibility of pressure induced superconductivity in the 1T transition metal dichalcogenides (TMD).

In order to address these questions I measured the transport properties of these materials, such as electrical resistivity and thermoelectric power. Resistivity measurement is sensitive to the scattering processes of the electrons, and from the thermoelectric power we can learn about the density of state, and the type

of charge carriers, which reflects in some sense the dispersion relation around the Fermi surface. Those two measurements together are exceptionally good tools to monitor changes which might happen in the electrical properties of a system. As control parameter beside temperature I used pressure, high pulsed magnetic field, and electron irradiation.

In the first part of my thesis I addressed the subject of pressure induced superconductivity in transition metal dichalcogenides (TMD) with 1T structure. Superconductivity has never been observed in pristine 1T TMD sample. My two candidates were the 1T-TiSe₂ and 1T-TaS₂. 1T-TiSe₂ has a CDW phase below 220 K which origin is an ongoing question. Although the excitonic mechanism got recently more experimental support, the Jahn-Teller distortion can not be excluded from the game neither. By applying pressure I discovered that the pristine sample is superconducting between 2.0 and 4.0 GPa. This pressure range has a remarkable coincidence with the disappearance of the CDW phase, where short range fluctuations are the strongest, and they disappear together at the same pressure. My thermoelectric power measurement showed that the high temperature state is non metallic throughout the whole pressure range which more or less eliminates the Peierls mechanism for the phase transition. This further supports the excitonic origin of the CDW phase. After those findings the interesting possibility arises that the superconductivity might share the same origin.

My further interest was to see how general is, to find superconductivity under pressure in the TMD materials with 1T structure. To answer that I chose an other remarkable member of that family, the 1T-TaS₄. This material generated a great interest in the past because of the wide variety of the two dimensional CDW phases it exhibits. At low temperature we can find a commensurate CDW (CCDW) phase having a Mott-state on top of it, formed from the electrons not involved in the charge density wave. By increasing temperature that phase melts to a nearly commensurate phase (NCCDW) where commensurate domains are separated with domain walls. I found that pressure melts the phase as well, and

reveal that the material is superconducting above 2.5 GPa with a T_c of 5.9 K. Beside the relatively high transition temperature, the superconducting phase shows other interesting properties. First of all, it develops from a non-metallic NCCDW phase, and stays remarkably stable up to the highest applied pressure of 24 GPa. It is even more remarkable, considering the fact that the phase above T_c changes from the non-metallic to metallic, varying the low temperature resistivity by 2 orders of magnitude.

In the second part I investigated the low temperature normal state of the high- T_c superconductor $\text{Bi}_2\text{Sr}_2\text{CaCu}_2\text{O}_8$. Contrary to earlier reports, I found that the ground state of the underdoped cuprate after the suppression of T_c in high magnetic field (up to 60 T) is metallic. I explain the discrepancy between the two findings with the sample quality. With a simple model of inhomogeneous sample I showed, that already a small reorganization of the dopant atoms can drastically change the overall measured behavior. In other words, the normal state may look metallic, but the majority of the sample is insulator. After suppressing superconductivity the majority phase takes over. I also investigated the magnetoresistance of the samples with different critical temperatures up to 60 T. At high temperatures I found the violation of the Köhler's rule, what is in agreement with earlier reported measurements. Surprisingly, at low temperatures (which means lower T_c and higher underdoping) the system obeys the Kohler's rule. My further contribution to high- T_c from these measurements is coming from the analysis of the superconducting fluctuation. I found that the amplitude and the range of the superconducting fluctuations is increases with increasing magnetic field.

In the last section I investigated the suggestion made by Igor Mazin, concerning the violation of the Matthiessen's rule in the two band superconductor MgB_2 . To have a good control over the parameters, I chose high quality single crystals, and introduced point defects by fast electron irradiation. The systematic study showed that the Matthiessen's rule is obeyed in the case of MgB_2 in the T_c range of 30–35 K. . This confirms that interband scattering does not play an important role at these levels of irradiation.

Throughout this thesis I investigated three different families of superconductors and I made interesting observations. But by no means is this the end of the road. There is a lot more to do even within these families. The further investigation of the excitonic mechanism, or the doping versus pressure phase diagram in the case of 1T-TiSe₂ are very important tasks. X-ray measurement under high pressure on 1T-TaS₂ would be very beneficial to reveal the nature of the charge density wave phase. Last but not least, to unravel the mystery of high- T_C superconductivity, more careful measurement on high quality samples are needed.

Appendix A

Calculation the Coulomb energy for different domain sizes in the case of 1T-TaS₂

The Coulomb energy related to the charge transfer within the superstructure shown in Fig. 3.29 is calculated starting from the usual expression,

$$E_{\text{Coul}} = \frac{1}{2} \int_{\text{s.c.}} d^3 \vec{r} \int d^3 \vec{r}' \frac{1}{4\pi\epsilon_0\epsilon_r} \frac{\rho(\vec{r})\rho(\vec{r}')}{|\vec{r} - \vec{r}'|}, \quad (\text{A.1})$$

where the first integral goes over the supercell in the TaS₂ plane, while the second integral goes over the whole space. $\rho(r)$ stands for the charge density produced by the charge transfer from domains to inter-domain space. E_{Coul} stands for the energy per supercell in the TaS₂ plane, while the energy E_c per electron transferred is obtained by dividing E_{Coul} by the number of David stars in the domain. Given the particular shape of the textured phase, we choose to calculate the integral in direct space, though with some simplifications. Firstly, being only interested in the long-wavelength aspect of the charge transfer, we do not consider the details of the charge distribution vertically within the layer, or on the scale of the basic TaS₂ cell. Accordingly, the Coulomb potential is regularized below

distance d , of the order of the separation between two neighbouring Ta atoms, and the planar charge density is assumed smooth on that scale. The latter is set within the domain by the requirement of one electron lacking per David star, and the requirement that each supercell remains neutral. Additionally, no variation in planar charge density is allowed within domains or within the inter-domain space. The former integral then transforms into the three-dimensional sum of convolutions of planar integrals over pairs of planar supercells. The sum is rapidly converging upon choosing the high-symmetry supercell, while all integrals are numerically calculated by subdividing the planar supercell into small triangles (size of the order of d). The requirement that the states above the gap in domains are kept void, determines the contributions to the dielectric constant ε_r that enters the calculation. Specifically, the contribution from electrons from metallic, "triangular" parts should be excluded, and only the contributions that relate to gapped charge-density wave should be included. Since these contributions also determine the screening of the electron-electron interaction in the Mott phase, the approximate value for appropriate ε_r may be determined from the proximity of that phase. The collapse of the Mott state on triangular lattice[1] is known to occur at $U/t \sim 10$. The value of U is given by $e^2/r_{DS}\varepsilon_r$, where r_{DS} is of the order of the radius of the David star in 1T-TaS₂, $e^2/r_{DS} \sim 2$ eV. The transfer integral t relevant for the Hubbard model one may read from the relevant band-width W in the band structure calculation[2], $W = 8t \approx 0.1$ eV. This leads to $\varepsilon_r \sim 10$, used in our calculation.

Bibliography

- [1] M. Capone, L. Capriotti, F Becca, and S Caprara. Mott metal-insulator transition in the half-filled Hubbard model on the triangular lattice. *Phys. Rev. B*, 63(8):085104, Feb 2001.
- [2] K. Rossnagel and N. V. Smith. Spin-orbit coupling in the band structure of reconstructed 1T-TaS₂. *Phys. Rev. B*, 73(7):073106, 2006.

Acknowledgement

The four years I spent in Lausanne were sometimes hard, but there are several people, now around the world, who made it really happy and joyful for me.

First of all I would like to express my deep and sincere gratitude to my supervisor, Professor László Forró, whose personality made our group so special. Without his support and patience it wouldn't have been possible for me to finish this PhD.

I'm also thankful to Richard Gaal, for always being helpful, but also for pointing out with great sarcasm all my weaknesses. All the technicians in the group, who were always helpful even when I arrived in the last minute with my requests also deserve thanks. Monique Bettinger, who is simply the best secretary on the earth. Eduard Tutiš for one of my best scientific discussions of my life. Anna Kusmartseva, who not only was involved in that conversation, but was also shared her great philosophy. All the members of to group who shared all the joy both in, and outside the lab. The small Hungarian community including Tamas, Janos, Rea and Nadia, who were always around to try my cooking creations. Bibe and Camillo, for the great festivals. My basketball and dancing clubs for adding color to my life. Gøran, for correcting this work and being a perfect flatmate for a few months. And everyone else who I can't name here because of lack of space – especially who shared skiing experiences, happiness, craziness, talks, and time with me.

And I just can't express well enough my gratefulness for my family. They were located far away, but always here with me.

CURRICULUM VITAE

BALÁZS SIPOS

PERSONAL DETAILS

Date of birth	February 28, 1981
Place of birth	Budapest, Hungary
Citizen of	Hungary
Civil status	single

EDUCATION

1991–1999	High School Studies, ELTE Trefort Ágoston Gyakorlóiskola és Gimnázium
1999–2004	Undergraduate Studies in Physics, Eötvös Lóránd University, Budapest
Since 2004	Ph.D. student, École Polytechnique Fédérale De Lausanne

RESEARCH

1999–2001	Undergraduate research, Eötvös Lóránd University: <i>Automatic foreground star removal from galactic images</i>
July 2001	One month summer internship in the group of prof. László Forró: <i>Thermoelectric power measurements on oxygen sensitive powder samples</i>
July 2002	One month summer internship in the group of prof. László Forró: <i>Transport measurements on high-T_c materials</i>
July 2003	One month summer internship in the group of prof. László Forró: <i>Brake junction tunneling measurements on underdoped $Bi_2Sr_2CaCu_2O_{8-\delta}$</i>

AWARDS

2001	2 nd place prize, Hungarian Conference of Undergraduate Research
------	---

SKILLS

Languages	English, French – fluent German – basic Hungarian – mother tongue
Software	Expert in Linux system administration; \LaTeX , Matlab, Origin, MS Office, good knowledge of programming languages (python, C, C++, IDL)

CONFERENCE TALKS

- **Pressure induced superconductivity in the proximity of CDW phase in dichalcogenides** at *Swiss Workshop on Materials with Novel Electronic Properties* (2007)

PUBLICATIONS

- **From Mott state to superconductivity using pressure in 1T-TaS₂**
B. Sipoš, A.F. Kusmartseva, A. Akrap, H. Berger, L. Forró and E. Tutiš *Nature Materials* **7** 960 (2008)
- **Matthiessen's rule in MgB₂: Resistivity and T_c as a function of point defect concentration**
B. Sipoš, N. Barisic, R. Gaal, L. Forró, J. Karpinski and F. Rullier-Albenque *Physical Review B* **76** 132504 (2007)
- **Pressure induced superconductivity in 1T-TiSe₂** A.F. Kusmartseva, B. Sipoš, H. Berger, L. Forró and E. Tutiš *Phys. Rev. Lett.*, *submitted*
- **Mechanical and electronic properties of VO_x nanotubes**
B. Sipoš, M. Duchamp, A. Magrez, N. Barisic, A. Kis, J.W. Seo and L. Forró *Jour. of App. Phys.*, *submitted*
- **High-pressure infrared spectroscopy: Tuning of the low-energy excitations in correlated electron systems**
I. Kezsmarki, R. Gaal, C.C. Homes, B. Sipoš, H. Berger, S. Bordacs, G. Mihály and L. Forró *Physical Review B* **76** 205114 (2007)
- **Ni-doped cobaltates as potential materials for high temperature solar thermoelectric converters**
R. Robert, L. Bocher, B. Sipoš, M. Dobeli and A. Weidenkaff *Progress In Solid State Chemistry* **35** 447 (2007)